BULLETIN OF BIOTECHNOLOGY

e-ISSN: 2717-8323

Cilt: 6 Volume: 1 Year: 2025

BULLETIN OF BIOTECHNOLOGY

Cilt: 6 Volume: 1 Year: 2025

Published Biannually

Corresponding Address
Karamanoğlu Mehmetbey University, Faculty of Health, Sciences, Department of Nutrition and Dietetics, Karaman, Türkiye
E-mail: mtdogan1@gmail.com
Web: https://www.dergipark.org.tr/biotech

Owner / Publisher
Assoc. Prof. Dr. Muhammet DOĞAN
This journal is peer-reviewed and published twice (June, December) a year.
All responsibility of the articles belongs to the authors.

e-ISSN 2717-8323

BULLETIN OF BIOTECHNOLOGY

e-ISSN 2717-8323

Cilt: 6 Volume: 1 Year: 2025

Contents

Research Articles

RESEARCH ARTICLE
Bull Biotechnol (2025) 6(1):1-10
https://doi.org/10.51539/biotech.1564289
Journal homepage: www.dergipark.org.tr/biotech

Bulletin of Biotechnology

Application of chitosan-alginate biocomposite for adsorption of Erythrosine B dye from wastewater: isotherm and kinetic study

Zeynep Mine Şenol[1*], Zehra Seba Keskin[2]

[*1] *Department of Nutrition and Diet, Faculty of Health Sciences, Sivas Cumhuriyet University, Sivas, Türkiye*
[2] *Department of Pharmacy, Health Services Vocational School, Sivas Cumhuriyet University, Sivas, Türkiye*

*Corresponding author: msenol@cumhuriyet.edu.tr
Orcid No: https://orcid.org/0000-0002-5250-126

Received : 10/10/2024
Accepted : 03/02/2025

To Cite: Şenol ZM, Keskin ZS (2025) Application of chitosan-alginate biocomposite for adsorption of Erythrosine B dye from wastewater: isotherm and kinetic study. Bull Biotechnol 6(1):1-10 https://doi.org/10.51539/biotech.1564289

Abstract: Biocomposite materials are effective and efficient adsorbents in the treatment of dye-contaminated wastewater. In this study, the adsorption properties of chitosan (Ch)-alginate (A) biocomposite for Erythrosine B (EB) dye were investigated. FT-IR, SEM-EDX, and zero-charge point analyses support the idea that the adsorption process may occur via hydrogen bonds and electrostatic interactions between dye molecules and functional groups on the surface of Ch-A biocomposite. The maximum adsorption capacity of Ch-A biocomposite was found to be 319 mg g^{-1}. The adsorption energy value was found to be 7.76 kJ mol^{-1}, which indicates the physical nature of the adsorption process. Adsorption kinetics showed that the adsorption process first occurs as rapid adsorption onto the surface and then as relatively slow intraparticle diffusion. Adsorption thermodynamic studies showed that the adsorption process is endothermic and spontaneous. When all adsorption studies are evaluated together, Ch-A biocomposite is an alternative, effective, efficient, and promising adsorbent for better environmental protection and public health safety in removing EB dye from wastewater. We hope this study can successfully guide the development of new and more powerful approaches to reduce EB dye pollution in wastewater. It is of critical importance to protect the environment and human health from the toxic effects of EB dye that threatens life and enters wastewater. Because a clean environment means a more livable world for future generations.

Keywords: Chitosan; alginate; biocomposite; Erythrosine B; removal; wastewater treatment

1 Introduction

Although water is one of the most abundant natural resources on earth, only about 0.007% is available for human consumption. As a result, billions of people today lack access to clean, drinkable water, and the demand is growing daily (Sağlam, Türk, and Arslanoğlu 2023) (Alsawat 2024). Furthermore, the discharge of wastewater, generated by rapid industrialization and urbanization, into natural water sources without treatment represents a significant challenge in terms of water access. The dyes present in this wastewater, due to their toxic and stable nature, cause visual and chemical pollution, thereby posing a considerable threat to the environment (M. F. Ahmad et al. 2024). The presence of dyes in wastewater impairs the photosynthetic activities of aquatic organisms and alters their biological processes. Furthermore, these dyes can undergo degradation into mutagenic, toxic, and carcinogenic compounds that pose a threat to the health of living organisms (Raji et al. 2023).

Erythrosine B is a member of the anionic xanthene dye class and exhibits high solubility in water. It is employed extensively in the food, cosmetic, and pharmaceutical industries (Nascimento et al. 2022). The World Health Organization (WHO) has established a maximum daily intake of EB at 0–1.25 mg kg^{-1} (Lai, Li, and Zhang 2021). However, ingestion of quantities over these limits can result in the development of allergic reactions, as well as carcinogenic and mutagenic effects, and thyroid disorders in humans (Pipíška et al. 2022). Given the detrimental impact of EB dye on public health and the natural environment, it is imperative to develop effective strategies for the treatment of wastewater contaminated with this substance. Consequently, a variety of techniques, including ion exchange, coagulation, membrane technology, chemical oxidation, photocatalytic degradation, ozonation, and adsorption, are utilized to eliminate synthetic dyes such as EB from wastewater (Umesh, Puttaiahgowda, and Thottathil 2024) (T. Ahmad et al. 2024).

Nevertheless, a disadvantage of these methods is the utilization of chemical reagents that result in secondary pollution and their considerable electricity costs. In contrast, adsorption is a more frequently preferred method due to its low cost, simplicity, environmental friendliness, process flexibility, and high efficiency (Umesh et al. 2024) (Arni et al. 2023). In the removal of dyes from aqueous solutions through adsorption, a variety of adsorbents have been employed, including activated carbon (Raji et al. 2023), biomass (Şenol, Messaoudi, et al. 2023), biochar (Zhang, He, and Liu 2023), graphene (Khan Rind et al. 2023), clays (Ighnih et al. 2023), nanocomposites (Rehan et al. 2023), and natural polymers (Hevira, Ighalo, and Sondari 2024). However, due to the high cost and toxicity of activated carbon, graphene, and carbon nanotubes, recent studies have focused on the effectiveness of natural polymers like chitosan and alginate, as well as biocomposites synthesized from them, in dye removal (Şen and Şenol 2023a).

Chitosan is a polysaccharide derived from the deacetylation of chitin and represents one of the most prevalent natural polymers on Earth. Chitosan is employed in a multitude of industries, including agriculture, medicine, biomedicine, food, paper, textiles, and cosmetics. The aforementioned characteristics of chitosan, namely its hydrophilicity, abundant availability, high biocompatibility, strong chemical reactivity, non-toxicity, low cost, recyclability, antimicrobial activity, and functional groups (-NH_2 and -OH) that support adsorption, render it an attractive adsorbent. Nevertheless, the utilization of chitosan (as an adsorbent is constrained by several factors, including its inadequate mechanical strength, limited specific surface area, susceptibility to depolymerization in acidic conditions, proclivity to agglomerate, and elevated swelling index (Abdulhameed et al. 2024) (Kashi et al. 2024) (Sabbagh, Tahvildari, and Mehrdad Sharif 2021). To enhance these structural characteristics, chitosan has been modified through techniques such as cross-linking, covalent grafting, and ionic liquid impregnation with minerals, metal nanoparticles, synthetic polymers, metal oxides, glutaraldehyde, clay, and polysaccharides like alginate (Issahaku, Tetteh, and Tetteh 2023). The utilization of cross-linkers, such as epichlorohydrin and tripolyphosphate, has the potential to enhance the surface properties, chemical stability, and mechanical strength of the synthesized biocomposite (Bellaj et al. 2024) (Hisham et al. 2024). Due to its abundant natural availability, low cost, non-toxicity, hydrophilic nature, biodegradability, and ability to cross-link with divalent cations, various studies have reported that chitosan can be cross-linked to synthesize a biocomposite with enhanced properties (Şenol, Elma, et al. 2023). Additionally, in several studies, chitosan's high amino functional groups have been shown to attract dye anions through electrostatic interactions (Chiou and Chuang 2006) (Chiou, Ho, and Li 2004).

Alginate, a linear polysaccharide derived from brown seaweed, is a widely utilized material in a multitude of industries, including cosmetics, pharmaceuticals, textiles, food production, and the manufacture of medical products (Kazemi and Javanbakht 2020). The alginate is a natural anionic biopolymer with free hydroxyl (–OH) and carboxyl (–COOH) groups. It has attracted great attention due to its widespread availability, low cost, biocompatibility, and biodegradability. Its ability to bind metal cations (usually divalent cations) through ionic interactions has made alginate an alternative to traditional treatment methods for heavy metal removal. However, the poor mechanical and chemical resistance of this biopolymer limits its industrial use on a large scale (Sachan 2009). One of the new approaches used to solve this disadvantage of biopolymers is to use them as composite material components.

This paper investigated the adsorption properties of Ch-A biocomposite cross-linked with tripolyphosphate and epichlorohydrin to effectively remove anionic EB dye from aqueous solutions. Extensive research in the literature revealed that this study is the first to investigate the performance of cross-linked Ch-A biocomposite in the removal of EB dye. The effects of initial EB concentration, pH, contact time, adsorbent dose, and temperature on the adsorption process were investigated. Furthermore, the adsorption mechanism was explained using isotherm and kinetic models and the adsorption capacity for EB dye was evaluated. The findings demonstrated that Ch-A biocomposite is an effective, environmentally friendly, and cost-effective alternative adsorbent for the removal of EB dye.

2 Materials and Method

2.1 Chemicals

The EB ($C_{20}H_6I_4Na_2O_5$) dye was purchased from Merck (Germany). The chemical structure of EB was given in Fig. 1. Medium molecular weight Ch, A, epichlorohydrin (ECH), NaOH, sodium tripolyphosphate (NaTPP), KNO_3, and HCl, were obtained from Sigma-Aldrich.

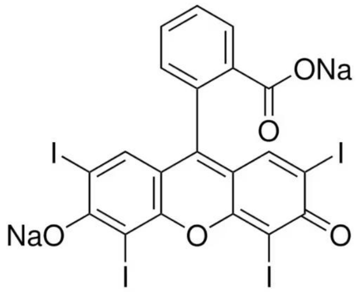

Fig. 1 Chemical structure of EB

2.2 Preparation of Ch-A biocomposite beads

In the synthesis of Ch-A biocomposite beads, the method of (Şenol 2021) was followed. Then, the Ch-A biocomposite was ground into powder and stored.

2.3 Batch adsorption experiments

The batch experimental conditions are given in Table 1. The EB dye concentration was determined at 528 nm (Kaur and Datta 2013) in a UV–vis spectrophotometer. Removal% and

Q adsorbed amount of EB dye (mg g^{-1}) were calculated using Eq. 1 and Eq. 2.

$$Removal\% = \left[\frac{C_i - C_f}{C_i}\right] x100 \qquad \textbf{(1)}$$

$$Q = \left[\frac{C_i - C_f}{m}\right] xV \qquad \textbf{(2)}$$

Table 1. Experimental conditions

Aim of experiment	**pH**	**$[EB]_0$ (mg L^{-1})**	**m (g L^{-1})**	**t (min)**	**T (^{0}C)**
Effect of pH	2.0-12.0	500	5	1440	25
Effect of concentration	6.5	10-1000	5	1440	25
Effect of time	6.5	500	15	2-1440	25
Effect of adsorbent dose	6.5	500	1, 3, 5, 10	1440	25
Effect of temperature	6.5	500	5	1440	5, 25, 40

3 Results

3.1 FT-IR and SEM-EDX analysis

The FT-IR spectra of Ch, A, and the Ch-A biocomposite are shown in Fig. 2. The broad band observed in the FTIR spectrum of chitosan (Ch) between 3656 and 3010 cm^{-1} is attributed to the stretching vibrations of N-H and O-H. The peaks observed at 2882, 1619, and 1538 cm^{-1} are attributed to the stretching of the C-H bond, the bending of the N-H bond, and the bending of the primary amine N-H bond, respectively (He et al. 2023) (Benhouria et al. 2023). The distinctive peaks of chitosan at 1438, 1329, and 1032 cm^{-1} are attributed to C-O stretching, and C-H bending, (Tran et al. 2023) (Meng et al. 2023) (Şenol and Şimşek 2020). The broad band observed in the FT-IR spectrum of alginate between 3676 and 2975 cm^{-1} is attributed to O-H group stretching vibrations. The peak at 2914 cm^{-1} is attributed to C-H stretching, while the peaks at 1599 and 1407 cm^{-1} are assigned to COO^- group stretching vibrations. The peak at 1081 cm-1 is associated with C-H bending, and the peak at 1028 cm^{-1} corresponds to C-O stretching vibrations (Nandanwar et al. 2023) (Wen et al. 2024) (Khapre, Pandey, and Jugade 2021). The FT-IR spectrum of the Ch-A biobiocomposite displays the presence of characteristic peaks at 2882, 1619, and 1538 cm^{-1}, which are associated with chitosan, and peaks at 1407, 1081, and 1028 cm^{-1}, which are characteristic of alginate. The appearance of these peaks serves as confirmation that the synthesis of the biocomposite was accomplished.

The FT-IR spectra of the Ch-A biocomposite are presented in Fig. 2, illustrating the spectra of the biocomposite before adsorption and after the adsorption of the EB dye. A comparison of the FT-IR spectra of the EB-loaded Ch-A biocomposite with that of the unloaded Ch-A spectrum reveals notable differences. Following the adsorption of EB dye molecules, alterations in the position and intensity of the characteristic peaks of Ch-A can be ascribed to the electrostatic interaction between the EB dye molecules and Ch-A bio. Furthermore, the emergence of new peaks in the FT-IR spectrum of EB-loaded Ch-A at 645 cm^{-1} and 1326 cm^{-1} can be attributed to the C-I stretching vibration of the EB dye (Ramalakshmi, Murugan, and Jeyabal 2022) and the C-H deformation of the xanthene ring (Kaur and Datta 2013), respectively. The broadband for O-H and N-H seen around 3200-3500 cm^{-1} has shifted and increased in intensity due to the hydrogen bonding of EB and biocomposite. It was observed that the intensities of amide I and amide II bands increased around 1650 cm^{-1} and 1560 cm^{-1}, which indicates the interaction of the biocomposite with EB dye. The increases in the intensity of the peaks seen around 1600 cm^{-1} and 1400 cm^{-1} corresponding to the carboxylate groups indicate the interaction of the carboxylate groups of alginate with EB dye and were evaluated as evidence for EB dye adsorption.

The structures constituting the Ch-A biocomposite and its components and the SEM images and EDX spectra after EB adsorption are presented comparatively in Fig. 3(a-d). The SEM images revealed that chitosan possesses a porous surface (Fig. 3(a)), whereas alginate exhibits a rough and porous structure (Fig. 3(b)). The SEM image of the Ch-A biocomposite (Fig. 3(c)) has a completely different morphology from its components. After EB adsorption, there is a significant change in the surface morphology of the Ch-A biocomposite and its surface appears to have become smoother (Fig. 3(d)). This may be due to surface complexation. EDX spectra showed that Ch contained C, N, and O (Fig. 3(e)), while alginate contained C, O, and Na (Fig. 3(f)). The Ch-A biocomposite showed that both Ch and alginate contained C, N, O, and Na elements (Fig. 3(g)). The EDX data of the Ch-A biocomposite after EB adsorption (Fig. 3(h)) confirms the adsorption of the dye, as does the presence of iodine, which is not present in the elemental composition of Ch-A.

3.2 Effect of pH of EB dye solution

Adsorption efficiency is strongly dependent on the pH of the solution medium. The pH of the solution medium is affected by the surface properties of the adsorbent and the ionization of the dye molecules. The pH effect on the adsorption of EB dye molecules onto the Ch-A composite was investigated in the pH range of 2.0-12.0 (Fig. 4). EB is an acidic dye and since the functional groups of acidic dyes are anionic, they release negative charges to their aqueous solutions. Acid dyes have chromophore groups with negative electrical charges. At acidic pH values, the adsorbent surface is positive due to the high concentration of H^+ ions. This increases the electrostatic interaction between the adsorbent and the anionic dye molecules. In acidic conditions, the electrostatic interactions between the positively charged adsorbent surface and the COO^- groups of the EB dye molecules play an important role in the adsorption process. Therefore, the adsorption efficiency was found to be high at pH: 2.0. In the pH range of 4.0-12.0, it was observed that the adsorption efficiency gradually decreased. With increasing pH values, the number of negatively charged sites on the adsorbent surface increases and the number of positively charged sites decreases. The lower adsorption efficiency under alkaline conditions is due to the competition between anionic EB dye molecules and OH- ions for adsorption sites. The surface of the adsorbent was negatively charged at basic pH values, which hindered the adsorption of anionic EB dye molecules by electrostatic repulsion (Pan and Zhang 2009). In addition to the electrostatic interactions between the Ch-A composite adsorbent and anionic EB dye molecules, intermolecular interactions such as physical forces such as hydrogen bonding also occur (Ansari and Mosayebzadeh 2010). The surface charge of the adsorbent was found by point of zero charge (pHpzc) analysis (Şenol et al. 2024). The surface charge of the Ch-A composite adsorbent was found to be 4.59 (Fig. 4). The Ch-A composite will be positively charged in solutions with pH below the pHpzc value and negatively charged in solutions with pH above it. At strong acidic pH values (pH<pHpzc), the adsorbent surface will be positively charged and the anionic EB dye adsorption efficiency will increase. At basic pH values (pH>pHpzc), hydroxyl ions deprotonate all nitrogen atoms in the Ch-A composite adsorbent and the surface charge becomes significantly negative. In this case, the adsorption efficiency also decreased. These two sets of findings were in agreement with the predicted framework for the pH effect on the removal of EB dye molecules onto the Ch-A biocomposite.

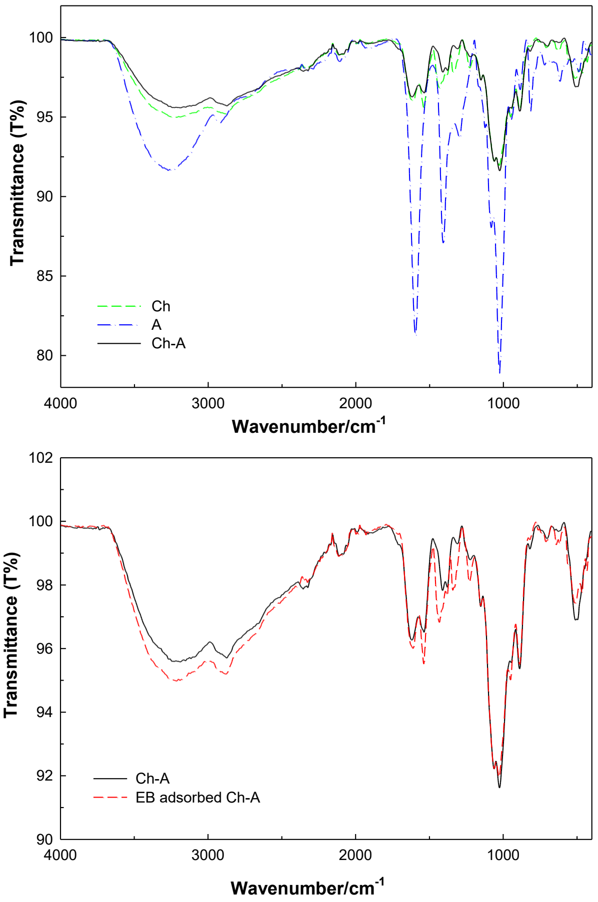

Fig. 2 FT-IR spectrum of Ch, A, Ch-A, and EB adsorbed Ch-A biocomposite

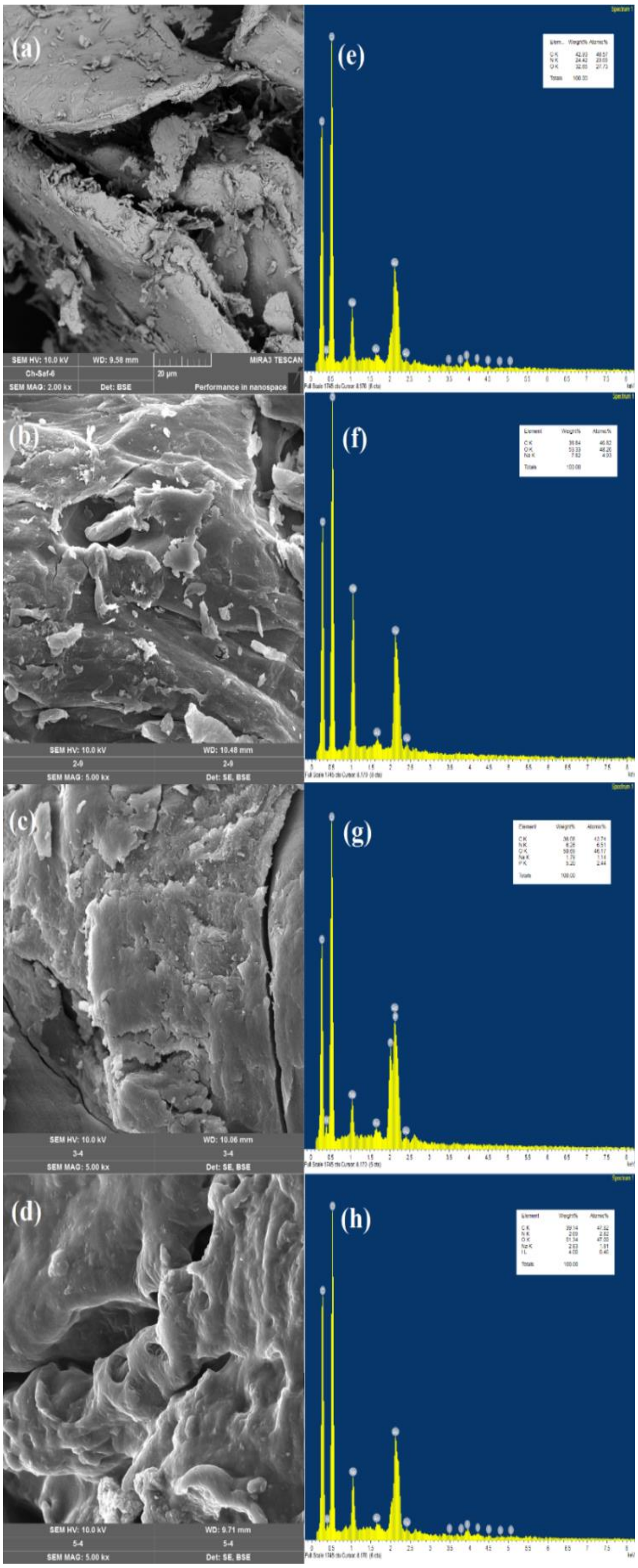

Fig. 3 SEM morphologies of Ch (a), A (b), Ch-A (c), and EB adsorbed Ch-A (d) and EDX spectra of Ch (e), A (f), Ch-A (g), and EB adsorbed Ch-A (h)

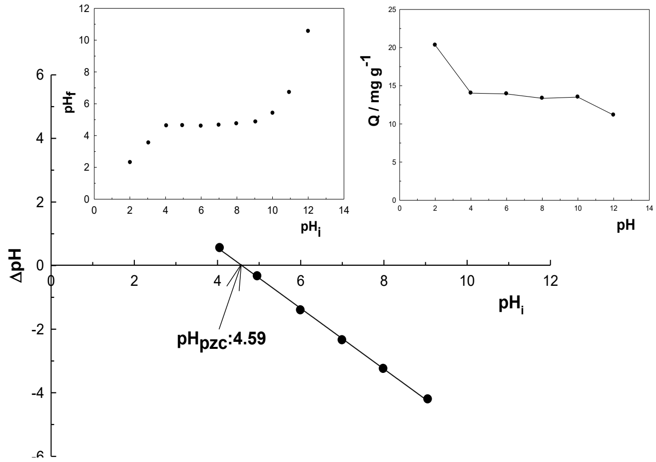

Fig. 4 Effect of pH and pHpzc for Ch-A

3.3 Effect of the biocomposite dose

The efficiency of dye removal from wastewater is contingent upon the number of active adsorption sites on the adsorbent surface. The determination of the optimal quantity of adsorbent to be employed represents a pivotal element in the evaluation of the cost per unit of dye solution (Elgarahy et al. 2021). The impact of varying concentrations of Ch-A (1-20 g L^{-1}) on the adsorption of EB dye molecules was examined while maintaining other experimental variables at a constant level. Fig. 5 illustrates the relationship between the percentage removal of EB dye and the adsorption capacity of Ch-A concerning the adsorbent amount. The increase in the amount of Ch-A resulted in a notable enhancement in the percentage removal of EB dye, rising from 88% to 94% (Fig. 5). This increase can be attributed to the proportional rise in the number of active binding sites and surface area with the greater amount of Ch-A. Consequently, anionic EB dye molecules are more readily retained by the active centers on the Ch-A surface (Şen and Şenol 2023b). Nevertheless, the augmented Ch-A quantity resulted in a reduction in the quantity of EB dye adsorbed per unit. This reduction can be attributed to the fact that the increased number of active sites on Ch-A may not have reached saturation with the EB dye molecules, resulting in the clustering of adsorption sites and longer diffusion distances. The highest adsorption capacity identified was achieved with a 1 g L^{-1} adsorbent dose (Ezeh et al. 2017).

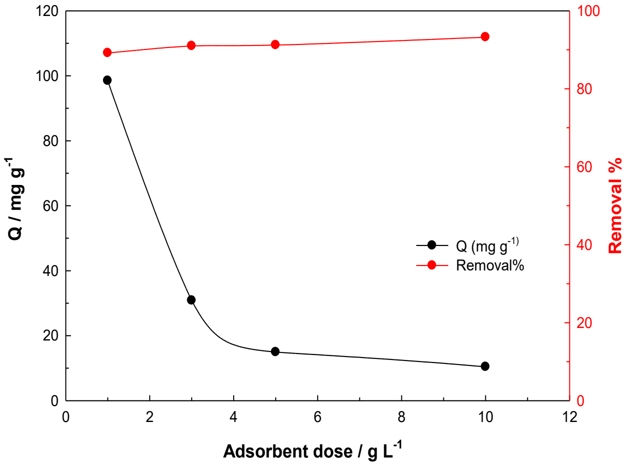

Fig. 5 Effect of the biocomposite dose

3.4 Modeling of Adsorption Process

In this study, Langmuir (Langmuir 1918), Freundlich (Freundlich 1907), and Dubinin-Radushkevich (D-R) (Dada 2012) isotherm models, were applied to the experimental data. The adsorption behavior of EB dye on Ch-A composite was analyzed using isotherm models and the fit of the isotherm plots is presented in Fig. 6. The derived isotherm parameters are listed in Table 2. Fig. 6 shows that the adsorption efficiency of EB dye is high at low concentrations due to the presence of vacant active sites on the surface of the Ch-A biocomposite. However, at higher concentrations, these active sites are filled and the adsorption efficiency decreases and eventually, equilibrium is reached. When the R^2 values from the Langmuir and Freundlich isotherm models are compared (Fig. 6, Table 2), it is seen that the adsorption is in good agreement with the Langmuir isotherm model. The maximum adsorption capacity obtained from this model is 319 mg g^{-1} and the Langmuir constant is 0.00227 L mg^{-1}. The high adsorption capacity of the Ch-A biocomposite indicates its potential as an effective adsorbent for removing EB dye from wastewater. According to the Freundlich isotherm model, the adsorption capacity (X_F) was found to be 0.113 and the surface heterogeneity factor (β) was found to be 0.908. The adsorption energy calculated from the D-R model indicates that the adsorption process is physical. A comparison of the EB dye adsorption capacities of various adsorbents (Table 3) shows that the Ch-A composite exhibits a relatively high sorption capacity (319 mg g^{-1}).

Table 2. Isotherm parameters

Isotherm model	Parameter	Value
Langmuir	Q_L (mg g^{-1})	319
$Q = \frac{Q_L C_e}{1 + K_L C_e}$	K_L x10^3 (L mg^{-1})	2.27
	R^2	0.991
Freundlich	X_F	0.113
$Q = X_F C_e^{\beta}$	β	0.908
	R^2	0.989
D-R	X_{DR} (mg g^{-1})	774
$Q = X_{DR} e^{-(K_{DR}\varepsilon^2)}$	-K_{DR}x10^9/mol^2 KJ^{-2}	8.31
$\varepsilon = RT\ln\left(1 + \frac{1}{C_e}\right)$	E_{DR}/kJ mol^{-1}	7.76
$E_{DR} = (2K_{DR})^{-0.5}$	R^2	0.977

Table 3. Comparison of adsorption capacity for adsorption of EB dye on various adsorbents reported in the literature

Adsorbent	pH	Q/ mg g^{-1}	Reference
Montmorillonite	7.5	578.03	(Kaur and Datta 2013)
Pumpkin seed hulls	-	16.4	(Carmen Apostol et al. 2016)
Chitosan/ hydrogel SiO_2 hybrid material	-	71.27	(Copello et al. 2011)
Chitin/hydrogel SiO_2 hybrid material	-	131.98	(Copello et al. 2011)
Crystal violet modified montmorillonite	-	123.18	(Rytwo et al. 2006)
Bottom ash and de-oiled soya	2.0	16.17 and 9.52	(Mittal et al. 2006)
Sugarcane bagasse	9.0	500	(Sharma and Kaur 2011)
TiO_2 and ZnO surfaces	5.0-6.8	17.54 and 3.06	(Hasnat et al. 2007)
Cross-linked lysozyme crystals	-	70.39	(Cvetkovic et al. 2005)
Hen feathers	3.0	15.43	(Gupta et al. 2006)
Ch-A biocomposite	6.5	319	This study

3.5 Effect of contact time

In the adsorption process, it is vital that the adsorption reaches equilibrium in a short time. Kinetic studies help us predict the mechanism of the adsorption process at the solid-liquid interface. In the adsorption process, the solution transfer at the solid-liquid interface is expressed as either external mass transfer (boundary layer diffusion), intraparticle diffusion, or both. In general, three steps accompany the adsorption process; i) transport of the adsorbate from the bulk solution to the external surface of the adsorbent via the liquid film ii) diffusion of the adsorbate into the pores of the adsorbent iii) sorption of the adsorbate from the pores of the adsorbent to the inner surface of the capillary cavities. The third step is considered as an equilibrium reaction. The third of these three steps is assumed to be fast and negligible.

Upon examining the adsorption kinetics presented in Fig. 7, it is observed that the adsorption of EB dye increases with contact time. Adsorption efficiency increases rapidly until the first 300 minutes. After the 300 minutes, it is seen that the adsorption rate decreases and reaches equilibrium. The high adsorption rate observed in the first 300 minutes is due to the number of vacant active centers on the Ch-A composite surface. As a result, the interactions between the EB dye molecules in the solution and the active centers on the Ch-A composite surface have increased. Over time, the number of active centers has decreased due to the attachment of EB dye molecules to the vacant active centers on the Ch-A composite surface. This causes the adsorption rate to decrease after the 300 minutes. To study the effect of contact time on the adsorption process in detail, the kinetic data were analyzed as pseudo-first-order (PFO) (Ho and McKay 1998), pseudo-second-order (PSO) (Ho and McKay 1999) and intraparticle diffusion (IPD) (Wu, Tseng, and Juang 2009) the fit to the velocity models were investigated (Fig. 7).

The parameters obtained from the fit of PFO, PSO, and IPD kinetic models are summarized in Table 4. When the kinetic parameters in Table 4 are examined, it is seen that the adsorption process provides a better fit to the PSO kinetics. In addition, the experimental Q_t values and the theoretically calculated Q_e values are much closer to each other, which reveals the fit of the PSO model. In addition, the multicollinearity observed in the IPD plot indicates that the adsorption process involves two or more steps. Therefore, the adsorption of EB dye on the Ch-A composite can be described using both PSO and IPD models instead of a single kinetic model.

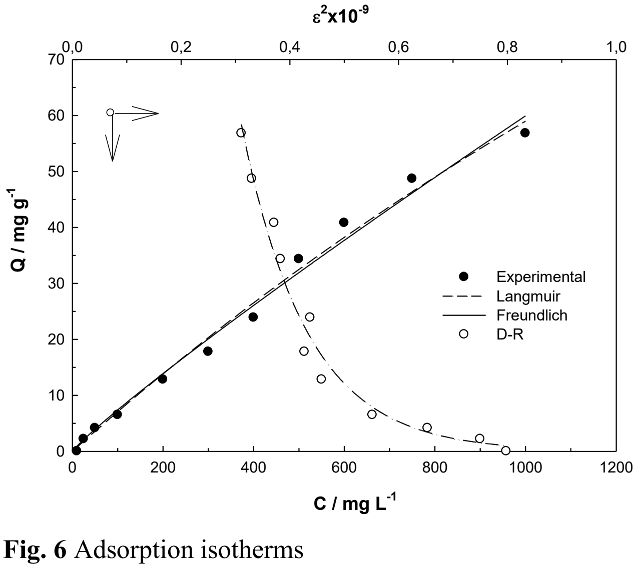

Fig. 6 Adsorption isotherms

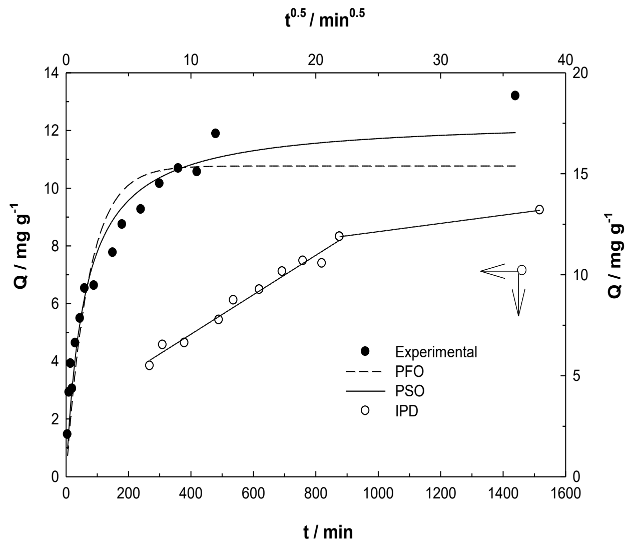

Fig. 7 Adsorption kinetics

Table 4. Kinetic parameters

Kinetic model	Parameter	Value
PFO	Q_t/mg g^{-1}	13.2
$Q_t = Q_e[1 - e^{-k_1 t}]$	Q_e/mg g^{-1}	10.8
$H_1 = k_1 Q_e$	k_1 x10^3/min^{-1}	13.9
	H_1x10^3/mg g^{-1} min^{-1}	150
	R^2	0.883
PSO	Q_t/mg g^{-1}	13.2
$Q_t = \frac{t}{\left[\frac{1}{k_2 Q_e^2}\right] + \left[\frac{t}{Q_e}\right]}$	Q_e/mg g^{-1}	12.4
	k_2 x10^3/mg^{-1} g min^{-1} H_2x10^3/mg g^{-1} min^{-1}	1.36 209
$H_2 = k_2 Q_e^2$	R^2	0.951
IPD	k_i x10^3/mg g^{-1} min$^{-0.5}$	3143
$Q_t = k_i t^{0.5}$	R^2	0.978

3.6 Effect of temperature

An investigation into the effect of temperature on adsorption allows insights to be gained into the thermodynamic parameters, which in turn facilitate an understanding of the process's feasibility and efficiency. To elucidate the nature of EB dye adsorption by Ch-A and its relationship with temperature, thermodynamic studies were conducted at 278, 298, and 313 K. The resulting data enabled the calculation of thermodynamic parameters, including enthalpy change (ΔH°), Gibbs free energy (ΔG°), and entropy change (ΔS°), using the following equations (Eq. 3-6) (Lima et al. 2019).

$$K_d = \frac{Q}{C_e} \qquad \textbf{(3)}$$

$$\Delta G^\circ = -RT\ln(K_d) \qquad \textbf{(4)}$$

$$lnK_D = \frac{\Delta S^\circ}{R} - \frac{\Delta H^\circ}{RT} \qquad \textbf{(5)}$$

$$\Delta G^o = \Delta H^o - T\Delta S^o \qquad \textbf{(6)}$$

Here, K_D represents the equilibrium adsorption rate constant (L mol^{-1}), R denotes the universal gas constant (8.314 J mol^{-1} K^{-1}), and T stands for the absolute temperature (K). The ΔH° and ΔS° parameters were calculated from the slope and the intercept of the line obtained from the lnK_D-1/T graph, which was drawn using the Van't Hoff equation, respectively (Fig. 8). The resulting values are presented in Table 5. The negative value of ΔH° (-15.4 kJ mol^{-1}) indicates that the adsorption of the EB dye onto Ch-A is exothermic and occurs physically. In general, ΔH° values in the range of -2.1 to -20.9 kJ mol^{-1} are indicative of physical adsorption, while values between -80 and -200 kJ mol^{-1} are indicative of chemical adsorption (Nannu Shankar et al. 2023). The positive ΔS° value (46.6 J mol^{-1} K^{-1}) indicates that during the adsorption of EB onto Ch-A, there is an increase in the degrees of freedom at the solid-liquid interface. This can also be attributed to the high affinity of Ch-A for the EB dye molecules. As demonstrated in Table 3, the negative ΔG° values at varying temperatures indicate that the adsorption process of the EB dye is both feasible and spontaneous, with favorable outcomes. Furthermore, the reduction in ΔG° values with rising temperature indicates that elevated temperatures serve as a driving force for adsorption (Akdemir et al. 2023). Furthermore, the observed increase in ΔG° values with rising temperature indicates that a greater driving force is required for adsorption at higher temperatures.

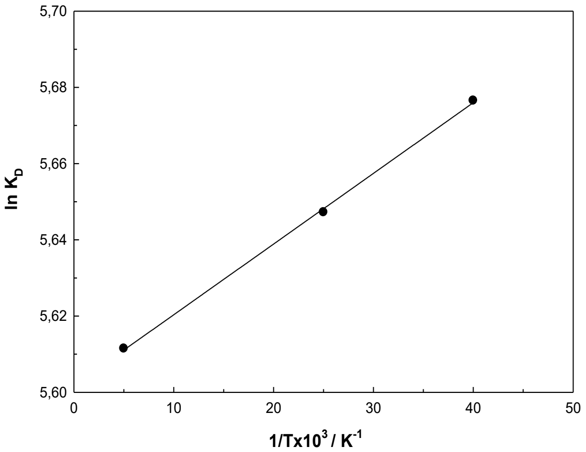

Fig. 8 The effect of temperature

Table 5. Thermodynamic parameters

T (°C)	ΔH^0 (kJ mol^{-1})	ΔG^0 (kJ mol^{-1})	ΔS^0 (Jmol^{-1} K^{-1})	R^2
5		-28.4		
25	-15.4	-29.3	46.6	0.999
40		-30.1		

3.7 Possible removal mechanism

Fig. 9 shows the possible interactions between Ch-A biocomposite and EB dye molecules. The adsorption process of anionic EB dye molecules with Ch-A biocomposite is accompanied by multiple mechanisms such as H-bonding and electrostatic interactions. Amine groups on the surface of the Ch-A biocomposite can be easily protonated and anionic EB dye molecules can be bonded by electrostatic interaction. In addition, H-bonding can occur between electronegative groups of dye molecules and active centers on the surface of Ch-A biocomposite. In this study, electrostatic interactions and H-bonding were important factors in the entire adsorption process.

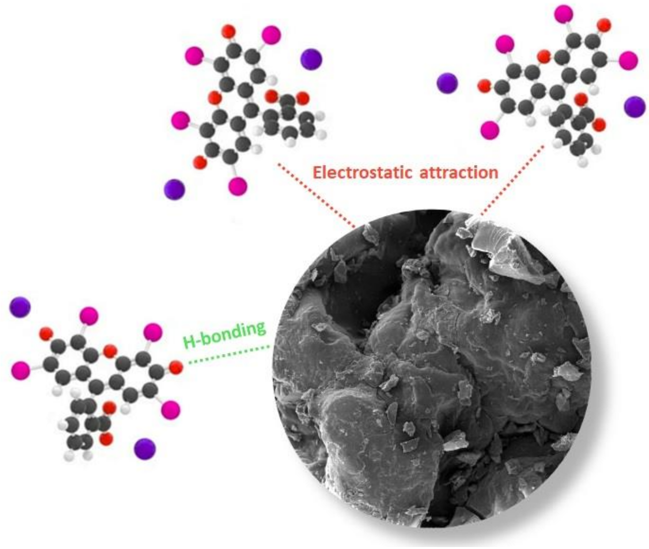

Fig. 9 Possible interactions of EB dye onto the Ch-A

5 Conclusion

In this study, the removal of EB dye from an aqueous solution was investigated using Ch-A biocomposite. Maximum adsorption capacity was achieved at pH 6.5 at 25 ºC. The maximum adsorption capacity of the Ch-A biocomposite for EB dye was found to be 319 mg g^{-1} at 25 °C (R^2 values, Langmuir isotherm model). Thus, the results fitted best the Langmuir model. The adsorption energy showed that adsorption was physical. Adsorption kinetics showed that the adsorption process followed the PSO and IPD patterns. Adsorption thermodynamics showed that the adsorption process is endothermic, entropy-increasing, and spontaneous. All obtained results showed that the Ch-A biocomposite will be an alternative, effective, and efficient adsorbent material for the removal of colored pollutants from wastewater.

Acknowledgements

This study was presented as an oral presentation at the 7th International Eurasian Conference on Biological and Chemical Sciences (EurasianBioChem 2024).

The present study was supported by the Sivas Cumhuriyet University Projects Commission (Project number: SBF-2023-101).

Authors' contributions:

ZMŞ: experimental work, visualization, supervision, writing, guidance, editing, and review

ZSK: writing, editing, and review

Conflict of interest disclosure:

The authors declare no conflict of interest.

References

Dada AO (2012) Langmuir, Freundlich, Temkin and Dubinin–Radushkevich Isotherms Studies of Equilibrium Sorption of Zn2+ Unto Phosphoric Acid Modified Rice Husk. IOSR J Appl Chem 3(1):38–45. doi: 10.9790/5736-0313845.

Abdulhameed AS, Mohammad KAK, Hassan A, Mohammad KY, and Sameer A (2024) Newly Developed Polymer Nanocomposite of Chitosan-Citrate/ZrO2 Nanoparticles for Safranin O Dye Adsorption: Physiochemical Properties and Response Surface Methodology. Mater Chem Phys 324:129699. doi: 10.1016/j.matchemphys.2024.129699.

Ahmad MF, Safia H, Zahid I, Danial M, Sumra A, Syed AU (2024) Green Approach to Water Purification: Investigating Methyl Orange Dye Adsorption Using Chitosan/Polyethylene Glycol Composite Membrane. J Polym Environ 32(1). doi: 10.1007/s10924-023-02994-9.

Ahmad T, Mohammad SM, Sardaraz K, Manal A. Al-Sharafi, Jordana G, Dison S.P.F, Nisar U (2024) Enhanced Adsorption of Bisphenol-A from Water through the Application of Isocyanurate Based Hyper Crosslinked Resin. J Mol Liq 395:123861. doi: 10.1016/j.molliq.2023.123861.

Akdemir M, Birol I, Fatih C, and Ozlem C (2023) High-Performing Natural Materials (Leonurus Cardiaca): Dye Biosorption Studies and Statistical Analysis. Biomass Convers Biorefin 13(15). doi: 10.1007/s13399-023-04469-2.

Alsawat M (2024) Congo Red Dye Adsorption Using CuSnO2TiO2 Nanocomposites: Adsorption Data Interpretation by Statistical Modeling. Int J Electrochem Sci 19(7):100611. doi: 10.1016/j.ijoes.2024.100611.

Ansari R, Zahra M (2010) Removal of Eosin Y, an Anionic DYE, from Aqueous Solutions Using Conducting Electroactive Polymers. Iran Polym J 19(7).

Arni LA, Ahmad H, Ahmed SA, Tumirah K, Zeid A, ALOthman LD, Wilson AHJ (202) Design of Separable Magnetic Chitosan Grafted-Benzaldehyde for Azo Dye Removal via a Response Surface Methodology: Characterization and Adsorption Mechanism. Int J Biol Macromol 242. doi: 10.1016/j.ijbiomac.2023.125086.

Bellaj M, Khalid A, Mounir EA, Mohammadine EH, Lhoucine G, Tonni AK, Zhonghao C, Pow SY, Faissal A (2024) Cationic and Anionic Dyes Adsorption from Wastewater by Clay-Chitosan Composite: An Integrated Experimental and Modeling Study. Chem Eng Sci 285. doi: 10.1016/j.ces.2023.119615.

Benhouria A, Zaghouane-Boudiaf H, Riadh B, Ferhat D, Hameed BH, Mokhtar B (2023) Cross-Linked Chitosan-Epichlorohydrin/Bentonite Composite for Reactive Orange 16 Dye Removal: Experimental Study and Molecular Dynamic Simulation. Int J Biol Macromol 242. doi: 10.1016/j.ijbiomac.2023.124786.

Carmen A, Laura, CG, Madalena A, Maria G (2016) Removal of Erythrosine B Dye from Water Effluents Using Crop Waste Pumpkin Seed Hulls as Adsorbent. Desalin Water Treat 57(47).

doi: 10.1080/19443994.2015.1132477.

Chiou MS, Guo SC (2006) Competitive Adsorption of Dye Metanil Yellow and RB15 in Acid Solutions on Chemically Cross-Linked Chitosan Beads. Chemosphere 62(5). doi: 10.1016/j.chemosphere.2005.04.068.

Chiou MS, Pang YH, Hsing YL (2004) Adsorption of Anionic Dyes in Acid Solutions Using Chemically Cross-Linked Chitosan Beads. Dyes and Pigm 60(1). doi: 10.1016/S0143-7208(03)00140-2.

Copello GJ, Andrea MM, Raineri M, Mariela PP, Luis ED (2011) Removal of Dyes from Water Using Chitosan Hydrogel/SiO2 and Chitin Hydrogel/SiO2 Hybrid Materials Obtained by the Sol-Gel Method. J Hazard Mater 186(1). doi: 10.1016/j.jhazmat.2010.11.097.

Cvetkovic A, Adrie JJS, Rajamani K, Luuk AMVDW (2005) Adsorption of Xanthene Dyes by Lysozyme Crystals. Langmuir 21(4). doi: 10.1021/la0478090.

Elgarahy AM, Elwakeel KZ, Mohammad SH, Elshoubaky GA (2021) A Critical Review of Biosorption of Dyes, Heavy Metals and Metalloids from Wastewater as an Efficient and Green Process. Clean Eng Technol 4:100209. doi: 10.1016/j.clet.2021.100209

Ezeh K, Ogbu IC, Akpomie KG, Ojukwu NC, Ibe JC (2017) Utilizing the Sorption Capacity of Local Nigerian Sawdust for Attenuation of Heavy Metals from Solution: Isotherm, Kinetic, and Thermodynamic Investigations. Pac J Sci Technol 18(1).

Freundlich H (1907) Über Die Adsorption in Lösungen. *Zeitschrift Für Physikalische Chemie* 57U(1). doi: 10.1515/zpch-1907-5723.

Gupta VK, Alok M, Lisha K, Jyoti M (2006) Adsorption of a Hazardous Dye, Erythrosine, over Hen Feathers. J Colloid Interface Sci 304(1). doi: 10.1016/j.jcis.2006.08.032.

Hasnat MA, Uddin MM, Samed AJF, Alam SS, Hossain S (2007) Adsorption and Photocatalytic Decolorization of a Synthetic Dye Erythrosine on Anatase TiO2 and ZnO Surfaces. J Hazard Mater 147(1–2). doi: 10.1016/j.jhazmat.2007.01.040.

He F, Baozhong M, Chengyan W, Yongqiang C, Xiujuan H (2023) Adsorption of Pb(II) and Cd(II) Hydrates via Inexpensive Limonitic Laterite: Adsorption Characteristics and Mechanisms. Sep Purif Technol 310:123234. doi: 10.1016/J.SEPPUR.2023.123234.

Hevira L, Joshua OI, Dewi S (2024) Chitosan-Based Polysaccharides for Effective Synthetic Dye Adsorption. J Mol Liq 393.

Hisham F, Maziati Akmal MH, Farah Ahmad KA, Noorasikin S (2024) Biopolymer Chitosan: Potential Sources, Extraction Methods, and Emerging Applications. Ain Shams Eng 15(2).

Ho YS, McKay G (1999) Pseudo-Second Order Model for Sorption Processes. Process Biochem 34(5). doi: 10.1016/S0032-9592(98)00112-5.

Ho YSS, McKay G (1998) Sorption of Dye from Aqueous Solution by Peat. Chem Eng J 70(2):115–24. doi: https://doi.org/10.1016/S0923-0467(98)00076-1.

Ighnih H, Redouane H, Hassan O, Abdelmajid R, Brahim EI, Naima H, Amane J, Mohamed LT, Abdelaziz Ait A (2023) Efficient Removal of Hazardous Dye from Aqueous Solutions Using Magnetic Kaolinite Nanocomposite: Experimental and Monte Carlo Simulation Studies. Inorg Chem Commun 153. doi: 10.1016/j.inoche.2023.110886.

Issahaku I, Isaac KTe, Antonia YT (2023) Chitosan and Chitosan Derivatives: Recent Advancements in Production and Applications in Environmental Remediation. Environ Adv 11.

Kashi E, Surip SN, Tumirah K, Wan IN, Yannis DL, Zaher MY, Ali HJ (2024) High Adsorptive Performance of Chitosan-Microalgae-Carbon-Doped TiO2 (Kronos)/ Salicylaldehyde for Brilliant Green Dye Adsorption: Optimization and Mechanistic Approach. Int J Biol Macromol 259. doi: 10.1016/j.ijbiomac.2023.129147.

Kaur M, Monika D (2013) Adsorption Equilibrium and Kinetics of Toxic Dye-Erythrosine B Adsorption onto Montmorillonite. Sep Scı Technol 48(9). doi: 10.1080/01496395.2012.727939.

Kazemi J, Vahid J (2020) Alginate Beads Impregnated with Magnetic Chitosan@Zeolite Nanocomposite for Cationic Methylene Blue Dye Removal from Aqueous Solution. Int J Biol Macromol 154. doi: 10.1016/j.ijbiomac.2019.11.024.

Khan RI, Sarı A, Tuzen M, Lanjwani MF, Saleh TA (2023) Synthesis of Graphene/Silica Composites and Its Removal Efficiency of Methylene Blue Dye from Water. Inorg Chem Commun 158. doi: 10.1016/j.inoche.2023.111507.

Khapre MA, Sadanand P, Ravin MJ (2021) Glutaraldehyde-Cross-Linked Chitosan–Alginate Composite for Organic Dyes Removal from Aqueous Solutions. Int J Biol Macromol 190. doi: 10.1016/j.ijbiomac.2021.09.026.

Lai H, Gongke L, Zhuomin Z (2021) Ti3C2Tx-AgNPs@beta-Cyclodextrin SERS Substrate for Rapid and Selective Determination of Erythrosin B in Dyed Food. Sens Actuators B: Chem 346. doi: 10.1016/j.snb.2021.130595.

Langmuir I (1918) Adsorption of Gases on Glass, Mica and Platinum. J Am Chem Soc 40(1914):1361–1403.

Lima EC, Ahmad HB, Juan Carlos Moreno-Piraján, and Ioannis Anastopoulos. 2019. “A Critical Review of the Estimation of the Thermodynamic Parameters on Adsorption Equilibria. Wrong Use of Equilibrium Constant in the Van’t Hoof Equation for Calculation of Thermodynamic Parameters of Adsorption.” J Mol Liq 273. doi: 10.1016/j.molliq.2018.10.048.

Meng W, Hongnan S, Taihua M, Marco GV (2023) Pickering Emulsions with Chitosan and Macroalgal Polyphenols Stabilized by Layer-by-Layer Electrostatic Deposition. Carbohydr Polym 300:120256. doi: 10.1016/J.CARBPOL.2022.120256.

Mittal A, Jyoti M, Lisha K, Singh AK (2006) Process Development for the Removal and Recovery of Hazardous Dye Erythrosine from Wastewater by Waste Materials-Bottom Ash and De-Oiled Soya as Adsorbents. J Hazard Mater 138(1). doi: 10.1016/j.jhazmat.2006.05.038.

Nandanwar P, Ravin J, Vaishnavi G, Anita S, Apurva B, Dhandayutham S, Sadanand P (2023) Chitosan-Biopolymer-Entrapped Activated Charcoal for Adsorption of Reactive Orange Dye from Aqueous Phase and CO2 from Gaseous Phase. J Compos Sci 7(3). doi: 10.3390/jcs7030103.

Nannu S, Sripriya DRD, Dinesh KC, Gopikrishna M, Bhuvaneswari S, Udaya PNK (2023) Adsorption Kinetics, Equilibrium and Thermodynamics of a Textile Dye V5BN by a Natural Nanocomplex Material: Clinoptilolite. Energy Nexus 10. doi: 10.1016/j.nexus.2023.100197.

Nascimento RS, Corrêa JAM, Figueira BAM, Pinheiro PA, Silva JH, Freire PTC, Quaranta S (2022) From Mining Waste to Environmental Remediation: A Nanoadsorbent from Amazon Bauxite Tailings for the Removal of Erythrosine B Dye. Appl Clay Sci 222. doi: 10.1016/j.clay.2022.106482.

Pan X, Daoyong Z (2009) Removal of Malachite Green from Water by Firmiana Simplex Wood Fiber. Electron J Biotechnol 12(4). doi: 10.2225/vol12-issue4-fulltext-4.

Pipíška Ma, Eva KK, Milan H, Vladimír F, Libor Ď, Ivona Č, Mária K, Pellegrino C, and Gerhard S (2022) Biochar from Wood Chips and Corn Cobs for Adsorption of Thioflavin T and Erythrosine B. *Materials* 15(4). doi: 10.3390/ma15041492.

Raji Y, Ayoub N, Issam Me, Meriem S, Omar C, Souad Z (20239 High Adsorption Capacities of Crystal Violet Dye by Low-Cost Activated Carbon Prepared from Moroccan Moringa Oleifera Wastes: Characterization, Adsorption and Mechanism Study. Diam Relat Mater 135. doi: 10.1016/j.diamond.2023.109834.

Ramalakshmi RD, Murugan M, Jeyabal V (2022) Removal of Erythrosine B Using Prosopisspicigera L. Wood Carbon-Iron

Oxide Composite. Indian J Chem Technol 29(3). doi: 10.56042/ijct.v29i3.53865.

Rehan AI, Adiba IR, Awual ME, Waliullah RM, Mohammed SH, Khadiza TK, Md Shad S, Md Munjur H, Md Nazmul H, Md Chanmiya S, Hadi MM, Md Abdul K, Aminul I, Md Rabiul A (2023) Improving Toxic Dye Removal and Remediation Using Novel Nanocomposite Fibrous Adsorbent. Colloids Surf. A: Physicochem. Eng 673. doi: 10.1016/j.colsurfa.2023.131859.

Rytwo G, Huterer-Harari R, Dultz S, Gonen Y (2006) Adsorption of Fast Green and Erythrosin-B to Montmorillonite Modified with Crystal Violet. J Therm Anal Calorim 84(1). doi: 10.1007/s10973-005-7187-5.

Sabbagh N, Kambiz T, Amir AMS (2021) Application of Chitosan-Alginate Bio Composite for Adsorption of Malathion from Wastewater: Characterization and Response Surface Methodology. J Contam Hydro*l* 242. doi: 10.1016/j.jconhyd.2021.103868.

Sachan NK (2009) Sodium Alginate : The Wonder Polymer for Controlled Drug Delivery. J Pharm Res 2(7).

Sağlam S, Türk FN, Arslanoğlu H (2023) Use and Applications of Metal-Organic Frameworks (MOF) in Dye Adsorption: Review. J Environ Chem Eng 11(5).

Şen, Neşet Erek, and Zeynep Mine Şenol. 2023b. Effective Removal of Allura Red Food Dye from Water Using Cross-Linked Chitosan-Diatomite Composite Beads. Int J Biol Macromol 253:126632. doi: 10.1016/j.ijbiomac.2023.126632.

Şenol ZM (2021) A Chitosan-Based Composite for Adsorption of Uranyl Ions; Mechanism, Isothems, Kinetics and Thermodynamics. Int J Biol Macromol 183:1640–48. doi: 10.1016/j.ijbiomac.2021.05.130.

Şenol ZM, Elma E, El Messaoudi N, Mehmeti V (2023) Performance of Cross-Linked Chitosan-Zeolite Composite Adsorbent for Removal of Pb2+ Ions from Aqueous Solutions: Experimental and Monte Carlo Simulations Studies. J Mol Liq 391(July). doi: 10.1016/j.molliq.2023.123310.

Şenol ZM, Keskin ZS, Dinçer E, Ben Ayed Amina (2024) Influential Lead Uptake Using Dried and Inactivated-Fungal Biomass Obtained from Panaeolus Papilionaceus: Biological Activity, Equilibrium, and Mechanism. Biomass Convers Biorefin doi: 10.1007/s13399-024-05584-4.

Şenol ZM, El Messaoudi N, Fernine Y, Keskin ZS (2023) Bioremoval of Rhodamine B Dye from Aqueous Solution by Using Agricultural Solid Waste (Almond Shell): Experimental and DFT Modeling Studies. *Biomass Convers Biorefin* doi: 10.1007/s13399-023-03781-1.

Şenol ZM, Şimşek S (2020) Equilibrium, Kinetics and Thermodynamics of Pb(II) Ions from Aqueous Solution by Adsorption onto Chitosan-Dolomite Composite Beads. Int. J. Environ. Anal doi: 10.1080/03067319.2020.1790546.

Sharma P, Harleen K (2011) Sugarcane Bagasse for the Removal of Erythrosin B and Methylene Blue from Aqueous Waste. Appl Water Sci 1(3–4):135–45. doi: 10.1007/s13201-011-0018-x.

Tran ML, Tran TTV, Juang RS, Nguyen CH (2023) Graphene Oxide Crosslinked Chitosan Composites for Enhanced Adsorption of Cationic Dye from Aqueous Solutions. J Taiwan Inst Chem 142:104678. doi: 10.1016/j.jtice.2023.104678.

Umesh AS, Yashoda MP, Swathi T (2024) Enhanced Adsorption: Reviewing the Potential of Reinforcing Polymers and Hydrogels with Nanomaterials for Methylene Blue Dye Removal. J Surf Interfac Mater 51:104670. doi: 10.1016/j.surfin.2024.104670.

Wen Z, Ruihan P, Die G, Jing L, Jia Z, Zhou L, Famin K, Zhining X, Dandan W (2024) Chitosan-Alginate Sponge with Multiple Cross-Linking Networks for Adsorption of Anionic Dyes: Preparation, Property Evaluation, Mechanism Exploration, and Application. J Chromatogr A 1713. doi: 10.1016/j.chroma.2023.464507.

Wu FC, Ru LT, Ruey SJ (2009) Initial Behavior of Intraparticle Diffusion Model Used in the Description of Adsorption Kinetics. Chem Eng J 153(1–3). doi: 10.1016/j.cej.2009.04.042.

Zhang Z, Yu CH, Youyan L (2023) Efficient Antibacterial and Dye Adsorption by Novel Fish Scale Silver Biochar Composite Gel. Int J Biol Macromol 248. doi: 10.1016/j.ijbiomac.2023.125804.

RESEARCH ARTICLE
Bull Biotechnol (2025) 6(1):11-17
https://doi.org/10.51539/biotech.1629972
Journal homepage: www.dergipark.org.tr/biotech

Bulletin of Biotechnology

Inhibitory efficiency of various natural and synthetic antibacterial agents against bacteria isolated from a hospital environment

Serpil Ugras*, Beyza Nur Akbaba

*[1]*Department of Pharmaceutical Microbiology, Hamidiye Faculty of Pharmacy, University of Health Sciences, Istanbul, Türkiye*
[2]*Department of Chemistry, Duzce University, Institute of Science, 81620, Duzce, Türkiye*

*Corresponding author : serpilkus@gmail.com
Orcid No: 0000-0002-1867-5781

Received : 31/01/2025
Accepted : 20/02/2025

To Cite: Ugras S, Akbaba BN (2025) Inhibitory efficiency of various natural and synthetic antibacterial agents against bacteria isolated from a hospital environment. Bull Biotechnol 6(1):11-17 https://doi.org/10.51539/biotech.1629972

Abstract: Nosocomial infections pose significant challenges to healthcare systems worldwide. Despite frequent environmental cleaning and disinfection measures, the emergence of antibiotic and disinfectant-resistant bacterial pathogens continues to rise due to the misuse of antimicrobials. In this study, we aimed to identify bacteria isolated from the hospital environment, analyze their antibiotic resistance profiles, and assess their susceptibility to various antimicrobials (thymol (T), thyme oil (TO), zinc pyrithione (ZnPt), magnesium monoperoxyphthalate (MMPP)). Bacteria were isolated from the hospital environment and identified using the VITEK system. Antibiotic resistance profiles were determined using the disc diffusion technique, while the efficacy of different antimicrobials was assessed using the agar well diffusion technique. The isolates comprised 13.0% *Staphylococcus hominis*, 13.0% *Micrococcus* sp., 13.0% *Staphylococcus sciuri*, 27.0% *Staphylococcus haemolyticus*, 7.0% *Staphylococcus warneri*, 13.0% *Escherichia vulneris*, 7.0% *Sphingomonas paucimobilis*, and 7.0% *Kocuria kristinae*. It was observed that 10% of the isolates exhibited resistance to the tested antibiotics, while 74% were susceptible. Furthermore, the bacterial isolates demonstrated higher sensitivity to ZnPt compared to other substances, with the sensitivity ranking of alternative disinfectants as ZnPt>T>TO>MMPP. Our findings indicate that bacterial isolates showed a high sensitivity to ZnPt. Therefore, disinfectants containing ZnPt (0.1% concentration) could be effective in combating nosocomial infections.

Keywords: Antibiotic resistance; Bacteria; Disinfectant; Hospital, Nosocomial infection.

1 Introduction

Nosocomial infections have remained a significant challenge for healthcare systems throughout history. They not only prolong hospital stays but also contribute to the development of new infections (Kireçci et al. 2018). Numerous studies have highlighted that weakened immune systems and vulnerable patient populations, such as children, are particularly susceptible to nosocomial infections caused by opportunistic pathogenic microorganisms (Çavdar et al. 2022). Patient contact with contaminated environmental surfaces is a key factor in the transmission of hospital-acquired infections, with environmental surfaces estimated to play a role in 15-20% of such cases (Ekrami et al. 2011; Sserwadda et al. 2018). This is primarily because the hospital environment can serve as a reservoir for pathogenic organisms (Muhammad et al. 2013; Misgana et al. 2015). Consequently, regular microbiological monitoring of hospital equipment and the environment is crucial for detecting the presence of multidrug-resistant or virulent pathogens that could lead to nosocomial infections (Mulu et al. 2012; Messele et al. 2009).

Despite frequent environmental cleaning and disinfection efforts, mismanagement policies, such as the inappropriate use of antiseptics and disinfectants in hospitals, have been linked to increased rates of nosocomial infections (Kihla et al. 2014). Misuse of antiseptics and disinfectants can contribute to the development of bacterial resistance, including cross-resistance to antibiotics (Mendonça et al. 2000). The detection of pathogens like *Acinetobacter. baumannii* and methicillin-resistant *Staphylococcus aureus* (MRSA) on environmental surfaces following cleaning and disinfection underscores the importance of implementing effective cleaning practices to mitigate the risk of nosocomial infections. The proliferation of resistant pathogens in hospital environments not only leads to prolonged hospital stays but also contributes to higher morbidity and mortality rates, as well as imposing a significant economic burden (Kamat et al. 2008).

Effective disinfectant selection is a critical step in preventing nosocomial infections (Fagon et al. 1989). However, contemporary challenges include the emergence of bacterial resistance to commonly used disinfectants. Therefore, there is a growing need for disinfectants with high efficacy and diverse mechanisms of action. In this study, we aimed to investigate the identification of bacteria isolated from the hospital environment, their antibiotic resistance profiles, and their susceptibility to different antimicrobials (thymol, thymol mixture, thyme oil, zinc pyrithione, magnesium monoperoxyphthalate).

2 Materials and Method

2.1 Bacterial Isolation

A total of 35 samples were collected from various sites within a private hospital in Duzce using sterile swab sticks. Sampling sites included the x-ray cassette (RK), urine specimen collection cabinet (HR), laboratory bench (LT), microscope (M), effort (EF), blood collection stretcher (KS), operating room endoscopy device (E), audiometer headset (OK), electrocardiography device (EKG), centrifuge (S), and operating room autoclave (O). These samples were inoculated onto petri dishes containing nutrient agar (NA, Merck) and then incubated at 37°C for 24 hours. Following incubation, bacteria were isolated and purified based on their colony morphology.

2.2 Identification of Isolates

Gram properties of the bacterial isolates were initially determined using the Potassium Hydroxide Test (3% KOH) (Suslow et al. 1982). Subsequently, the isolates were identified using the VITEK 2 system (BioMérieux). The bacterial isolates were incubated in Tryptic Soy Agar (TSA) medium for 16-18 hours at 37°C, and cultures from these incubations were used for card inoculation.

2.3 Antibiotic Susceptibility of Isolates

The antibiotic susceptibility of the isolates was assessed using the agar disc diffusion method with seven different antibiotic discs: IMC (imipenem-cilastatin, 20 µg, Bioanalyse), E (erythromycin, 15µg, Oxoid), CIP (ciprofloxacin, 5µg, Oxoid), S (streptomycin, 10µg, Oxoid), CD (cefdinir, 30µg, Bioanalyse), AZM (azithromycin, 15µg, Oxoid), and TOB (tobramycin, 10µg, Oxoid) (Maragkoudakis et al. 2006; Turhan-Eryılmaz, 2011). Bacterial isolates were first incubated in nutrient broth (NB, Merck) for 18-24 hours. Following incubation, bacterial dilutions were prepared to achieve a concentration of 10^8 cells/ml, and 100 µl of these dilutions were spread onto NA-containing petri dishes. Antibiotic discs were then placed on these petri dishes, and the dishes were incubated at 37°C for 16-18 hours. Antibiotic susceptibility was determined based on the inhibition zones around the antibiotic discs, with results interpreted according to guidelines provided by the Clinical and Laboratory Standards Institute (CLSI).

2.4 Susceptibility Profile of Isolates to Some Antimicrobial Agents

Alternative disinfectants used in this study included T (1-10% (v/v) Thymol), TO (1-10% (v/v) Thyme Oil), ZnPt (0.1-10% (v/v) zinc pyrithione,), and MMPP (1-10% (v/v) Magnesium monoperoxyphthalate,). The solutions were prepared using distilled water. The antibacterial activities of these molecules against bacterial isolates were assessed using the agar well diffusion method (Aytar et al. 2019). Bacterial isolates were incubated in NB for 18-24 hours, and bacterial dilutions were prepared at a concentration of 10^8 cells/ml. Subsequently, 100 µl of the bacterial dilutions were spread onto petri dishes containing NA. Wells (6 mm) were then drilled under aseptic conditions on the petri dish, and 100 µl of the antimicrobial substances (alternative disinfectants) were added to the wells. The dishes were incubated at 37°C for 16-18 hours, after which the sensitivity of the isolates to the antimicrobial substances was determined based on the zones around the wells.

3 Results

3.1 Identification of Bacteria

The samples were collected from 35 different hospital environments, resulting in the culturing of 15 different bacterial isolates. Subsequently, the gram properties of these isolates were assessed, revealing 14 Gram-positive and 1 Gram-negative bacteria (Table 1). Using the VITEK identification system, the isolates were further characterized, yielding the following distribution: 13.0% *Staphylococcus hominis*, 13.0% *Micrococcus* sp., 13.0% *Staphylococcus sciuri*, 27.0% *Staphylococcus haemolyticus*, 7.0% *Staphylococcus warneri*, 13.0% *Esherichia vulneris*, 7.0% *Sphingomonas paucimobilis*, and 7.0% *Kocuria kristinae* (Figure 1 and Table 1).

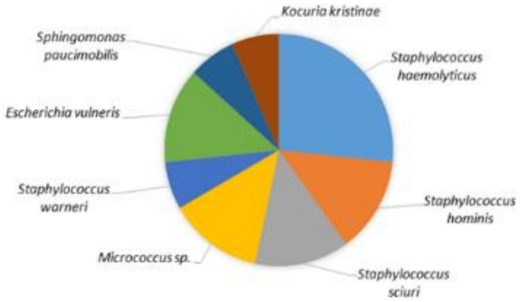

Fig. 1 Identification of isolates with VITEK.

Antibiotic susceptibility analysis of the bacterial isolates revealed high sensitivity to Imipenem and Ciprofloxacin antibiotics. However, *S. paucimobilis* (IK3) and *S. sciuri* (E1) exhibited resistance to approximately 43% of antibiotics. Specifically, E1 demonstrated resistance to Tobramycin, Azithromycin, and Cefdinir antibiotics, while IK3 displayed resistance to Tobramycin, Streptomycin, and Cefdinir antibiotics.

Table 1 VITEK identification results of bacterial isolates

Isolate Code	Source	Gram Properties	Colony Morphology	Bacterial Isolate
RK1	X-Ray Cassette	G (+)	Yellow	*Micrococcus* sp.
IK2	Urine Sample Collection Cabinet	G (+)	White	*Staphylococcus hominis*
LT1	Laboratory Bench	G (+)	White, Mucous	*Staphylococcus sciuri*
M2	Microscope	G (+)	White	*Staphylococcus haemolyticus*
EF2	Effort	G (+)	Yellow, Matte	*Staphylococcus haemolyticus*
KS5	Blood Collection Stretcher	G (+)	Orangey yellow	*Staphylococcus warneri*
IK1	Urine Sample Collection Cabinet	G (-)	Light yellow	*Escherichia vulneris*
IK3	Urine Sample Collection Cabinet	G (+)	White	*Sphingomonas paucimobilis*
E1	Operating Room Endoscopy Device	G (+)	White	*Staphylococcus sciuri*
E5	Operating Room Endoscopy Device	G (+)	White, Matte	*Staphylococcus haemolyticus*
OK1	Audiometer Headset	G (+)	White, Matte	*Staphylococcus hominis*
RK5	X-Ray Cassette	G (+)	Transparent	*Escherichia vulneris*
EKG2	Electrocardiography Device	G (+)	White	*Staphylococcus haemolyticus*
OK4	Audiometer Headset	G (+)	Light yellow	*Kocuria kristinae*
O2	Operating Room Autoclave	G (+)	Yellow	*Micrococcus* sp.

Table 2 Antibiotic susceptibility profiles of bacterial isolates

Isolate Code	Antibiotics / Zone of Inhibition (mm)						
	IMC20	**TOB10**	**AZM30**	**S25**	**E30**	**CD30**	**CIP30**
RK1	$>30^{a}$	17.25 ± 1.23^{b}	19.75 ± 1.26^{a}	20.50 ± 1.29^{a}	24.50 ± 0.58^{a}	10.75 ± 1.26^{c}	27.25 ± 0.50^{a}
IK2	$>30^{a}$	18.50 ± 0.50^{b}	27.25 ± 1.26^{a}	23.50 ± 2.08^{a}	$>30^{a}$	23.50 ± 1.29^{a}	$>30^{a}$
LT1	$>30^{a}$	14.75 ± 1.26^{b}	18.75 ± 0.96^{a}	20.25 ± 0.50^{a}	21.00 ± 0.82^{a}	12.00 ± 0.82^{c}	$>30^{a}$
M2	$>30^{a}$	18.75 ± 1.26^{b}	16.75 ± 0.96^{b}	20.50 ± 1.00^{a}	21.75 ± 1.26^{a}	22.00 ± 0.82^{a}	$>30^{a}$
EF2	$>30^{a}$	16.25 ± 1.26^{b}	20.50 ± 1.29^{a}	19.75 ± 0.50^{a}	24.50 ± 1.29^{a}	20.50 ± 1.29^{a}	22.75 ± 2.63^{a}
KS5	$>30^{a}$	17.25 ± 0.50^{b}	22.75 ± 1.71^{a}	20.00 ± 3.56^{a}	29.00 ± 0.82^{a}	25.50 ± 1.29^{a}	$>30^{a}$
IK1	21.75 ± 1.26^{a}	19.00 ± 0.82^{b}	21.75 ± 1.26^{a}	24.00 ± 0.82^{a}	15.25 ± 0.96^{b}	19.75 ± 0.26^{a}	$>30^{a}$
IK3	$>30^{a}$	11.50 ± 1.29^{c}	18.50 ± 0.58^{a}	10.00 ± 1.63^{c}	20.50 ± 0.29^{a}	13.00 ± 2.16^{c}	21.50 ± 0.58^{a}
E1	$>30^{a}$	11.00 ± 0.82^{c}	00.00 ± 0.00^{c}	20.25 ± 0.50^{a}	22.75 ± 0.50^{a}	00.00 ± 0.00^{c}	29.25 ± 1.26^{a}
E5	$>30^{a}$	18.75 ± 0.25^{b}	$>30^{a}$	22.50 ± 3.11^{a}	$>30^{a}$	$>30^{a}$	$>30^{a}$
OK1	$>30^{a}$	19.75 ± 1.26^{a}	25.75 ± 0.96^{a}	22.00 ± 1.41^{a}	$>30^{a}$	28.75 ± 0.96^{a}	$>30^{a}$
RK5	$>30^{a}$	17.25 ± 1.26^{b}	20.75 ± 1.26^{a}	20.75 ± 1.26^{a}	23.50 ± 1.00^{a}	10.50 ± 3.32^{c}	21.75 ± 0.96^{a}
EKG2	$>30^{a}$	12.50 ± 1.29^{c}	21.00 ± 2.16^{a}	17.75 ± 1.71^{b}	20.25 ± 0.50^{a}	14.50 ± 0.25^{b}	$>30^{a}$
OK4	$>30^{a}$	23.75 ± 0.50^{a}	$>30^{a}$	$>30^{a}$	25.50 ± 1.29^{a}	27.75 ± 1.71^{a}	$>30^{a}$
O2	$>30^{a}$	10.50 ± 1.29^{c}	16.50 ± 1.29^{b}	20.00 ± 0.82^{a}	19.75 ± 0.50^{b}	20.75 ± 0.36^{a}	21.75 ± 0.50^{a}

IMC20; imipenem-cilastatin (10-10 µg/disc), TOB10; tobramycin (10 µg/disc), AZM30; azithromycin (30 µg/disc), S25; streptomycin (25 µg/disc), E30; erythromycin (30 µg/disc), CD30; cefdinir (30 µg/disc), CIP30; ciprofloxacin, (30 µg/disc). Antibiotic susceptibility: a: Sensitive, b: Intermediate, c: Resistant.

Additionally, *Micrococcus* sp. (RK1), *S. sciuri* (LT1), and *E. vulneris* (RK5) were found to be resistant to Cefdinir. *S. haemolyticus* (EKG2) and *Micrococcus* sp. (O2) exhibited resistance to Tobramycin antibiotic, whereas *K. kristinae* (OK4) displayed overall sensitivity. Overall, 10.48% of the isolates were resistant to the tested antibiotics, 14.29% showed intermediate sensitivity, and 75.24% were susceptible (Table 2, Figures 2). Furthermore, the inhibition activities of T, TO, ZnPt, and MMPP were assessed using the well diffusion method against the bacterial isolates. The sensitivity of bacterial isolates was determined based on the inhibition diameters around the wells, with ZnPt demonstrating the highest sensitivity compared to other substances. The sensitivity ratios were ranked as follows: ZnPt > T > TO > MMPP (Table 3)

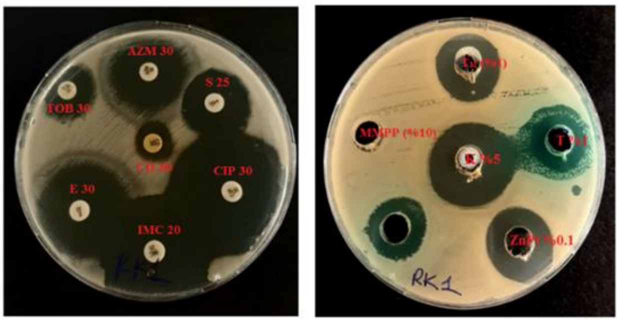

Fig. 2 Antibiotic and disinfectant susceptibility of the isolate *Micrococcus* sp.

Table 3 Susceptibility profiles of bacterial isolates against antimicrobials

Code	**Antimicrobial Agents / Zone of Inhibition (mm)**								
	(T)		**(TO)**			**(ZnPt)**		**(MMPP)**	
	1%	**10%**	**1%**	**5%**	**10%**	**0.1%**	**1-10%**	**1%**	**10%**
RK1	13.75±0.50	>30	-	25.50±1.29	>30	20.00±1.29	>30	-	-
IK2	09.00±1.29	>30	11.75±1.26	>30	>30	17.25±1.26	>30	-	08.50±1.00
LT1	-	10.50±0.50	-	-	10.25±1.25	15.25±1.26	>30	-	-
M2	16.25±0.50	>30	11.25±0.82	11.50±0.50	>30	20.25±0.50	>30	-	09.50±0.50
EF2	10.75±1.26	>30	-	19.50±1.00	>30	23.50±1.00	>30	-	13.25±1.29
KS5	12.50±1.25	>30	10.25±2.63	21.75±2.00	>30	20.00±0.80	>30	-	18.25±1.00
IK1	09.50±1.00	>30	10.50±1.25	11.00±1.26	>30	>30	>30	-	-
IK3	-	10.50±2.50	-	-	09.75±1.26	17.00±0.50	>30	-	-
E1	-	10.50±1.26	-	-	10.25±2.65	16.25±1.26	>30	-	-
E5	17.00±1.29	>30	08.25±1.63	>30	>30	18.00±0.50	>30	-	09.00±0.50
KS4	10.75±0.82	>30	>30	>30	>30	>30	>30	-	17.25±0.82
OK1	>30	20.75±1.26	18.75±1.00	25.00±1.29	>30	24.75±1.29	>30	-	10.00±1.00
RK5	12.50±1.26	>30	-	12.00±0.82	>30	16.50±0.82	>30	-	10.75±0.50
EKG2	>30	>30	07.25±1.00	30.25±1.26	>30	17.00±1.29	>30	-	-
S3	22.00±2.00	>30	12.75±0.50	27.75±1.29	>30	21.50±1.29	>30	-	-
OK4	>30	>30	-	18.00±0.50	>30	16.00±1.26	>30	-	-
O2	>30	>30	20.25±2.50	29.00±1.00	>30	21.25±0.50	>30	-	-

(T); Thymol, (TO); Thyme Oil, (ZnPt); Zinc Pyrithione, (MMPP); Magnesium monoperoxyphthalate. (-); no inhibition activity.

4 Discussion

Nosocomial infections pose a significant threat in developing countries, contributing substantially to morbidity and mortality rates (Orji et al. 2005). Environmental surfaces are estimated to be involved in 15-20% of these infections (Ekrami et al. 2011; Sserwadda et al. 2018). A study revealed that 65% of nurses' gowns carrying methicillin-resistant *Staphylococcus aureus* (MRSA) transmitted the bacteria during patient care activities (Orji et al. 2005; Boyce et al. 1997). Treating infections caused by antibiotic-resistant bacteria is incredibly challenging, with an estimated 33,000 deaths reported in Europe in 2015 due to resistant pathogens. The greatest impact on mortality is attributed to third-generation cephalosporin-resistant *Escherichia coli*, methicillin-resistant *S. aureus* (MRSA), third-generation cephalosporin-resistant *Klebsiella pneumoniae*, and carbapenem-resistant *Pseudomonas aeruginosa* (Cassini et al. 2019).

This study aimed to investigate the levels of antibiotic resistance among bacteria isolated from hospital environments. The findings revealed that 9% of the isolates developed resistance to the tested antibiotics, with 10% showing intermediate sensitivity and 81% being susceptible. While 9% resistance is concerning, it may exacerbate as resistance spreads to other bacteria over time. Hospital environments are regularly disinfected to mitigate the transmission risk of such pathogens. However, the development of bacterial resistance is exacerbated by mismanagement policies, such as the use of high-concentration and low-efficacy antiseptics and disinfectants in hospitals (Mendonça et al. 2000; Kihla et al. 2014; Kireçci et al. 2018; Sserwadda et al. 2018).

Despite routine cleaning efforts throughout the day, this study identified several bacterial species in the hospital environment, including *Micrococcus* sp., *Staphylococcus hominis*, *Staphylococcus sciuri*, *Staphylococcus haemolyticus*, *Staphylococcus warneri*, *Escherichia vulneris*, *Sphingomonas paucimobilis*, and *Kocuria kristinae*. These findings indicate that standard disinfection procedures may not be sufficient to eliminate all potentially harmful bacteria. Moreover, other studies have reported the isolation of various bacterial species from hospital environments. For example, in a study evaluating 288 Deep Tracheal Aspirate (DTA) samples, bacterial growth was detected in 140 samples, with *Acinetobacter* spp. accounting for 45%, *Pseudomonas aeruginosa* for 21.4%, *Klebsiella pneumoniae* for 16.4%, *Enterobacter* spp. for 6.4%, *Staphylococcus aureus* for 5%, *Escherichia coli* for 2.8%, and other species for 3%. Additionally, high rates of carbapenem resistance were observed, with rates of 87.3% for *Acinetobacter* spp., 65.2% for *K. pneumoniae* strains, and 40% for *P. aeruginosa* strains (Mizrakci 2022).

Considering these findings, the selection of appropriate disinfectants is crucial for preventing hospital infections (Fagon et al. 1989). Disinfectants with high efficacy and diverse mechanisms of action are required. Although many new disinfectants have been introduced in recent years, the lack of appropriate disinfection policies in hospitals may lead to their misuse, compromising the provision of quality and safe healthcare services. Therefore, it is essential to understand the properties of disinfectants, including their usage areas and potential toxic effects (Coates and Hutchinson, 1994). Ideally, selected disinfectants should be broad-spectrum, fragrant or odorless, non-irritating to the skin, unaffected by organic substances, possess cleaning properties, and maintain their activity when applied with detergent (Fraise, 2004; Suljagic, 2008). Commonly used disinfectants in hospitals include alcohol, aldehydes, halogen-based disinfectants, peroxides and peracids, phenol compounds, and quaternary ammonium compounds (Sehulster and Chin, 2003).

Eryılmaz et al. conducted a study isolating nosocomial infection factors, including thirty different strains of *S. aureus* (sixteen of which were methicillin-resistant (MRSA) and fourteen methicillin-susceptible (MSSA)), and twentyone different *Enterococcus* spp. (thirteen isolates of *E. faecalis*, seven isolates of *Enterococcus faecium*, and one untypeable isolate of *Enterococcus* spp.). All these isolates demonstrated sensitivity to 2% glutaraldehyde, 4% chlorhexidine gluconate, 7.5% povidone-iodine, 10% povidoneiodine, and 70% 2-propanol at varying contact times. However, it was noted that most of these isolates exhibited resistance to 3% hydrogen peroxide. Consequently, the study concluded that 2% glutaraldehyde, 4% chlorhexidine gluconate, 7.5% povidone iodine, 10% povidone-iodine, and 70% 2-propanol could be safely used for disinfection in İbn-i Sina Hospital against *S. aureus* and *Enterococcus* spp. strains. Nevertheless, it was suggested that hydrogen peroxide should not be preferred due to the presence of 3% resistance among isolates (Satar and Springthorpe 2008).

In this study, the inhibitory effects of four different antimicrobial agents thymol (T), thyme oil (TO), zinc pyrithione (ZnPt), and magnesium monoperoxyphthalate (MMPP) which are regarded as alternative disinfectants, were evaluated against bacteria isolated from a hospital setting. The results revealed that bacterial isolates exhibited varying degrees of sensitivity to these substances, with susceptibility ratios listed as ZnPt>T>TO>MMPP. ZnPt demonstrated particularly strong inhibitory activity against the tested isolates.

Thymol (T), utilized in this study, is a white crystalline solid natural monoterpene phenol renowned for its antimicrobial, anti-inflammatory, antitumor, and fungicidal effects (Eryılmaz 2011; Zhu 2016). It serves as the primary component of thyme (*Thymus vulgaris*) essential oil, a staple ingredient in the food industry and cosmetics due to its antioxidant and preservative properties (Milovanovic 2013). Thymol is present in various species such as *T. vulgaris*, *Ocimum gratissimum*, *Thymus ciliates*, and others, each containing thymol and offering diverse biological benefits, including antioxidant, antibacterial, antifungal, and antiparasitic activities (Salehi et al. 2018). Thymol functions as an antiseptic and disinfectant by enhancing the permeability of bacterial and fungal cytoplasmic membranes, thereby exerting bactericidal and fungicidal effects (Nagoor et al. 2017). In this study, thymol demonstrated potent bactericidal properties.

Thyme oil (TO), another substance employed in this research, possesses numerous pharmacological properties, including antioxidant, antimicrobial, antitumor, antidiabetic, and antihypertensive effects (Benkaci-Ali et al, 2007; Najafloo et al, 2020). Most of these attributes are attributed to compounds like thymoquinone, carvone, p-cimene, and notably thymol and carvacrol (Ali and Blunden, 2003; Ündeğer et al. 2009). Thyme oil's incorporation into products helps retard oxidation processes and extend product shelf life due to its antimicrobial activity. In the study, thyme oil exhibited robust antibacterial activity against bacterial isolates, albeit slightly less potent than thymol for some bacteria. This variance may be attributed to the diverse molecules present in thyme oil. Additionally, thyme oil displayed higher antimicrobial efficacy than thymol against certain bacteria, such as IK2 and KS4 strains, possibly due to the synergistic effects of other compounds present in thyme oil.

Zinc pyrithione (ZnPT), identified as another candidate for use as an alternative disinfectant in this study, is an organic metal compound renowned for its broad-spectrum antimicrobial properties, effectively inhibiting the growth of bacteria, fungi, algae, and molds. Its antimicrobial efficacy has been harnessed across various industries, with decades of use as a fungicide, particularly in anti-dandruff shampoos (Windler et al. 2013). This study determined ZnPT to possess the strongest antibacterial activity among the tested molecules, suggesting its potential as a potent disinfectant additive.

Magnesium monoperoxyphthalate (MMPP) is a water-soluble peroxy acid employed as an oxidant in organic synthesis. Its primary applications include the conversion of ketones to esters, epoxidation of alkenes, and oxidation of sulfides to sulfoxides and sulfones, among others (Carvalho et al. 2009). MMPP also serves as an active ingredient in certain surface disinfectants, showcasing a broad-spectrum biocidal action, including the inactivation of endospores (Baldry 1984). Its compatibility with a wide range of surfaces enables its use on sensitive materials such as plastic and rubber equipment in hospitals. Furthermore, MMPP has been explored as a potential antibacterial agent for mouthwashes and toothpastes (Scully et al. 1999). However, in this study, MMPP exhibited the lowest inhibitory activity compared to other antimicrobials tested.

5 Conclusion

Despite regular disinfection efforts in hospitals, this study underscores the persistent presence of bacteria in the hospital environment. Moreover, these bacteria have demonstrated the capacity to develop resistance against both antibiotics and traditional disinfectants. Given this challenge, there is a pressing need for novel antimicrobial agents to effectively combat these resilient pathogens.

The findings of this study highlight the remarkable sensitivity of bacterial isolates to low concentrations of Zinc pyrithione (ZnPt). This suggests the potential efficacy of ZnPt (at 0.1% concentration) as an additive in disinfectants aimed at combating nosocomial infections. Implementing ZnPt-based disinfectants could represent a promising strategy in enhancing the effectiveness of hospital sanitation protocols and reducing the risk of healthcare-associated infections.

Acknowledgements

The current study was not supported by any project.

Authors' contributions: SU: Design, data analysis, manuscript writing, BNA:laboratory experiments.

Conflict of interest disclosure:

The author declares no conflict of interest.

References

Ali BH, Blunden G (2003) Pharmacological and toxicological properties of Nigella sativa. Phytother Res 17(4):299-305.

Aytar M, Oryaşın E, Başbülbül G, Bozdoğan B (2019). Standardization study for agar well diffusion. JONAS 2(2): 138-145.

Baldry MGC (1984) The antimicrobial properties of magnesium monoperoxyphthalate hexahydrate. J Appl Bacteriol 57(3):499-503.

Benkaci-Ali F, Baaliouamer A, Meklati BY, Chemat F (2007) Chemical composition of seed essential oils from algerian nigella sativa extracted by microwave and hydrodistillation. Flavour Fragr J 22(2):148-153.

Boyce JM, Pott-Bynoe G, Cheneevert C, King T (1997) Environmental contamination due to methicillin resistant Staphylococcus aureus: possible infection control implications. Infect Control Hosp Epidemiol 18:622.

Carvalho J, Silva M, Sá E Melo M (2009). Highly efficient epoxidation of unsaturated steroids using magnesium bis(monoperoxyphthalate) hexahydrate. Tetrahedron 65(14):2773-81.

Cassini A, Högberg LD, Plachouras D, Quattrocchi A, Hoxha A, Simonsen GS, et al. (2019). Attributable deaths and disability-adjusted life-years caused by infections with antibiotic-resistant bacteria in the eu and the european economic area in 2015: a population-level modelling analysis. Lancet Infect Dis 19(1):56-66.

Coates D, Hutchinson DN (1994). How to produce a hospital disinfection policy. J Hosp Infect 26(1):57-68.

Çavdar G, Köroğlu M, Ölmez M, Şahin E, Altındiş M (2022) Microbiological analysis of hospital drinking and usage water; Sakarya. Online Turkish Journal of Health Sciences 7(3):346-355.

Ekrami A, Kayedani A, Jahangir M, Kalantar E, Jalali M (2011) Isolation of common aerobic bacterial pathogens from the environment of seven hospitals, ahvaz, iran. Jundishapur J Microbiol 4(2):75-82.

Eryılmaz M, Akın A, Arıkan Akan O (2011) Investigation of the efficacy of some disinfectants against nosocomial Staphylococcus aureus and Enterococcus spp. isolates. Find Microbiome 45(3):454-60.

Fagon JY, Chastre J, Domart Y, Trouillet L, Pierre J, Darne C, et al. (1989) Nosocomial pneumonia in patients receiving continuous mechanical ventilation. Prospective analysis of 52 episodes with use of a protected specimen brush and quantitative culture Techniques Am Rev Respir Dis 139(4):877-84.

Fraise AP (2004) Decontamination of the environment and medical equipment in hospitals, "Fraise AP, Lambert PA, Maillard JY (eds): "Russell, Hugo, Ayliffe's Principles and Practice of Disinfection, Preservation and Sterilization. Blackwell Publishing, Hoboken NJ . pp.563-85.

Kamat US, Ferreira AMA, Savio R, Motghare DD (2008) Antimicrobial resistance among nosocomial isolates in a teaching hospital in goa. Indian J Community Med 33(2):89-92.

Kihla AJ, Ngunde PJ, Mbianda SE, Gerard N, Ndip RN (2014) Risk factors for wound infection in health care facilities in buea, cameroon: aerobic bacterial pathogens and antibiogram of isolates. Pan African Medical Journal 18(1):6.

Kireçci M, Arslan E, Kirişci Ö, Karaman Ş (2018) Investigation of the potential resistance of the bacteria ısolated from the hospital environment to some disinfectants and antiseptcs. Flora 23(4):179-185.

Maragkoudakis PA, Zoumpopoulou G, Miaris C, Kalantzopoulos G, Pot B, Tsakalidou E (2006) Probiotic potential of lactobacillus strains isolated from dairy products. Int Dairy J 16(3):189-199.

Mendonça S, Ecclissato C, Sartori MS, Godoy AP, Guerzoni RA, Degger M, et al. (2000) Prevalence of helicobacter pylori resistance to metronidazole, clarithromycin, amoxicillin, tetracycline, and furazolidone in brazil. Helicobacter 5(2):79-83.

Messele G, Woldemedhin Y, Demissie M, Mamo K, Geyid A (2009) Common causes of nosocomial infections and their susceptibility patterns in two hospitals in addis ababa. Ethiop J Health Biomed Sci 2(1):3–8.

Milovanovic S, Stamenic M, Markovic D, Radetic M, Zizovic I (2013) Solubility of thymol in supercritical carbon dioxide and its impregnation on cotton gauze. J Supercrit Fluids 84:173-181.

Misgana GM, Abdissa K, Abebe G (2015) Bacterial contamination of mobile phones of health care workers at jimma university specialized hospital, jimma, southwest ethiopia. International Journal of Infection Control 11(1):1-8.

Mizrakci S (2022). Global overview of publications on rotavirus. BSJ Health Sci. 5(2):239-244.

Muhammad UK, Isa MA, Aliyu ZM (2013) Distribution of potential nosocomial pathogens isolated from environments of four selected hospital in Sokoto, Northwestern Nigeria. J Microbiol Biotechnol Res 3(1):139–43.

Mulu W, Kibru G, Beyene G, Damtie M (2012) Postoperative nosocomial infections and antimicrobial resistance pattern of bacteria isolates among patients admitted at felege hiwot referral hospital, bahirdar, Ethiopia. Ethiop J Health Sci 22(1):7–18.

Nagoor MMF, Javed H, Al Taee H, Azimullah S, Ojha SK (2017) Pharmacological properties and molecular mechanisms of thymol: prospects for its therapeutic potential and pharmaceutical development. Front Pharmacol 8:380.

Najafloo R, Behyari M, Imani R, Nour S (2020) A mini-review of thymol incorporated materials: applications in antibacterial wound dressing. J Drug Deliv Sci Technol 60:101904.

Orji MU, Mbata TI, Kalu OU (2005) Isolation of pathogenic bacteria from hospital staff appareli in Nigeria. Malawi Med J 17(4):128-130.

Salehi B, Mishra AP, Shukla I, Sharifi-Rad M, Contreras MDM, Segura-Carretero A, et al. (2018) Thymol, thyme, and other plant sources: health and potential uses. Phytother Res 32(9):1688-1706.

Sserwadda I, Lukenge M, Mwambi B, Mboowa G, Walusimbi A, Seguija F (2018) Microbial Contaminants Isolated From İtems And Work Surfaces in The Post-Operative Ward at Kawolo General Hospital, Uganda. BMC Infect Dis 68.

Satar SA, Springthorpe S (2008) The need for safer and better microbicides for infection control. In book: Disinfection and Decontamination. Principles, Applications and Related Issues Edition: First Publisher: CRC Press Editors: Gurusamy Manivannan. pp.41-58.

Scully C, El-Kabir M, Greenman J, Porter SR, Mutlu S, Barton I, et al. (1999) The effects of mouth rinses and dentifrice-containing magnesium monoperoxyphthalate (MMPP) on oral microflora, plaque reduction, and mucosa. J Clin Periodontol 26(4):234–238.

Sehulster L, Chinn R (2003) Centers for diseases control and prevention: guidelines for environmental infection control in health care fascilities. Recommendations of Cdc and The Healthcare Infection Control Practices Advisory Committee (Hicpac). 52(10):1-42.

Suljagic V (2008) A pragmatic approach to judicious selection and proper use of disinfectant and antiseptic agents in healthcare settings. In book: Disinfection and Decontamination. Principles, Applications and Related Issues Edition: FirstPublisher: CRC PressEditors: Gurusamy Manivannan. pp.124-154.

Suslow TV, Schroth MN, Isaka M (1982). Application of a rapid method for gram differentiation of plant pathogenic and saprophytic bacteria without staining. Phytopathol 72:917-918.

Turhan-Eryılmaz F (2011) Identification of potential probiotic properties of some lactic acid bacterial genera which is isolated from vaginal secretion. Ankara.

Ündeğer Ü, Başaran A, Degen GH, Başaran N (2009) Antioxidant activities of major thyme ingredients and lack of (oxidative) dna damage in v79 chinese hamster lung fibroblast cells at low levels of carvacrol and thymol. Food Chem Toxicol 47(8):2037-2043.

Windler L, Height M, Nowack B (2013) Comparative evaluation of antimicrobials for textile applications. Environ Int 53:62-73.

Zhu X, Pan H, Yang Z, Cui B, Zhang D, Ba-Thein W (2016) Self-medication practices with antibiotics among chinese university students. Public Health 130:78-83.

RESEARCH ARTICLE
Bull Biotechnol (2025) 6(1):18-24
https://doi.org/10.51539/biotech.1673256 Journal homepage: www.dergipark.org.tr/biotech

Bulletin of Biotechnology

Determination of molybdenum content of soils in Arsuz region of Hatay Province and relationships with some heavy metals in soil

Mehmet Yalçın *
Hatay Mustafa Kemal University, Faculty of Agriculture, Soil Science and Plant Nutrition, Hatay, Türkiye.

*Corresponding author : myalcin@mku.edu.tr
Orcid No: https://orcid.org/0000-0002-1690-7681

Received : 10/04/2025
Accepted : 16/06/2025

To Cite: Yalçın M (2025) Determination of molybdenum content of soils in Arsuz region of Hatay Province and relationships with some heavy metals in soil. Bull Biotechnol 6(1):18-24 https://doi.org/10.51539biotech.1673256

Abstract: In this study, it was aimed to determine the molybdenum content of the soils of Arsuz region of Hatay province and to determine their relationship with some heavy metals in the soil. For this purpose, a total of 70 soil samples were taken from 0-30 cm depth and 70 points to represent the soils of Arsuz district. According to the results of the research; Cd content of the soils was found between 0.01-0.03 µg/kg; Co content between 0.02-2.96 µg/kg; Cr content between 0.01-0.85 µg/kg; Ni content between 0.35-17.60 mg/kg; Fe content between 1.65-18.72 mg/kg and Mo content between 0.01-0.18 µg/kg. Positive significant relationships were determined between Mo and Cd, Co and Fe contents of soils. At the same time, positive significant relationships were determined between Cd and Co, Ni, Fe and Co and Ni and Fe. When the heavy metal contents of the soils of the region were compared with the limit values, no heavy metal pollution was found.

Keywords: molybdenum content; Arsuz district; heavy metals

1 Introduction

Soil is an active and essential natural part of the lithosphere, which includes many different types of organisms from very small organisms to very large trees. Soil is also a living entity that contains macro and micronutrients, which are an important source of nutrients for biological activity to take place, and helps to maintain the continuity of many different biodiversity and habitats (Küçük and Karaoğlu 2021). In general, metals with a specific gravity above 5 g cm^{-3} and an atomic mass above 20 are more commonly referred to as heavy metals. Both high and low concentrations of heavy metals in soils are toxic to soil organisms. At the same time, very low concentrations of some heavy metals (Fe, Cu, Zn, Mo and Ni) are necessary for plants in the soil. Some of them (Cd, Pb, Hg, As, etc.) show toxic effects on plants because they do not have a known physiological function in plants in the soil. However, heavy metals in nature pose a very important threat to human, animal and plant health at high concentrations. The development of industry and anthropogenic effects are the most important factors in the increase of heavy metal-induced environmental pollution (Yurdakul et al. 2023). Heavy metal pollution in soils in nature can be caused by human-induced practices such as the combustion of fossil fuels, thermal power plants, the use of waste or polluted water, fertilisers and pesticides in agricultural soils, mining wastes and landfill filtration, as well as the natural weathering process of minerals, erosion, forest fires and volcanic activities (Özyiğit 2021). Among sustainable agricultural inputs, one of the most important sources of pollution, especially in agricultural lands, is heavy metal pollution. The most important factors in the formation of heavy metal pollution are the uncontrolled application of urban wastes and sewage sludge to lands, the use of solid and liquid wastes from industry in agricultural environments, and the improper use of pesticides and fertilizers (Saltalı et al. 2018). In sustainable agricultural activities, plant products grown in soils contaminated with heavy metals negatively affect all life systems when they are added to the food chain. For this reason, heavy metal pollution in soil, which occurs naturally or artificially, is one of the very important issues that need to be controlled and monitored, especially in agricultural areas (Dedeoğlu and Başyiğit 2018). Depending on their amounts in the soil, heavy metals can potentially determine toxicity for plants in the soil and those who consume them. In general, toxic metals accumulate in the upper layer of the soil and enter the food chain through plants. With their entry into the food chain, bioaccumulation events occur and pose a significant risk to all living species (Çolak et al. 2021). In addition to the effect of heavy metal contents in the soil ecosystem, heavy metals in soils can cause acute or chronic diseases as a result of consumption in humans through the food chain. Due to these known damages, it is not desirable to have heavy metal concentrations above critical levels in soils. Along with the aforementioned effects the removal of heavy metal pollution in the soil from the environment is one of the most important issues for the continuation of biological vitality in the soil, the protection of soil health and quality, and the continuation of agricultural sustainability (Taciroğlu et al. 2016). Heavy metals as pollution factors pose a danger and risk to all living organisms and human life worldwide. They cause various diseases, especially cancer, in humans depending on factors such as exposure dose, genetics, immune resistance and general health status, age, nutritional level. Urgent measures should be taken to minimise soil pollution caused by heavy metals, which are a problem in the world and in our country. Plant products grown unhealthily in soils contaminated with heavy metals directly affect human and animal life negatively (Seven et al. 2018).Many studies on heavy metals have been carried out in our country. In a study carried out in the same region, Yalçın (2024) aimed to determine the molybdenum content of the soils of Kırıkhan-Kumlu region and to determine their relationship with some heavy metals in the soil. As a result of the study; Cd content of soils was found between 0.01-0.06 μg kg^{-1}; Co content between 0.02-0.22 μg kg^{-1}; Cr content between 0.03-0.77 μg kg^{-1}; Ni content between 0.70-6.56 mg kg^{-1}; Fe content between 4.04-13.09 mg kg^{-1} and Mo content between 0.01-0.23 μg kg^{-1}. Negative significant relationships were determined between Mo and Cr contents of soils. At the same time, positive significant relationships were determined between Cd and Ni, Co and Cr and Ni and Ni and Fe. When the heavy metal contents of the soils of the region were compared with the limit values, no heavy metal pollution was found. Yalçın (2023) aimed to determine the molybdenum content of agricultural soils in the Kırıkhan-Reyhanlı region and its relation with some heavy metals. According to the results of the study, Cd content of soils varied between 0.009-0.041 μg kg^{-1}, Co content between 0.011-0.317 μg kg^{-1}, Cr content between 0.008-0.187 μg kg^{-1}, Ni content between 0.787-6.211 mg kg^{-1}, Cu content between 1.11-3.77 mg kg^{-1}, Fe content between 2.80-15.09 mg kg^{-1} and Mo content between 0.006-0.101 μg kg^{-1}. Positive significant relationships were determined between Mo and Co and Ni contents of soils, but negative significant relationships were determined with Cr content. In addition, positive significant relationships were found between Cd and Co and Ni, between Co and Ni and Cu, and between Cu and Fe. When the heavy metal contents of the soils in the region were compared with the limit values, no heavy metal pollution was found. The study aimed to determine the relationships between the molybdenum level of soils in the Arsuz region of Hatay province and some heavy metals in these soils and to contribute this information to the productivity and quality of agricultural soils.

2 Materials and Method

2.1. Materials

In this study, surface soil samples (0-30 cm) were duly taken from 70 different locations in parsley cultivated agricultural fields in Arsuz district of Hatay province (Figure 1; Table 1). The soil samples were brought to the laboratory on the same day, air-dried in the shade and sieved through a 2 mm sieve to prepare them for analysis. The pH of the soils of the study area was determined as 8.07 in the range of 7.65-8.42 and the pH of the soil samples was slightly alkaline throughout the study area. While the lowest % salt content of Arsuz district soils was 0.013, the highest % salt content was 0.033. The average % salt content of the study area was 0.020. The lowest clay, sand and silt contents of the soils of Arsuz district of Hatay province were 18.88 %, 3.68 % and 18.00 %, respectively, while the highest clay, sand and silt contents were 60.32 %, 51.12 % and 64.00 %, respectively. The average clay, sand and silt contents of the 0-30 cm depth samples of the soils were found as 43.16 %, 19.09 % and 37.84 %, respectively. The lime contents of the soils of the research area were found to be between 0.62-28.04 %, with an average of 14.69 %, and they were commonly determined as medium to very calcareous soils. While the lowest organic matter content of Arsuz district soils was 1.68 %, the highest organic matter content was 4.09 %. The average organic matter content of the samples of the soils at 0-30 cm depth was found to be 2.50 % and commonly low to high organic matter (Yalçın and Çimrin 2021).

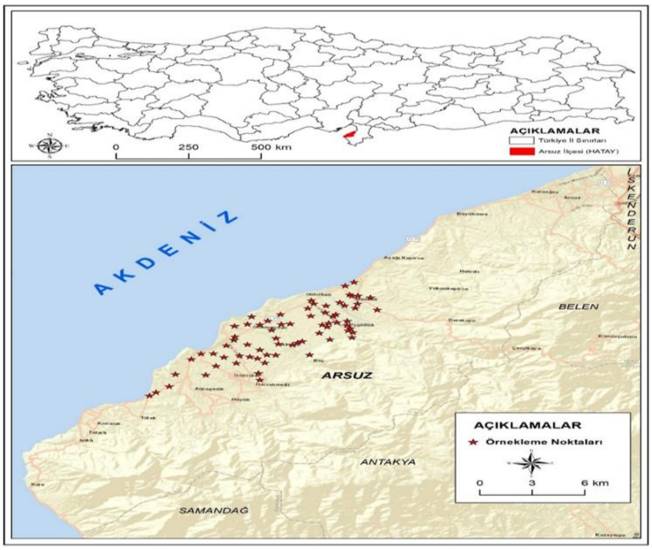

Figure 1. Representation of the soil samples on the map

2.2. Method

Soils were analysed for cadmium (Cd), cobalt (Co), chromium (Cr), nickel (Ni), copper (Cu), iron (Fe) and molybdenum (Mo) according to Lindsay and Norvell (1978) in 0.005 M DTPA+0.01 M $CaCl_2$+0.1 M TEA (pH 7.3). Correlation and regression analyses between soil properties and nutrients were performed using SPSS 17 statistical software (Düzgüneş et al. 1987).

Table 1. Locations where soil samples were taken

Soil Number	Sample Place	N/E Coordinates with GPS	Soil Number	Sample Place	N/E Coordinates with GPS
1	Madenli 1	(36.4718 - 35.9798)	36	Akçalı 8	(36.4113 - 35.9595)
2	Madenli 2	(36.4751 - 35.9852)	37	Akçalı 9	(36.4202 - 35.9392)
3	Madenli 3	(36.4641 - 35.9828)	38	Akçalı 10	(36.4251 - 35.9376)
4	Madenli 4	(36.4515 - 36.0009)	39	Akçalı 11	(36.4374 - 35.9404)
5	Madenli 5	(36.4620 - 35.9962)	40	Akçalı 12	(36.4459 - 35.9396)
6	Madenli 6	(36.4564 - 35.9883)	41	Akçalı 13	(36.4401 - 35.9318)
7	Madenli 7	(36.4631 - 35.9845)	42	Akçalı 14	(36.4258 - 35.9113)
8	Madenli 8	(36.4633 - 35.9881)	43	Akçalı 15	(36.4230 - 35.9109)
9	Madenli 9	(36.4547 - 35.9801)	44	Akçalı 16	(36.4192 - 35.9197)
10	Madenli 10	(36.4573 - 35.9770)	45	Akçalı 17	(36.4149 - 35.9276)
11	Üçgüllük 1	(36.4543 - 35.9683)	46	Akçalı 18	(36.4073 - 35.9264)
12	Üçgüllük 2	(36.4468 - 35.9747)	47	Akçalı 19	(36.4107 - 35.9323)
13	Üçgüllük 3	(36.4451 - 35.9731)	48	Akçalı 20	(36,4105 - 35,9379)
14	Üçgüllük 4	(36.4399 - 35.9758)	49	Gökmeydan 1	(36,4322 - 35,9345)
15	Üçgüllük 5	(36.4391 - 35.9705)	50	Gökmeydan 2	(36,4367 - 35,9268)
16	Üçgüllük 6	(36.4375 - 35.9664)	51	Gökmeydan 3	(36,4369 - 35,9189)
17	Üçgüllük 7	(36.4360 - 35.9697)	52	Gökmeydan 4	(36,4435 - 35,9214)
18	Üçgüllük 8	(36.4349 - 35.9844)	53	Gökmeydan 5	(36,4350 - 35,9107)
19	Üçgüllük 9	(36.4413 - 35.9822)	54	Çetellik 1	(36,4037 - 35,9313)
20	Üçgüllük 10	(36.4377 - 35.9822)	55	Çetellik 2	(36,3945 - 35,9276)
21	Üçgüllük 11	(36.4451 - 35.9567)	56	Çetellik 3	(36,3887 - 35,9287)
22	Üçgüllük 12	(36.4559 - 35.9588)	57	Çetellik 4	(36,4029 - 35,9132)
23	Üçgüllük 13	(36.4559 - 35.9603)	58	Çetellik 5	(36,4078 - 35,9051)
24	Üçgüllük 14	(36.4484 - 35.9679)	59	Çetellik 6	(36.4108 - 35.8982)
25	Üçgüllük 15	(36.4330 - 35.9831)	60	Çetellik 7	(36.4104 - 35.8905)
26	Üçgüllük 16	(36.4527 - 35.9868)	61	Çetellik 8	(36.4056 - 35.8844)
27	Üçgüllük 17	(36.4316 - 35.9861)	62	Çetellik 9	(36.3921 - 35.8941)
28	Üçgüllük 18	(36.4270 - 35.9859)	63	Çetellik 10	(36.3922 - 35.8749)
29	Akçalı 1	(36.4586 - 35.9587)	64	Çetellik 11	(36.3816 - 35.8713)
30	Akçalı 2	(36.4379 - 35.9461)	65	Çetellik 12	(36.3762 - 35.8631)
31	Akçalı 3	(36.4215 - 35.9513)	66	Çetellik 13	(36.3732 - 35.8592)
32	Akçalı 4	(36.4197 - 35.9482)	67	Çetellik 14	(36.4180 - 35.9062)
33	Akçalı 5	(36.4229 - 35.9544)	68	Çetellik 15	(36.4095 - 35.9149)
34	Akçalı 6	(36.4304 - 35.9658)	69	Çetellik 16	(36.4087 - 35.9216)
35	Akçalı 7	(36.4249 - 35.9719)	70	Çetellik 17	(36.4002 - 35.9004)

3. Findings and discussion

3.1. Some Heavy Metal Content of Soil Samples

The results of some heavy metal properties of the soil properties used in the study are given in Table 3.

Cadmium

The lowest cadmium content of the research soils was 0.01 µg kg^{-1} and the highest cadmium content was 0.03 µg kg^{-1}. The average Cd content of the soils was 0.01 µg kg^{-1} (Table 2.). Özkan and Demir (2023), who studied the heavy metal contents tea soils of Rize province, reported that the Cd content of the soils of the study area was much lower than the known limit values and presented similar results.

Cobalt

The lowest cobalt content of the Arsuz region soils was 0.02 µg kg^{-1} and the highest was 2.96 µg kg^{-1}. The average Co content of the soils was 0.49 µg kg^{-1} (Table 2.). Özkan and Demir (2023) reported similar results by determining the Co contents of the soils between 0-0.09 µg kg^{-1} in their study in which they aimed to determine the heavy metal contents of the soils cultivated in Rize province.

Table 2. Cd, Co, Cr, Ni, Fe, Mo contents of soils of Arsuz region of Hatay province

Soil Number	Depth	Cd µg kg^{-1}	Co µg kg^{-1}	Cr µg kg^{-1}	Ni mg kg^{-1}	Fe mg kg^{-1}	Mo µg kg^{-1}	Texture Class
1	0-30	0.01	0.03	0.04	0.82	4.30	0.01	C
2	0-30	0.01	0.03	0.04	0.60	2.96	0.02	SiC
3	0-30	0.01	0.04	0.06	0.57	4.00	0.01	SiC
4	0-30	0.01	0.04	0.79	1.44	3.68	0.02	C
5	0-30	0.01	0.04	0.07	1.42	1.65	0.01	CL
6	0-30	0.01	0.04	0.08	0.58	2.85	0.02	SiC
7	0-30	0.01	0.04	0.21	0.55	3.63	0.01	SiC
8	0-30	0.01	0.04	0.17	1.17	2.73	0.01	C
9	0-30	0.01	0.03	0.12	0.57	3.06	0.00	SC
10	0-30	0.01	0.03	0.17	0.95	2.50	0.01	C
11	0-30	0.01	0.02	0.08	1.80	3.25	0.01	L
12	0-30	0.01	0.05	0.52	0.98	4.15	0.01	SiCL
13	0-30	0.02	0.02	0.12	0.56	5.28	0.01	C
14	0-30	0.02	0.02	0.06	0.74	4.84	0.02	SiC
15	0-30	0.01	0.04	0.07	0.84	6.01	0.02	SiC
16	0-30	0.01	0.04	0.05	0.57	7.15	0.04	SiC
17	0-30	0.01	0.03	0.03	0.56	4.97	0.02	SiC
18	0-30	0.02	0.02	0.08	0.60	7.42	0.02	SiC
19	0-30	0.01	0.03	0.08	0.43	4.05	0.03	SiC
20	0-30	0.02	0.02	0.11	0.35	6.35	0.01	SiC
21	0-30	0.01	0.03	0.07	0.54	4.72	0.01	C
22	0-30	0.01	0.02	0.07	0.58	7.67	0.03	C
23	0-30	0.00	0.02	0.11	0.63	2.54	0.01	C
24	0-30	0.02	0.03	0.08	0.92	4.36	0.01	C
25	0-30	0.01	0.04	0.15	0.68	4.70	0.03	SiC
26	0-30	0.01	0.14	0.06	0.81	5.03	0.04	SiCL
27	0-30	0.02	0.05	0.10	0.86	3.86	0.03	SiCL
28	0-30	0.01	0.13	0.04	0.80	3.42	0.04	SiCL
29	0-30	0.02	0.03	0.12	0.70	5.23	0.01	C
30	0-30	0.01	0.03	0.04	0.66	6.07	0.02	SiC
31	0-30	0.01	0.04	0.06	0.58	4.08	0.02	SiL
32	0-30	0.01	0.03	0.04	0.94	4.47	0.01	CL
33	0-30	0.01	0.08	0.06	0.67	6.39	0.02	SiC
34	0-30	0.01	0.05	0.09	0.60	4.79	0.02	SiCL
35	0-30	0.01	0.05	0.11	0.66	5.17	0.01	CL
36	0-30	0.01	0.35	0.01	1.21	9.43	0.03	SiCL
37	0-30	0.02	0.49	0.01	2.40	6.84	0.02	CL
38	0-30	0.02	0.59	0.03	2.11	10.27	0.04	SiC
39	0-30	0.01	0.35	0.03	1.36	6.48	0.02	C
40	0-30	0.01	0.51	0.02	2.76	9.04	0.02	C

Table 2. (Continued)

Soil Number	Depth	Cd µg kg^{-1}	Co µg kg^{-1}	Cr µg kg^{-1}	Ni mg kg^{-1}	Fe mg kg^{-1}	Mo µg kg^{-1}	Texture Class
41	0-30	0.02	0.79	0.02	4.48	11.83	0.03	C
42	0-30	0.02	1.17	0.01	2.47	12.97	0.05	C
43	0-30	0.01	0.33	0.02	1.58	14.63	0.03	SiCL
44	0-30	0.02	1.77	0.02	5.99	9.51	0.03	C
45	0-30	0.02	1.08	0.01	3.00	9.59	0.05	CL
46	0-30	0.01	0.81	0.02	1.98	11.17	0.06	C
47	0-30	0.02	0.42	0.02	1.36	7.65	0.03	SiC
48	0-30	0.02	1.05	0.01	3.42	7.83	0.03	C
49	0-30	0.02	0.41	0.02	3.04	8.23	0.02	SiC
50	0-30	0.02	0.36	0.03	2.65	10.17	0.03	SiC
51	0-30	0.01	1.27	0.01	6.12	10.44	0.02	C
52	0-30	0.02	0.63	0.01	4.31	6.05	0.01	SC
53	0-30	0.01	1.04	0.04	10.41	9.20	0.03	C
54	0-30	0.03	1.32	0.02	2.31	9.44	0.04	CL
55	0-30	0.02	0.40	0.85	1.45	18.72	0.11	SiC
56	0-30	0.02	1.95	0.01	2.46	14.64	0.07	SiCL
57	0-30	0.02	0.30	0.01	1.59	12.57	0.04	C
58	0-30	0.03	1.27	0.18	3.19	17.35	0.08	C
59	0-30	0.02	0.59	0.57	2.37	16.43	0.02	C
60	0-30	0.02	0.94	0.63	5.50	10.90	0.03	C
61	0-30	0.02	1.70	0.01	13.56	6.04	0.02	CL
62	0-30	0.02	2.17	0.02	17.60	7.48	0.02	C
63	0-30	0.02	1.94	0.01	9.73	5.69	0.02	C
64	0-30	0.01	2.96	0.02	11.52	6.75	0.02	C
65	0-30	0.02	0.83	0.02	6.84	5.22	0.05	CL
66	0-30	0.01	0.07	0.02	1.41	3.35	0.01	CL
67	0-30	0.02	0.08	0.01	1.09	11.54	0.02	C
68	0-30	0.01	0.20	0.02	1.46	5.12	0.02	C
69	0-30	0.01	0.13	0.02	0.95	12.15	0.02	CL
70	0-30	0.02	0.24	0.01	7.18	7.26	0.01	L
Min.		**0.01**	**0.02**	**0.01**	**0.35**	**1.65**	**0.01**	
Max.		**0.03**	**2.96**	**0.85**	**17.60**	**18.72**	**0.11**	
Aver		**0.01**	**0.49**	**0.11**	**2.72**	**7.22**	**0.03**	

Chrome

The lowest chromium content of the soils was 0.01 µg kg^{-1} and the highest chromium was 0.85 µg kg^{-1}. The average Cr content of the soils was found to be 0.11 µg kg^{-1} (Table 2). In a study conducted in a different region, Taş and Demir (2022), who aimed to determine the heavy metal contents of the central districts of Van province, found similar results in terms of Cr content of soils.

Nickel

The lowest exchangeable nickel content of all agricultural soils in the study area was 0.35 mg kg^{-1} and the highest was 17.60 mg kg^{-1}. The average nickel content of the soils was found to be 2.72 mg kg^{-1} (Table 2.). In a study carried out in a different region, Taş and Demir (2022) determined that the Ni content of the soils was between 2.47-14.95 mg/kg as a result of the study in which they aimed to determine the fertility level and some heavy metal contents of the agricultural soils of Bingöl plain and presented similar results.

Iron

The minimum iron content of the soils of the study area was 1.65 mg kg^{-1}, the highest iron content was 18.72 mg kg^{-1} and the average iron content was 7.22 mg kg^{-1}. When the soil iron contents were classified according to the limit values of Lindsay and Norvel (1978), 1.43 % of the samples were found to be iron deficient (<2.5 mg kg^{-1}), 27.14% were found to be adequate (2.5-4.5 mg kg-1) and 71.43 % were found to be iron surplus (>4.5 mg kg^{-1}) (Table 2.). Bayram et al. (2023), who studied the fertility status of pistachio orchards in Adıyaman province, determined that 85 % of the Fe content of the soils was adequate and high and presented similar results.

Molybdenum

The lowest molybdenum content of Arsuz region soils was 0.01 µg kg^{-1}, while the highest molybdenum content was 0.11 µg kg^{-1}. The average molybdenum content of the soils was found as 0.03 µg kg^{-1}. The available molybdenum contents of all of the agricultural soils of Arsuz region were found to be sufficient (>1 ppm) according to Viets and Lindsay (1973) (Table 2.). Shaheen et al. (2021), who aimed to determine the heavy metal contents of the agricultural soils of Kafr El-Zayat city of Egypt, reported that the Mo content in Egyptian soils was very low and the Mo content in the soils was below the limit values.

3.2. Relationships between available Molybdenum Content and Some Other Soil Heavy Metal Properties

The relationships between heavy metal contents of the soils under investigation and available molybdenum are given in Table 3. As can be seen from the table, positive significant relationships were determined between Mo and Cd (r: 0.39***; Figure 2), Co (r: 0.34***; Figure 3) and Fe (r: 0.69***; Figure 4) contents of soils. In a study conducted by Yu et al. (2018) in which heavy metal contents of soils were determined, similar results were obtained for Mo content of soils. In addition, significant positive relationships were determined between Cd content and Co (r: 0.42***), Ni (r: 0.29*) and Fe (r: 0.51***) contents of soils. Similar results were obtained in a study conducted by Arıkan et al. (2019). A significant positive relationship was determined between Co content of soils and Ni (r: 0.80***) and Fe (r: 0.42***) contents. A study by Shaheen et al. (2021) showed similar results between Co and Ni in agricultural soils in Egypt.

Table 3. Correlation coefficients (r) between molybdenum and some soil heavy metal contents of soils of Arsuz region of Hatay province

	Mo µg kg^{-1}	Cd µg kg^{-1}	Co µg kg^{-1}	Cr µg kg^{-1}	Ni mg kg^{-1}
Cd µg kg^{-1}	0.39***				
Co µg kg^{-1}	0.34***	0.42***			
Cr µg kg^{-1}	0.22	0.02	-0.14		
Ni mg kg^{-1}	0.06	0.29*	0.80***	-0.12	
Fe mg kg^{-1}	0.69***	0.51***	0.42***	0.18	0.17

* 0.05 düzeyinde önemli, *** 0.001 düzeyinde önemli

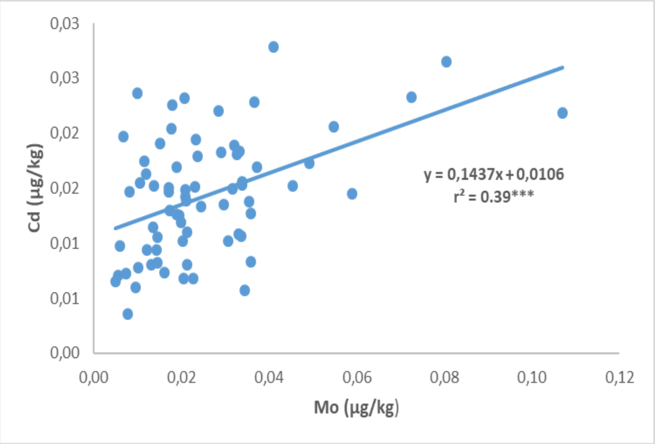

Figure 2. Relationship between useful Mo and Cd contents of soil prefixes

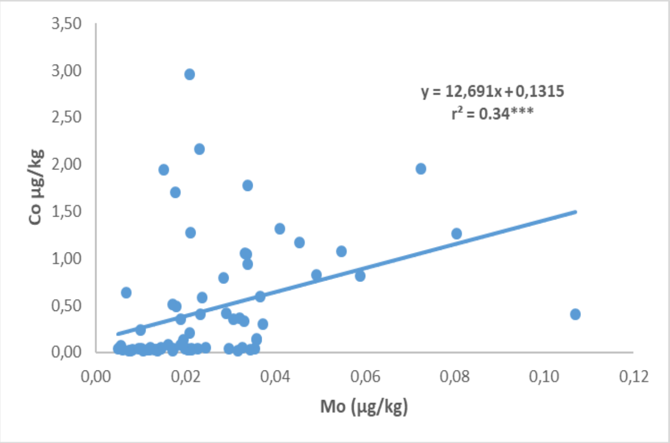

Figure 3. Relationship between Mo and Co contents of soil prefixes

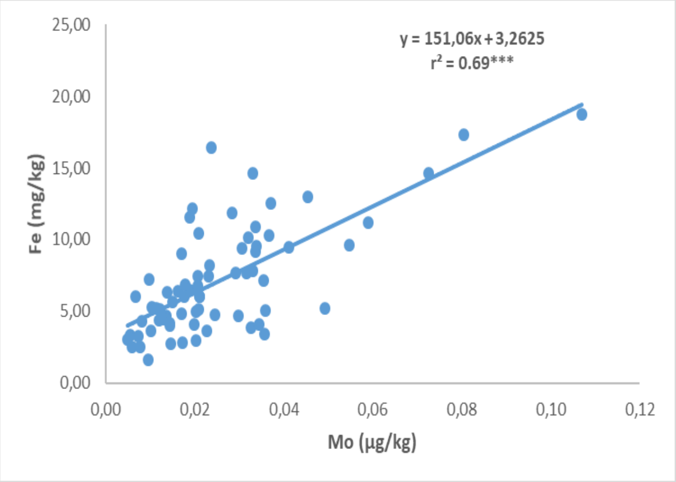

Figure 4. Relationship between Mo and Fe contents of soil prefixes

4. Discussion

Molybdenum content of soils in Arsuz region of Hatay province was analysed and its relationship with some heavy metal concentrations was investigated. The data obtained in this direction were compared with the permissible heavy metal limit values in soils determined in Turkey and worldwide. The results show that heavy metal accumulation in soils in the study area is within acceptable limits. This study reveals that the potential harm of heavy metal pollution caused by agricultural and industrial activities to human health is minimal. It is important to take necessary precautions to prevent the heavy metal contents in the agricultural soils in the study area, which do not reach harmful levels for human and animal health, from exceeding the specified limit values. In particular, it is necessary to carry out strict inspections of enterprises and factories in industrial and industrial zones located close to the study area.

References

Arıkan B, Çakmakçı G, Akıncı İE, Güler C (2019) Gaziantep ili tarım topraklarında ağır metal kirliliği ve bitki-gübre toprak ilişkisi. Anadolu Tarım Bilimleri Dergisi 34(3): 365-374.

Bayram CA, Büyük G, Kıyas N, Uçar A (2023) Adıyaman ili antepfıstığı bahçelerinin toprak örnekleri ile verimlilik durumlarının belirlenmesi. Mustafa Kemal Üniversitesi Tarım Bilimleri Dergisi 28(2): 308-318.

Çolak S, Akça ŞB, Yazıcı K (2021) Toprak kirliliğinin zenginleştirme, transfer ve birikim faktörleri ile değerlendirilmesi; Zonguldak/Çaycuma örneği. Ziraat Mühendisliği Dergisi (371): 59-73.

Düzgüneş O, Kesici T, Kavuncu O, Gürbüz F (1987) Araştırma deneme metotları (istatistik metotları-II). Ankara Üniversitesi Ziraat Fakültesi Yayınları:1021. Ankara, 381s.

Küçük C, Karaoğlu M (2021) Iğdır ili 080 devlet karayolu boyunca tarım topraklarında ağır metal kirliliği. Avrupa Bilim ve Teknoloji Dergisi (25): 325-333.

Lindsay WL, Norvel WA (1978) Development of a DTPA test for zinc. iron. manganese and copper. J. Soil Sci. Am. 42. 421-428.

Özkan F, Demir Y (2023) Rize ilinde geleneksel ve organik çay tarımı yapılan alanların topraklarında bazı verimlilik parametreleri ile ağır metal içeriklerinin karşılaştırılması. Iğdır Üniversitesi Fen Bilimleri Enstitüsü Dergisi 13(2): 1405-1417.

Özyiğit İİ (2021) Topraklarında ağır metaller; kökenleri, yayılışları ve etkileri. Ereğli Tarım Bilimleri Dergisi 1(1): 46-71.

Saltalı K, Gündoğan R, Demir ÖF, Kara Z, Yakupoğlu T, Dikici H, Yılmaz K (2018) Narlı ovası topraklarının ağır metal kapsamı üzerine çimento fabrikası baca tozlarının etkileri. Toprak Su Dergisi 7 (1): 11-20.

Seven T, Can B, Darende BN, Ocak S (2018) Hava ve toprakta ağır metal kirliliği. Ulusal Çevre Bilimleri Araştırma Dergisi 1(2): 91-103.

Shaheen ME, Tawfik W, Mankoula AF, Gagnon JE, Fryer BJ, El-Mekawy F (2021) Determination of heavy metal content and pollution indices in the agricultural soils using laser ablation inductively coupled plasma mass spectrometry. Environmental Science and Pollution Research 28: 36039–36052

Taciroğlu B, Kara E, Sak T (2016) Toprakta ağır metal gideriminde solucanların kullanımı. KSÜ Doğa Bilimleri Dergisi 19(2): 201-207.

Taş R, Demir Y (2022) Bingöl Ovası tarım topraklarının verimlilik düzeyi ile bazı ağır metal içeriklerinin belirlenmesi ve haritalanması. Düzce Üniversitesi Ormancılık Dergisi 18(2): 296-315.

Yu X, Sun B, Zhou J, Wang Y (2018) Distribution and relationship of molybdenum, cobalt, nickel and chromium in typical Chinese soils. Environmental Science and Pollution Research 25(8): 7970-7979.

Viets FG, Lindsay WL (1973). Testing soils for zinc. Copper. Managanese and iron. Soil Soc. Of Amer. Inc. Madison Wisconcin USA. 153-172.

Yalçın M (2024) Kırıkhan–Kumlu bölgesi topraklarının molibden içeriği ve topraktaki bazı ağır metaller ile ilişkilerinin belirlenmesi. MAS JAPS 9(2): 230–240.

Yalçın M, Çimrin KM (2021) Hatay ili Arsuz ilçesi topraklarının besin elementi durumları ve bunların bazı toprak özellikleri ile ilişkileri. MKU. Tarım Bilimleri Dergisi 26(3): 586-599.

Yalçın M (2023) Kırıkhan–Reyhanlı bölgesi tarım topraklarının molibden içeriği ve topraktaki bazı ağır metaller ile ilişkilerinin belirlenmesi. Eurasian Journal of Biological and Chemical Sciences 6(2): 63-72.

Yurdakul İ, Kalınbacak K, Altınkaynak D, Peker RM (2023) Molibden ve arseniğin tarla koşullarında buğday bitkisinin verimine ve toksikliğine etkilerinin belirlenmesi. Isparta Uygulamalı Bilimler Üniversitesi Ziraat Fakültesi Dergisi 18(1): 25-34.

RESEARCH ARTICLE
Bull Biotechnol (2025) 6(1):25-32
https://doi.org/10.51539/biotech.1708980
Journal homepage: www.dergipark.org.tr/biotech

Bulletin of Biotechnology

A Multi-Criteria Decision-Making Approach for Green Hydrogen Production via Renewable Energy Sources

Medine Türkmen*, Serap Ulusam Seçkiner

*1 *Industrial Engineering, Engineering Faculty, Gaziantep University, Gaziantep, Türkiye*

*Corresponding author: mt9006@mail2.gantep.edu.tr
Orcid No: https://orcid.org/0009-0007-6842-2049

Received : 29/05/2025
Accepted : 28/06/2025

To Cite: Türkmen M, Ulusam Seçkiner S (2025) A Multi-Criteria Decision-Making Approach for Green Hydrogen Production via Renewable Energy Sources. Bull Biotechnol 6(1):25-32 https://doi.org/10.51539/biotech.1708980

Abstract: The global transition toward cleaner energy systems has intensified interest in green hydrogen as a sustainable and low-emission alternative to fossil-based fuels. However, selecting the most appropriate hydrogen production method remains a complex decision-making challenge due to the interplay of technical, economic, environmental, and social factors. This study applies the Analytic Hierarchy Process (AHP), a widely recognized multi-criteria decision-making (MCDM) approach, to systematically evaluate and rank various green hydrogen production technologies. A hierarchical framework was developed incorporating critical criteria such as investment cost, operational efficiency, environmental sustainability, and technological maturity. Expert judgments were used to assign relative weights to each criterion, and competing alternatives were assessed accordingly. The AHP analysis identified RW-Biomass: Bio Photolysis as the most favorable hydrogen production method, achieving the highest overall priority score (0.102), indicating its strong performance across the selected evaluation criteria. These results highlight the method's potential in aligning sustainability goals with practical energy planning, providing valuable insights for decision-makers in shaping future hydrogen strategies. The study confirms the effectiveness of AHP in delivering structured, transparent, and evidence-based assessments in the context of sustainable energy development.

Keywords: Green Hydrogen; Multi-Criteria Decision Making (MCDM); Analytic Hierarchy Process (AHP); Sustainability; Hydrogen Production Technologies;

1 Introduction

The ongoing global shift toward low-carbon energy systems has underscored the pivotal role of hydrogen in achieving long-term climate and energy goals. As nations strive to reduce emissions across the power, transport, and industrial sectors, hydrogen emerges as a promising alternative energy carrier. Among various production routes, green hydrogen produced via the electrolysis of water powered by renewable electricity offers significant environmental benefits due to its near-zero greenhouse gas emissions. It has been increasingly recognized as a vital element in decarbonization pathways and a central contributor to climate neutrality targets (Cetinkaya et al. 2012).

Nonetheless, technical, economic, and infrastructural barriers remain challenging the realization of green hydrogen's full potential. The variability of renewable energy sources, substantial capital investment for electrolysis infrastructure, and the lack of hydrogen transport and storage systems hinder its large-scale deployment (Valente et al. 2016). In this context, developing comprehensive and robust planning strategies is crucial to strike a balance between environmental performance, economic viability, and production scalability.

Strategic planning for hydrogen systems must address conflicting objectives under uncertain and dynamic conditions. This complexity necessitates the adoption of the MCDM methods capable of integrating diverse performance indicators such as energy efficiency, environmental footprint, production cost, technological maturity, and social acceptance. Previous studies have demonstrated that life cycle-based evaluations are effective in quantifying environmental and economic impacts of hydrogen production technologies (Valente et al. 2016), while decision-support frameworks can assist stakeholders in ranking alternatives based on sustainability criteria (Cetinkaya et al. 2012).

Li et al. (2020) further contribute to this field by proposing a novel MCDM framework that incorporates objective grey relational analysis (GRA) with DEMATEL for determining criteria weights. Their approach eliminates the reliance on subjective expert evaluations by using data-driven methods to establish interrelationships among criteria. This hybrid methodology enhances the objectivity of sustainability assessments and provides a clearer prioritization of hydrogen production technologies. Their work also highlights the necessity of evaluating environmental, economic, technological, and sociopolitical dimensions to guide decision-makers toward selecting the most sustainable pathways.

This study aims to explore how green hydrogen production planning can be optimized by systematically evaluating production alternatives using an integrated multi-criteria framework. By applying tools such as AHP and integrating expert judgments with quantitative performance metrics, the research seeks to identify viable options that balance capacity, cost, and environmental objectives.

From a theoretical perspective, this study extends the application of MCDM approaches in green hydrogen planning. Practically, it offers a structured, reproducible evaluation model to assist policymakers and industry stakeholders in making informed, balanced decisions aligned with broader sustainability goals.

The methodological approach used to implement this evaluation framework is presented in the next section, with a focus on the AHP model design, criteria weighting, and alternative assessment procedures.

2 Materials and Method

This study adopts a structured, three-stage methodology to evaluate green hydrogen production alternatives under multiple criteria using the AHP model. The approach integrates expert judgment with quantitative analysis to ensure a robust and context-specific decision framework. The methodology comprises the following phases:

- **Analytic Hierarchy Process (AHP):** Identification of the alternatives, criteria, and the hierarchical structure based on an extensive review of relevant literature and consultations with domain experts.
- **Data Gathering:** Collection of pairwise comparison judgments and performance evaluations from experts through structured questionnaires to determine criteria weights and alternative performance.
- **Sensitivity Analysis:** Evaluation of how variations in the criteria weights affect the final rankings of alternatives to examine the robustness of the decision-making model.

Each stage of the methodology is elaborated in the following subsections.

2.1 Analytic Hierarchy Process (AHP)

The AHP, developed by Saaty (1980), provides a systematic approach for solving multi-criteria decision problems by decomposing the decision into a hierarchy of goals, criteria, sub-criteria, and alternatives.

- **Goal:** Optimal selection of green hydrogen production method,
- **Criteria/Sub-criteria:** Cost, efficiency, sustainability, and technology readiness,
- **Alternatives:** Different hydrogen production pathways, such as electrolysis, biomass gasification, and photolysis.

This hierarchical structure enables structured comparison and prioritization of alternatives based on consistent and traceable logic. In line with Russo and Camanho (2015), the hierarchical structure in this study was constructed as shown in Fig 1.

The selection and formulation of criteria were guided by an extensive literature review and validated through expert consultation. Russo and Camanho (2015) emphasize the importance of contextual relevance, measurability, and clarity in criteria design, which was carefully observed in this study.

The decision-making framework incorporated a diverse range of hydrogen production pathways as shown in Fig 2, including conventional fossil-based processes, renewable biomass conversion methods, and advanced water-splitting technologies. These alternatives were selected to reflect the full spectrum of current technological options.

Particular emphasis was placed on ensuring a balanced representation of both mature and emerging technologies, thereby allowing for a comprehensive evaluation across economic, environmental, and technical dimensions. This inclusive selection supports a robust comparative analysis aligned with multi-criteria decision-making methodologies.

This study employed AHP to identify the most suitable production method through a multi-criteria evaluation that aligns technical, environmental, and economic considerations. Four main criteria were identified, each with multiple sub-criteria, and fourteen alternatives were identified for this model as shown in Table 1.

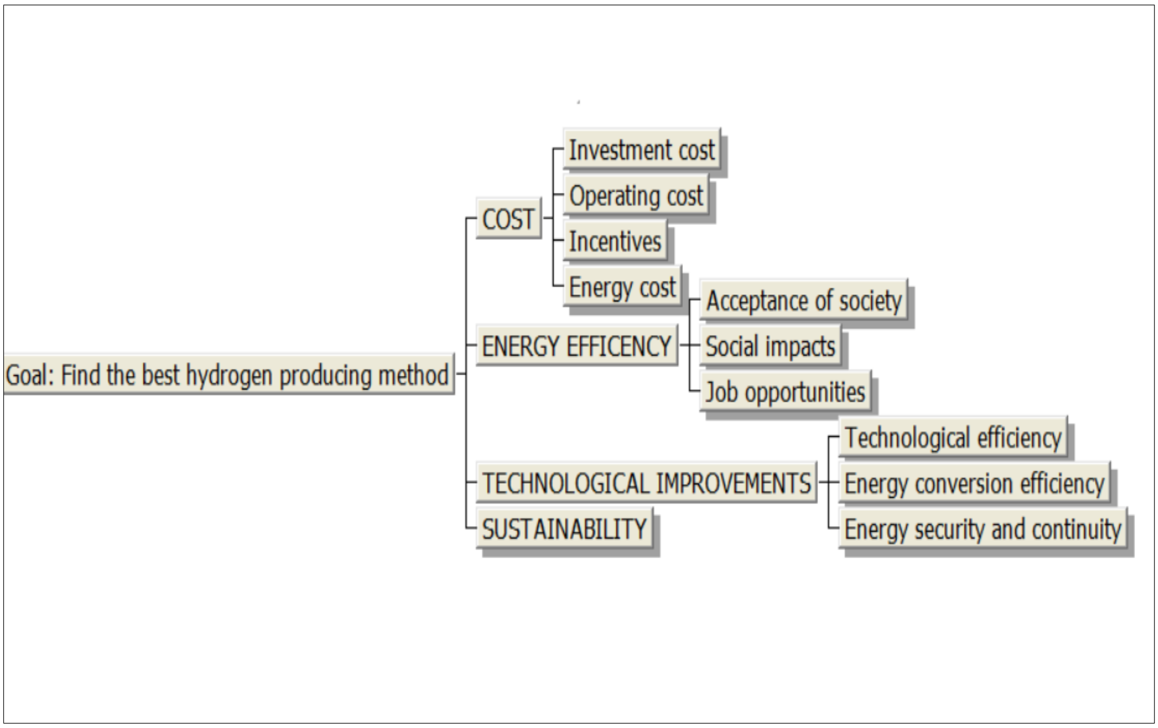

Fig. 1. The hierarchical structure of the AHP model

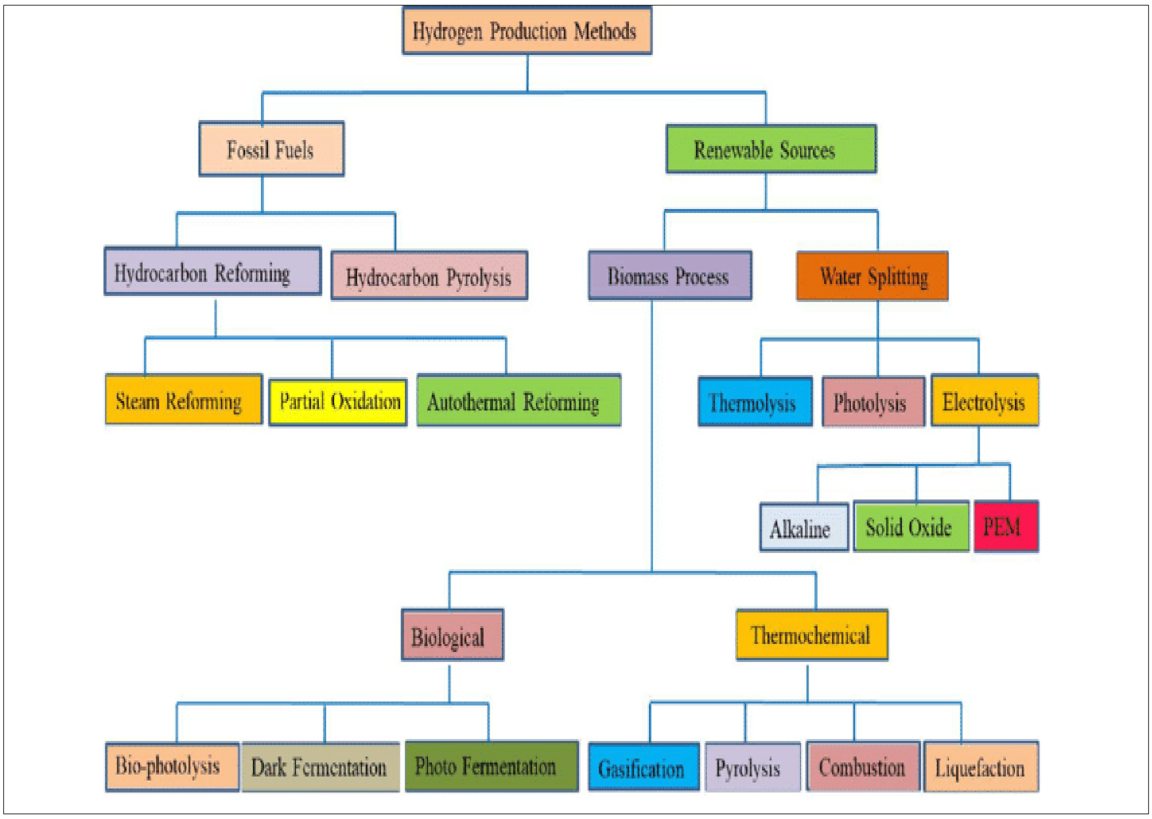

Fig. 2. Hydrogen Production Methods

Table 1 Criteria and Alternatives

Criteria and Sub-Criteria	Alternatives
Cost	**Fossil-Based**
• Investment Cost	• Steam Reforming
• Operating Cost	• Partial Oxidation
• Incentives	• Autothermal Reforming
• Energy Cost	• Hydrocarbon Pyrolysis
Technological Improvements	**Renewable-Biomass- Based**
• Technological Efficiency	• Bio-Photolysis
• Energy Conversion Efficiency	• Dark Fermentation
• Energy Security and Continuity	• Photo-Fermentation
Energy Efficiency	• Thermochemical Pyrolysis
• Social Acceptance	• Gasification
• Job Opportunities	• Combustion
• Social Impacts	• Liquefaction
Sustainability	**Renewable- Water Splitting**
	• Electrolysis
	• Thermolysis
	• Photolysis

2.2 Data Gathering

The pairwise comparisons were collected using Saaty's 1–9 fundamental scale to reflect the relative importance of each criterion concerning others. Data for criteria weights and alternative evaluations were collected through structured surveys conducted with domain experts, including academics and industry professionals in energy planning and hydrogen production. A total of 10 experts participated in the pairwise comparison process. The pairwise comparison matrix was constructed, and the priority weights were derived from the principal eigenvector. In Equation 1 was used to estimate weights:

$$A \cdot w = \lambda_{max} \cdot w \qquad (1)$$

Where A is the pairwise comparison matrix, w is the eigenvector of weights, λ_{max} is the maximum eigenvalue of matrix A. To ensure consistency of expert judgments, the Consistency Ratio (CR) was calculated in Equation 2:

$$CR = \frac{CI}{RI}\ ,\ CI = \frac{\lambda max - n}{n-1} \qquad (2)$$

Where CI is the random consistency index. A CR value below 0.10 was deemed acceptable (Saaty, 1980). For the alternative evaluations, experts provided performance scores for each hydrogen production method against each criterion. This data formed the decision matrix for final ranking calculations.

2.3 Sensitivity Analysis

To assess the robustness of the decision model, a sensitivity analysis was conducted by varying the weights of key criteria and observing the impact on the final rankings of the alternatives. This process identifies whether small changes in judgments or priorities result in significant shifts in outcomes. Such analyses are especially critical in energy planning studies, where uncertainty and evolving technological landscapes are common. As highlighted by Govindan and Jepsen (2016), sensitivity analysis in MCDM frameworks improves decision-maker confidence and enhances transparency in sustainable system assessments.

Following the implementation of the AHP model and synthesis of expert judgments, the subsequent section reports the results obtained and discusses their implications for green hydrogen production planning.

3 Results and discussion

In this study, AHP was applied to determine the most suitable hydrogen production method based on four main criteria: Cost, Energy Efficiency, Technological Improvements, and Sustainability. The AHP methodology allowed for the quantification of expert preferences and the prioritization of these criteria according to their relative importance. The performance of fourteen hydrogen production technologies was evaluated using these weighted criteria.

While the current results support Fossil-based hydrogen production methods, largely due to their cost-effectiveness, this does not necessarily reflect long-term sustainability goals. If future policies emphasize Sustainability or Technological Advancements, Renewable Water-Splitting and Biomass-based methods may rank higher. Therefore, a multi-scenario or dynamic weighting approach could be beneficial in strategic energy planning to accommodate shifts in policy or resource availability.

Based on the pairwise comparison matrix constructed using expert judgments, the following criterion weights were obtained:

- **Cost**: 52.52%
- **Energy Efficiency**: 19.77%
- **Technological Improvements**: 17.87%
- **Sustainability**: 9.84%

These results reveal that **Cost** is the most influential criterion in determining the optimal hydrogen production method, reflecting the economic sensitivity of current energy planning strategies. Using these weights, each alternative's overall AHP score was computed as the weighted sum of its performance across the four criteria. The alternative with the highest AHP score was Fossil-Steam Reforming, followed closely by Fossil-Partial Oxidation and Fossil-Autothermal Reforming. These alternatives generally exhibit low production costs and acceptable levels of efficiency, explaining their high ranking.

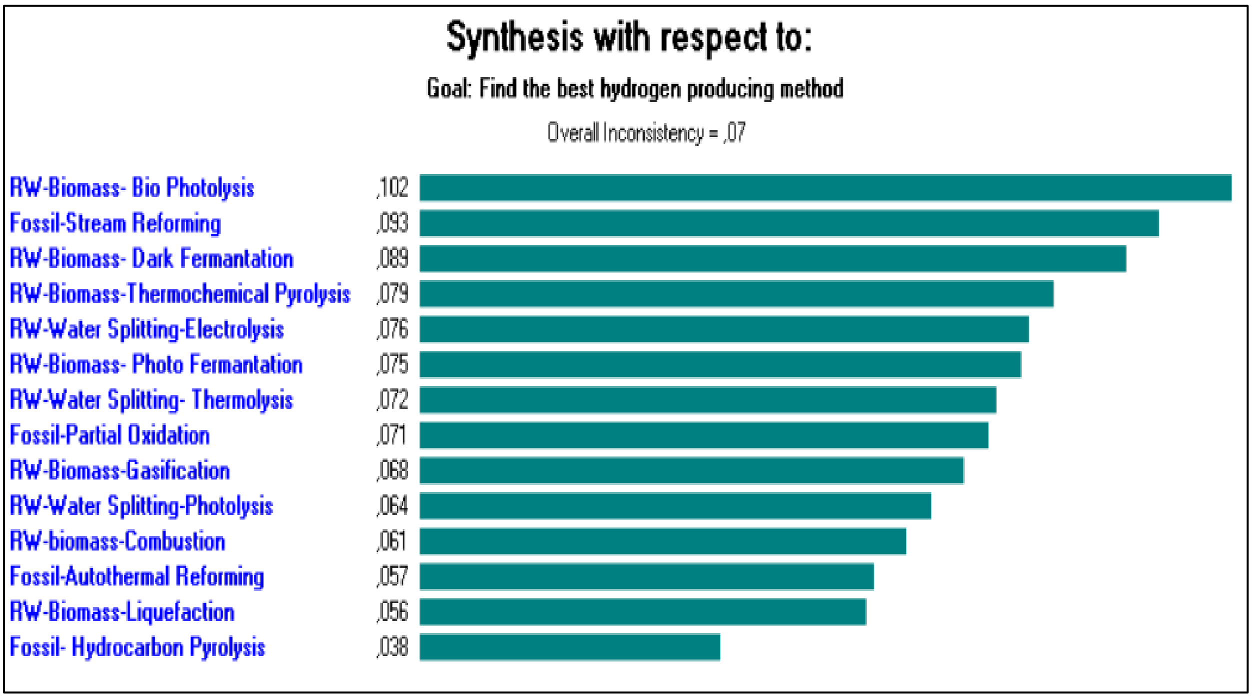

Fig. 3. The results of the AHP model

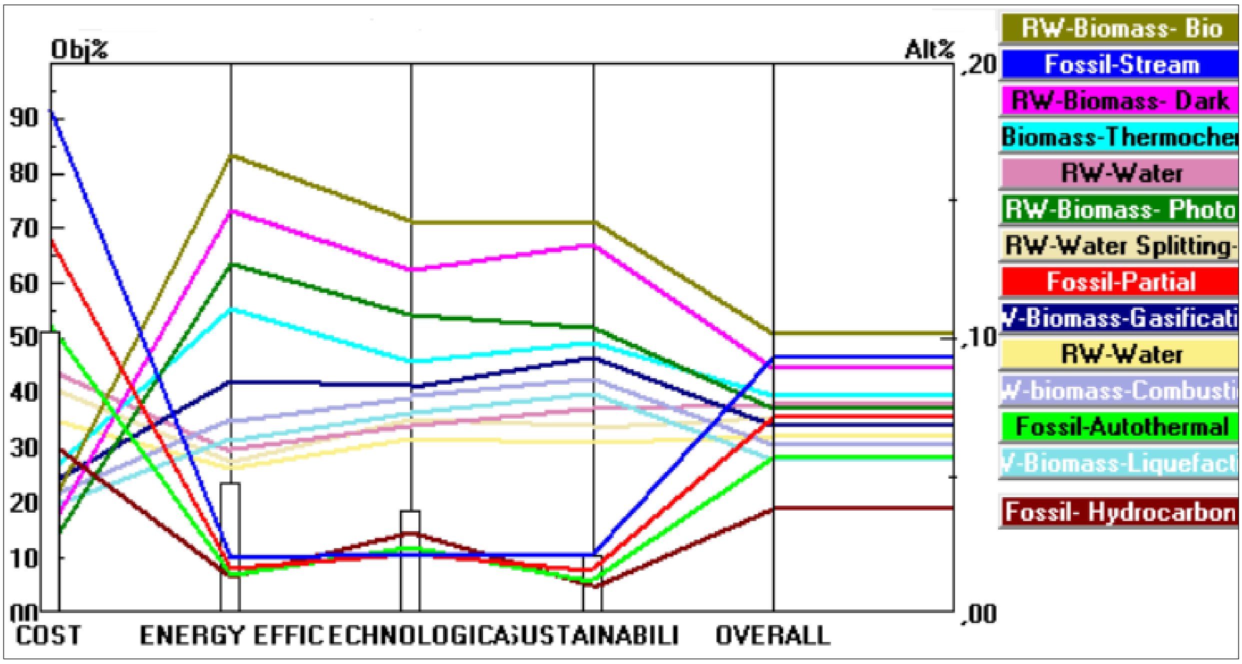

Fig. 4. Performance sensitivity analysis of the AHP model

As shown in Fig 3, RW-Biomass Bio Photolysis is ranked the highest with a weight of 0.102, suggesting it is the most preferred method when all considered criteria are aggregated. Fossil-Stream Reforming follows closely with a weight of 0.093, reflecting its strong performance, likely driven by cost efficiency. Other renewable-based technologies, such as RW-Biomass Dark Fermentation (0.089), RW-Biomass Thermochemical Pyrolysis (0.079), and Water Splitting via Electrolysis (0.076), also received relatively high scores, demonstrating the increasing viability of renewable and water-based hydrogen production pathways.

Conversely, methods such as Fossil-Hydrocarbon Pyrolysis (0.038) and RW-Biomass Liquefaction (0.056) received the lowest preference scores, indicating comparatively lower performance against the evaluation criteria.

The overall inconsistency ratio of the pairwise comparisons is reported as 0.07, which is within the acceptable threshold (<0.10), confirming the logical consistency of the decision-makers' judgments.

The sensitivity analysis, as illustrated in Fig 4, shows the performance variation of green hydrogen production alternatives in response to changing weights of the evaluation criteria: Cost, Energy Efficiency, Technological Advancement, and Sustainability. This analysis is essential for evaluating the robustness of the AHP model and understanding the sensitivity of final rankings to shifts in decision-maker priorities.

The results indicate that the Cost criterion exerts the most significant influence on the overall performance of the alternatives. Alternatives such as Fossil-Steam Reforming (blue line) and RW-Biomass Bio (goldenrod line) display high sensitivity to cost fluctuations, with their performance scores peaking under cost-dominant scenarios. This implies that initial investment and operational expenses remain crucial determinants in the selection process, especially for cost-intensive or fossil-based technologies.

In contrast, under the Energy Efficiency and Technological Improvement criteria, the performance scores of the alternatives show minimal divergence. Most alternatives remain within a narrow performance band, suggesting that these criteria do not substantially disrupt the overall rankings. This indicates a relative equilibrium in technological maturity and energy conversion efficiency among the compared options. A notable observation is the convergence of performance scores across alternatives when Sustainability is emphasized. The graph shows less variation under this criterion, implying that while sustainability is an essential evaluation factor, it is less discriminating among alternatives. This could be attributed to the fact that most green hydrogen pathways inherently align with environmental sustainability principles. Alternatives such as RW-Biomass Bio, RW-Biomass Dark, and RW-Water consistently perform well across all criteria and maintain relatively high scores even when the weights shift. Their robustness under different conditions highlights their suitability for long-term deployment. Conversely, fossil-fuel-based options such as Fossil-Partial Oxidation and Fossil-Hydrocarbon Reforming (red and brown lines) exhibit consistently lower performance and less adaptability, emphasizing their comparative disadvantages in sustainable energy planning.

Overall, the sensitivity analysis validates the stability and resilience of the AHP model. The top-ranked alternatives maintain their superiority across a wide range of weight configurations, affirming that the final decision is not overly sensitive to minor judgmental variations. These findings support previous MCDM studies, which emphasize the importance of cost criteria while also acknowledging the moderating role of technological and environmental factors (Govindan and Jepsen, 2016).

To further assess the stability of the model and examine the influence of individual criteria on the final prioritization of hydrogen production alternatives, a dynamic sensitivity analysis was conducted.

As shown in Fig 5, this analysis provides a visual representation of how each alternative's ranking responds to variations in the relative weights of the four main criteria: Cost (50.2%), Energy Efficiency (22.5%), Technological Improvements (17.8%), and Sustainability (9.4%).

The left panel of the figure illustrates the default weights assigned to each criterion, which were derived from expert judgments using the AHP pairwise comparison method. The results indicate that Cost is the most dominant factor, accounting for over half of the total decision weight. This aligns with current literature in energy planning, where initial investment and operating expenditures significantly shape the viability of hydrogen technologies (Dincer and Acar, 2015).

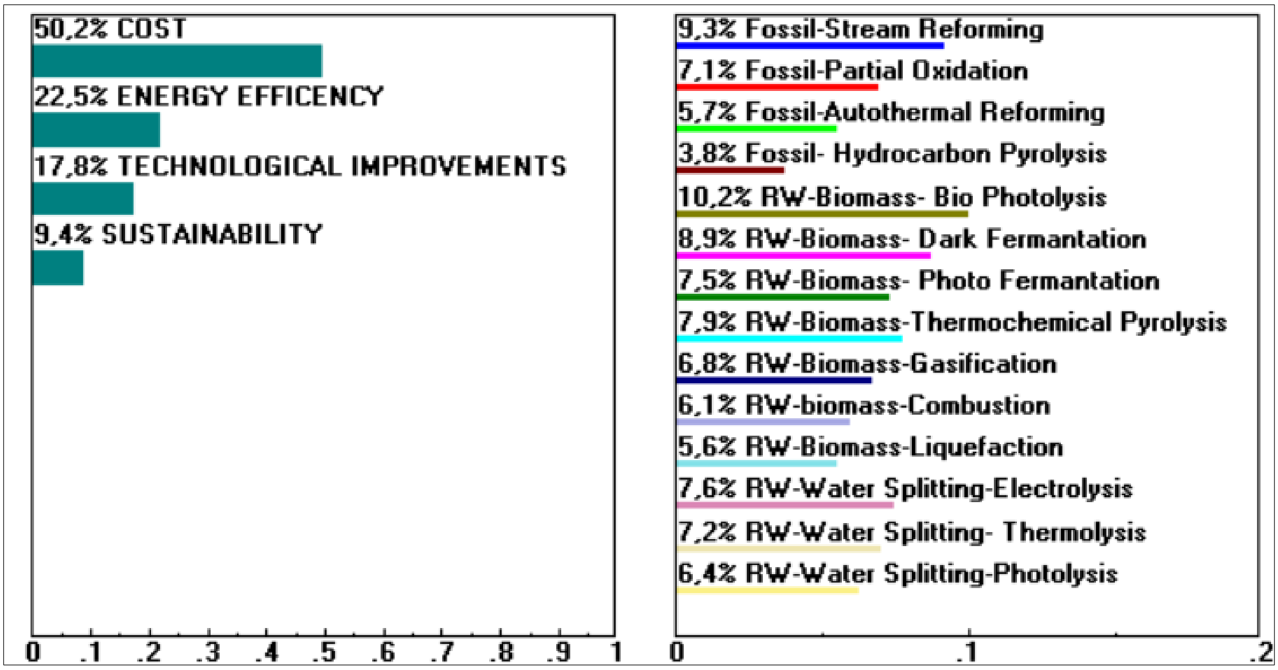

Fig. 5. Dynamic sensitivity analysis of the AHP model

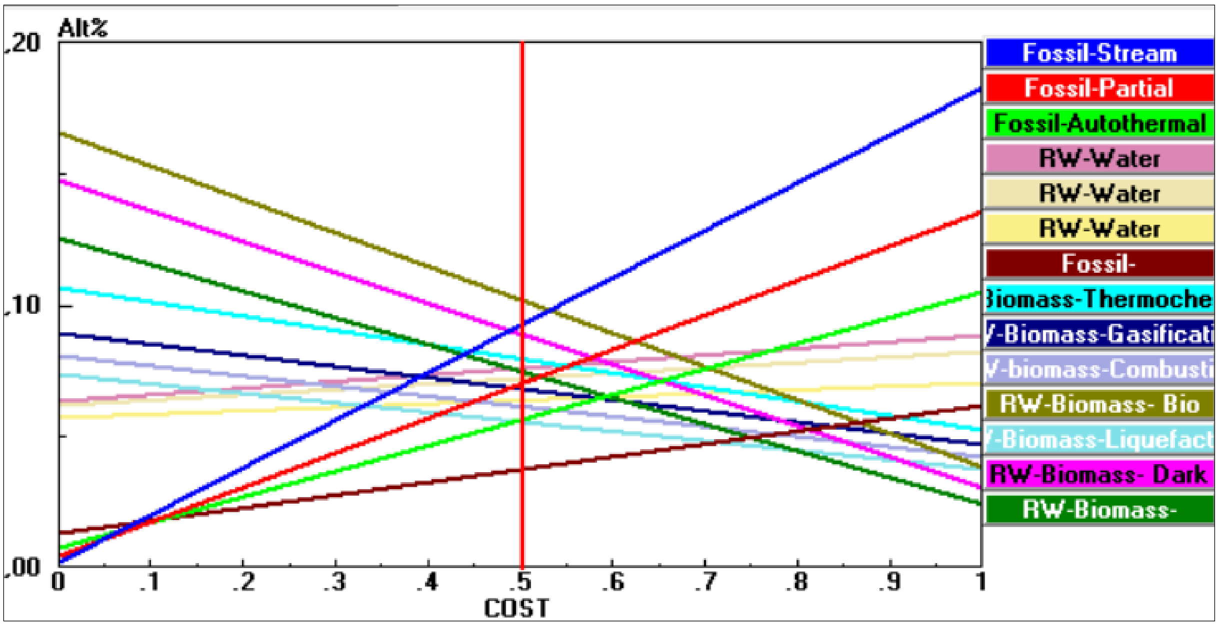

Fig. 6. Gradient Sensitivity Analysis for Cost Criterion in AHP Model

The right panel of the figure depicts the overall priority percentages of the 14 evaluated green hydrogen production alternatives. RW-Biomass Bio Photolysis (10.2%), RW-Biomass Dark Fermentation (8.9%), and RW-Biomass Thermochemical Pyrolysis (7.9%) emerge as the top-performing alternatives under the given weighting scheme. These biomass-based methods demonstrate strong performance across cost-effectiveness and technological feasibility, reflecting their increasing prominence in renewable hydrogen pathways (IEA, 2022).

Conversely, fossil-based alternatives such as Fossil-Hydrocarbon Pyrolysis (3.8%) and Fossil-Autothermal Reforming (5.7%) rank lower in the prioritization due to their higher environmental impacts and lower sustainability scores. These findings confirm that the model appropriately penalizes alternatives that are misaligned with long-term decarbonization goals.

The dynamic sensitivity analysis reveals that minor shifts in criterion weights, especially in cost and technological advancement, have a significant impact on the relative rankings of alternatives. This underscores the importance of understanding decision-maker preferences and conducting robust justification of weights, especially in policy-driven environments. Additionally, the relatively low sensitivity of rankings to the sustainability criterion indicates that while environmental impact is essential, its lower weight diminishes its discriminatory power in the current model structure.

Such dynamic visual tools are particularly useful for stakeholders to simulate real-world trade-offs and conduct “what-if” analyses under different strategic priorities, as recommended in multi-criteria energy system planning literature (Pohekar and Ramachandran, 2004).

To complement the static and dynamic analyses, a gradient sensitivity analysis was conducted to assess how variations in a single dominant criterion is Cost, impact the global rankings of hydrogen production alternatives. As depicted in Fig 6, this technique examines the trajectory (i.e., gradient) of each alternative’s overall score as the weight of the cost criterion increases from 0% to 100%, while maintaining proportional adjustments in the weights of the remaining criteria.

This form of analysis is particularly useful in evaluating the marginal impact of a criterion on the decision outcome and detecting any ranking reversals or crossing points among alternatives (Peniwati, 2007). The vertical red line in the graph marks the baseline cost weight at 50.2%, as determined from expert judgments.

Key Observations:

- Fossil-Steam Reforming (blue line) and Fossil-Partial Oxidation (red line) show sharply increasing slopes, indicating that their ranking significantly improves as cost becomes a more dominant criterion. This suggests their relative strength in economic feasibility compared to environmental or technological considerations.
- Conversely, RW-Biomass Bio Photolysis, RW-Biomass Dark Fermentation, and RW-Biomass Thermochemical Pyrolysis exhibit negative gradients, meaning their prioritization declines as the cost criterion weight increases. This behaviour reflects the higher upfront investment associated with biomass-based green hydrogen technologies, despite their advantages in sustainability and innovation.
- Several alternatives—such as RW-Water Electrolysis, Gasification, and Autothermal Reforming—show relatively flat gradients, implying that their rankings remain fairly stable across varying cost emphases. These pathways may represent more balanced trade-offs between economic and non-economic factors.

The presence of multiple intersection points among lines indicates potential ranking reversals depending on how much importance is assigned to cost. This insight is crucial for decision-makers operating under uncertain financial constraints or dynamic policy environments. It reinforces the notion that criteria prioritization should align with long-term sustainability goals, not just short-term cost considerations (Macharis et al. 2004). In summary, the gradient sensitivity analysis confirms that cost is a highly influential and volatile criterion, and alternative rankings are sensitive to its assigned weight. Therefore, any AHP-based decision support system should carefully justify the weight distribution to reflect stakeholder priorities accurately and transparently.

5 Conclusion

This study presents a comprehensive decision-making framework for evaluating green hydrogen production alternatives using the AHP model. In an era where sustainable energy planning is increasingly complex, the proposed model offers a systematic method for integrating technical, economic, environmental, and social criteria into strategic decision-making. The results demonstrate that AHP is a robust and transparent tool capable of managing multidimensional assessments in emerging energy systems.

The analysis revealed that biomass-based hydrogen production pathways, particularly RW-Biomass Bio Photolysis and Dark Fermentation, consistently outperformed fossil-based options under the baseline criteria weights. These alternatives provide synergies between environmental sustainability and technological innovation, although they are often limited by higher initial investment costs.

The sensitivity analyses, including performance-based, dynamic, and gradient sensitivity techniques, confirmed the dominant influence of the cost criterion, which accounted for over 50% of the total decision weight. Alternatives such as Fossil-Steam Reforming and Partial Oxidation gained priority when cost was emphasized, reflecting their economic viability but highlighting trade-offs in sustainability and long-term decarbonization compatibility.

Conversely, the performance stability of several renewable-based methods across different weight configurations suggests their strategic value under policy frameworks prioritizing environmental impact, technological maturity, and energy security. The sensitivity results also underscore the importance of aligning decision models with evolving national and regional energy strategies, as even small shifts in stakeholder priorities may lead to ranking reversals.

From a practical perspective, this study offers energy planners and policymakers a decision-support tool that is adaptable, scalable, and grounded in expert knowledge. It provides a transparent mechanism for justifying investment decisions in green hydrogen technologies, decisions that must carefully balance economic feasibility with long-term environmental objectives.

For future work, the integration of Fuzzy AHP, hybrid MCDM approaches (e.g., AHP-TOPSIS), or life cycle-based indicators can further enhance the decision model's depth and realism. Additionally, the application of the framework to specific regional contexts or dynamic policy scenarios (e.g., carbon pricing, subsidies) would strengthen its relevance for real-world planning.

In conclusion, AHP proves to be a valuable methodological tool for navigating the multifaceted landscape of green hydrogen production planning, offering a structured path toward sustainable energy transition.

Acknowledgements

This study was conducted without the support of any external funding from governmental, commercial, or non-profit organizations.

Authors' contributions:

MT conceptualized the study, conducted the data analysis, literature review and drafted the manuscript. SUS contributed to the methodology design and manuscript revision. Both authors read and approved the final version of the manuscript.

Conflict of interest disclosure:

The author declares no conflict of interest.

References

Çetinkaya E, Dinçer I, Naterer GF (2012) Life cycle assessment of various hydrogen production methods. Int J Hydrogen Energy 37:2071–2080

Dinçer I, Acar C (2015) Review and evaluation of hydrogen production methods for better sustainability. Int J Hydrogen Energy 40:11094–11111

Govindan K, Jepsen MB (2016) ELECTRE: A comprehensive literature review on methodologies and applications. Eur J Oper Res 250:1–29

International Energy Agency (2022) Global Hydrogen Review 2022. https://www.iea.org/reports/global-hydrogen-review-2022

Li W, Ren X, Ding S, Dong L (2020) A multi-criterion decision-making for sustainability assessment of hydrogen production technologies based on objective grey relational analysis. Int J Hydrogen Energy 45:34385–34395

Macharis C, Springael J, De Brucker K, Verbeke A (2004) PROMETHEE and AHP: The design of operational synergies in multicriteria analysis. Eur J Oper Res 153:307–317

Pohekar SD, Ramachandran M (2004) Application of multi-criteria decision making to sustainable energy planning—A review. Renew Sustain Energy Rev 8:365–381

Peniwati K (2007) Criteria for evaluating group decision-making methods. Math Comput Model 46:935–947

Russo RFSM, Camanho R (2015) Criteria in AHP: A systematic review of literature. Procedia Comput Sci 55:1123–1132

Saaty TL (1980) The analytic hierarchy process (AHP). J Oper Res Soc 41:1073–1076

Valente A, Iribarren D, Dufour J (2016) Life cycle assessment of hydrogen energy systems: A review of methodological choices. Int J Life Cycle Assess 22:346–363

Yıldırım B, Kantürk Figen A, Karakılçık M (2024) Hidrojen üretim yöntemleri. Hidrojen Teknolojileri 19

RESEARCH ARTICLE
Bull Biotechnol (2025) 6(1):33-45
https://doi.org/10.51539/biotech.1702926 Journal homepage: www.dergipark.org.tr/biotech

Bulletin of Biotechnology

Multi Epitope Based Vaccine Design against *Capnocytophaga canimorsus* through Immunoinformatics Approaches

Levent Cavas*, Atakan Vatansever

Department of Chemistry, Faculty of Science, Dokuz Eylül University, Main Campus 35390, İzmir, Türkiye

*Corresponding author:levent.cavas@deu.edu.tr
Orcid No: https://orcid.org/0000-0003-2136-6928

Received : 20/05/2025
Accepted : 29/06/2025

To Cite: Cavas L, Vatansever A (2025) Multi Epitope Based Vaccine Design against *Capnocytophaga canimorsus* through Immunoinformatics Approaches. Bull Biotechnol 6(1):33-45 https://doi.org/10.51539/biotech.1702926

Abstract: Immunoinformatics has provided an important contribution to the acceleration of vaccine research. The *in silico* tools developed under immunoinformatics efficiently filter candidate vaccines and select the most appropriate ones for *in vitro* and *in vivo* studies. Multi epitope-based vaccine design against *Capnocytophaga canimorsus* infections through immunoinformatics approaches was proposed in the present investigation. Outer membrane protein (OMP) of *C. canimorsus* was used to develop peptide-based vaccines. IEDB tools are used in this research. The antigenic potential of *C. canimorsus* OMP was evaluated via VaxiJen v2.0 and the Overall Prediction for the Protective Antigen was found to be 0.6049. MHC-I and -II binding epitopes with maximum scores were found to be "QEIGKLKKY" for HLAB*44:03 and "FNAVQEIGK" for HLA-DRB5*01:01, respectively. ABCPrep analysis identified multiple epitopes. The maximum score of 0.91 was associated with the sequence "KNMRIGYVDMDFILEN". Discontinuous epitopes were also detected in this research with the maximum score observed for the regions A:L247, A:E248, A:Q250 and A:K251. The population coverage for the global population was calculated to be 96.45% for a defined set of epitopes. In conclusion, since the adoption of dogs and cats as pets has increased after COVID-19, there is a clear risk for *C. canimorsus* infections. The proposed peptide-based vaccines in this report may mitigate this risk on a global level.

Keywords: Antigenic potential; *Capnocytophaga canimorsus*; immunoinformatics; health biotechnology; vaccine

1 Introduction

Cats and dogs are important animals in human life. The domestication of dogs and cats has a significant effect on their evolutionary trajectory and their interactions with mankind (Ammerman, 2017). Moreover, this relationship is a crucial strategy for survival in a world where the influence of mankind has become dominant (Oltenacu, 2004). Archaeological evidence suggests that the domestication of dogs began at least 14,000 years ago. Additionally, the origin of unconscious domestication extends up to 35,000 years. Cats, on the other hand, were domesticated approximately 9,500 years ago (Galibert et al. 2011; Vigne et al. 2004). Not only did this co-evolution strengthen the bond between humans and animals, but it also gave benefits in tasks such as hunting and protection and had deep cultural importance in art, mythology, and literature (Schleidt and Shalter, 2003; De Tiège et al. 2021). However, this interaction also created a potential channel for the transmission of infections (Esposito et al. 2023). Animal caused diseases known as zoonoses, present a critical challenge to global public health because the infections in animals can pass to humans, which causes different kinds of diseases (Saklani et al. 2024). These diseases are caused by a wide variety of pathogens, such as bacteria, viruses, parasites, and fungi. Also, the transmission routes differ (Rees et al. 2021). Those diseases pass to humans through direct contact with animals, exposure to their saliva, bodily fluids, or excretions, or even indirectly, such as interaction with contaminated environments (Desvars-Larrive et al. 2024). Some of the most common zoonotic diseases are *Campylobacteriosis*, *Salmonellosis*, infection with Shiga toxin-producing *Escherichia coli* (STEC), *Yersiniosis*, *Listeriosis*, *Tularaemia*, *Echinococcosis*, Q fever, West Nile virus infection, *Brucellosis*, *Trichinellosis*, rabies, and congenital toxoplasmosis (EFSA, 2024). Although many zoonotic diseases are well understood, it is important to remember that understanding whether the zoonotic pathogens are related to their host is crucial because the change in host-pathogen interactions may result in the emergence of new diseases (Ko et al. 2009). These interactions are also related with recent trends, such as the rise in pet adoption during the COVID-19 pandemic (Pieracci et al. 2021; Hedman et al.

2021). As the COVID-19 pandemic started, the limitations imposed on people increased the level of stress and anxiety. Owning a pet was found to be the best choice for saving the well-being of humans, and a noteworthy increase in pet ownership was recorded during that period because pets provided companionship and social support during lockdown (Ho et al. 2021; Bowen et al. 2020). As people were stressed during isolation in the COVID-19 pandemic, pets gave a source of comfort and emotional connection (Dogbey et al. 2024). Even though the increase in human animal relationships has provided strong companionship, as it is mentioned earlier in the text, it has also poten-tially increased certain zoonotic risks (Powell et al. 2022). Increased contact with pets, like licking, scratching, and bit-ing could lead to a higher probability of transmission of com-mensal bacteria found in animal oral flora, such as *Capno-cytophaga* species. All seven species that constitute the genus *Capnocytophaga* are found in the oral cavities of humans and domestic animals (Shin et al, 2007). However, *C. canimorsus* is recognized as the most important species that causes human infections (Lion et al. 1996). This pathogen is part of the normal flora of the oral cavity of dogs and cats and is known to cause meningitis, sepsis, and other life-threatening diseases in human, especially those with compromised immune systems. *C. canimorsus* can be transmitted through dog bites or cat scratches (Butler, 2015). *C. canimorsus* also has high virulence and can evade the innate immune system. The bacteria have mechanisms such as catalase and cytotoxin production to evade phagocytosis, gliding motility to facilitate tissue invasion, and serum complement resistance (Shin et al. 2007). Symptoms that may be seen in affected individuals include sepsis, septic shock, multiorgan failure, purpura fulminans secondary to DIC and meningitis (Mader et al. 2020; Lee et al. 2020). The appearance of *C. canimorsus* has revealed the potential for zoonotic risk of the oral flora of animals and the need for clinician awareness of infections associated with animal bites (O'Riordan et al. 2021). Van Samkar et al. (2016) reported three cases of *C. canimorsus* meningitis, of which two, occurred in healthy individuals who were bitten by a dog. Even though the infections caused by *C. canimorsus* were firstly identified in 1976 by Bobo and Newton, who isolated it from a patient with septicemia following a dog bite, there is no commercially available vaccine for prevention (Butler, 2015; Popiel and Vinh, 2013) to the best of our knowledge. The complexity of the interaction between human and animal ecosystems creates a new call for preventing strategies from those dangers effec-tively, especially while facing zoonotic threats. Fortunately, thanks to the applications that have advanced immuno-informatics technologies, either the development of vaccines or the application of vaccine development immunotherapeutic treatments can be made efficiently without any time-consuming procedures. Vaccines targeting pathogens like *Neisseria meningitidis* and *Bacillus anthracis* are early examples of vaccines that were successfully developed using immunoinformatics and reverse vaccinology (Damas et al. 2022; Shamakhi and Kordbacheh, 2021). Additionally, the benefits of this approach were also explained in the report by Ortega-Tirado et al. (2020), as the facilities provided by immunoinformatics have made it possible to identify the immunogenic T-cell peptides of *Mycobacterium tuberculosis* for a new vaccine. Platforms like VaxiJel, UniProt, NCBI (National Center for Biotechnology Information), and IEDB (Immune Epitope Database) have became predominant in this field. These tools accelerate studies of biotechnology and immunology, thus allowing for more sensitive and effective results.

In this study, an immunoinformatics approach using epitope mapping, immunogenicity prediction, population coverage for MHC-I and II alleles, and detection of probable B and T-cell epitopes via IEDB.org tools was proposed for the development of linear and non-linear peptide-based vaccine candidates for *C. canimor-sus* outer membrane protein (OMP) coded A0A0B7H4B5.

2 Materials and Method

2.1 Data

The FASTA-encoded primary amino acid sequence of *C. canimorsus* OMP was obtained from the UniProt Knowledgebase (UniProtKB), specifically from the UniProt release version 2024 06. The protein sequence was accessed by the accession code of A0A0B7H4B5 (Coudert et al. 2023; Bateman et al. 2023).

2.2 Determination of vaccine potential via VaxiJen servers

The antigenic potential of OMP was evaluated using the VaxiJen v3.0 online tool (Dimitrov et al. 2020). This bioinformatics tool predicts antigenicity based on the physicochemical properties of protein sequences, as evidenced by papers containing data for novel immunogenic proteins tested on humans until March 2017 (Zaharieva et al. 2019). The sequences with a bacterial threshold of over 0.4 are classified as a probable antigen. Thus, the antigenic protein sequences of *C. canimorsus* OMP were analysed and ranked according to their antigenic scores, which demonstrates its importance for vaccine development.

2.3 MHC-I binding predictions

MHC-I binding prediction is one of the tools provided by IEDB.org (Andreatta and Nielsen, 2016; Lundegaard et al. 2008). In this analysis, the following criteria were used to predict MHC-I binding epitopes. NetMHCpan 4.1 (EL) was selected as the prediction method. Humans were the MHC source species. All alleles were selected with the 9 and 10-mer lengths as the default settings. The epitopes were ranked based on descending scores.

2.4 MHC-II binding predictions

To predict MHC class II binding epitopes, the IEDB prediction tool had been used, which provides a comprehensive platform for computational epitope identification. Specifically, the NetMHCIIpan 4.1 EL algorithm was preferred as the epitope prediction model.

NetMHCIIpan 4.1 EL predicts binding affinities of peptide sequences to multiple human leukocyte antigen (HLA) class II alleles by integrating peptide sequence motifs and structural information. The model takes into account the peptide length variations and it was designed to improve prediction accuracy by integrating both eluted ligand and binding affinity data (Wang et al. 2008). The predictions were performed for a predefined set of HLA class II alleles.

All predicted epitopes were ranked based on their percentile scores, with lower percentile values indicating higher binding affinities. Only peptides falling within the top 2% rank were considered for further immunogenicity assessment, as suggested by previous benchmarking studies (Wang et al. 2010).

2.5 Prediction of T-cell epitopes and cleavage sites

Neural network-based prediction servers were used for the detection of cleavage sites (NetChop) and T-cell epitopes (NetCTL and NetCTLpan). NetChop is a predictor of proteasomal processing based upon a neural network (Nielsen et al. 2005). NetCTL and NetCTLpan are predictors of T cell epitopes along a protein sequence. It also employs a neural network architecture (Larsen et al. 2007). For the detection of the possible T-cell epitopes, all available twelve supertype alleles on NetCTL were used and the following filters were applied to each supertype: weight on C terminal cleavage: 0.15; weight on TAP transport efficiency: 0.05; threshold: 0.75. For the prediction of possible cleavage sites on the protein, the C-term 3.0 method was used, and a threshold value of 0.5 was used on NetChop.

2.6 B-cell epitope prediction on protein sequence

For B-cell epitope prediction, IEDB Analysis Resources (BepiPred 2.0, ElliPro and ABCpred tools) are preferred due to their effectiveness. Each tool uses specific algorithms and threshold values to identify sequences that can generate an immune response in our body. The IEDB Analysis Resource provides tools for predicting linear and conformational epitopes (Larsen et al. 2006). The BepiPred-2.0 server predicts B-cell epitopes from a protein sequence, using a Random Forest algorithm trained on epitopes and non-epitope amino acids determined from crystal structures (Jespersen et al. 2017). ElliPro predicts linear and discontinuous antibody epitopes based on a protein antigen's 3D structure (Ponomarenko et al. 2008). ABCpred server is based on machine learning techniques using fixed length patterns, to predict B-cell epitopes on an antigenic sequence (Saha and Raghava, 2006a). Together, these servers provide useful approaches to analyse antigenic features. ABCPred was employed using default settings, with a threshold value of 0.51 to obtain more precise predictions. ElliPro analysis was conducted by uploading the PDB file of *C. canimorsus* (fasta sequence of OMP was searched via alpha fold)(Jumper et al. 2021). Minimum score and maximum distance (Angstrom) parameters were used with default settings of 0.5 and 6, respectively.

2.7 Immunogenicity

The key property of *C. canimorsus* is its ability to produce an immunogenic response that results in the activation of T-cells. To identify the immunogenicity of OMP, ten distinct peptide sequences determined in MHC-I binding prediction (Table-1) were used by following the methodology outlined by Calis et al. (2013). In this stage of the research, selected immunogenic peptide sequences were analysed and ranked based on their immunogenicity score. These scores were calculated using the default settings where first, second, and C-terminus amino acids are masked.

2.8 Predictions of signal peptides within the protein sequence

Signal peptides play a critical role in the pathogenicity of microbial species and are of great importance for immune recognition by T and B cells (Owji et al. 2018). Signal peptide predictions were made on SignalP 6.0, server that predicts the presence of signal peptides and the location of their cleavage sites in proteins (Teufel et al. 2022). For the detection of signal peptides, the organism was chosen as others; the output format was set to long to view the signal peptides diagram, and the model mode was chosen as slow for an accurate result.

2.9 Population coverage

After predicting MHC class I and II binding epitopes for the OMP (Figure-1), a population coverage analysis was conducted on IEDB Population Coverage server to determine the percentage of individuals who could recognize specific epitope/HLA combinations for Türkiye and globally (Bui et al. 2006). While more than 380 MHC alleles were used for the global analyses, HLA-DQA1*01:01, HLA-DQA1*02:01, HLA-DQA1*03:01, HLA-DQA1*04:01, HLA-DQA1*05:01, HLA-DQA1*06:01, HLA-DQB1*02:01, HLA-DQB1*03:01, HLA-DQB1*04:01, HLA-DQB1*05:01, HLA-DQB1 *06:09, HLA-DRB1*01:01, HLA DRB1*03:01, and HLA-DRB1*04:01 alleles were used for the population coverage of Türkiye. Two analyses were performed separately for combined MHC classes (MHC-I and II), using the critical sixteen immunogenic epitopes (ten for MHC-I and six for MHC-II). The following filters were applied for IEDB Population Coverage of Türkiye: number of epitopes: 16; query by: area country ethnicity; calculation options: class I and II combined; selected area or population: Türkiye. For global, the number of epitopes was set as 16; query by: area country ethnicity; calculation options: class I and II combined; selected area or population: world.

2.10 Kolaskar and Tongaonkar antigenity

The Kolascar and Tongaonkar Antigenity method is a semi-empirical approach preferred to predict antigenic determinants, or B-cell epitopes, on protein antigens. This method uses the physicochemical properties of amino acid residues, such as hydrophilicity, accessibility, and flexibility, along with their frequencies of occurrence in experimentally determined epitopic regions. By analyzing these parameters, the method identifies potential antigenic sites within a protein sequence. In the present study, the Kolaskar and Tongaonkar Antigenicity method to was applied OMP to identify immunogenic regions (Kolaskar and Tongaonkar, 1990).

2.11 Prediction of antigenity of protein sequence

The allergenicity of protein sequences was predicted using two bioinformatics tools, namely AlgPred and Allermatch-TM. Algpred allows prediction of allergens based on similarity of known epitope with any region of the protein, and this tool integrates motif-based detection, SVM-based classification, and epitope mapping to predict allergenic proteins (Saha and Raghava, 2006b). Input sequences were analyzed for the presence of IgE-binding motifs and allergen representative peptides. AllermatchTM uses a FASTA-based search to compare protein sequences against known allergen databases (AllergenOnline)(Fiers et al. 2004).

3 Results

3.1 Determination of vaccine potential of *C. canimorsus* OMP via VaxiJen v2.0 and 3.0.

The overall predicted value for the Protective Antigen was found to be 0.6049, when the VaxiJen 2.0 version was used. On the other hand, VaxiJen 3.0 version gives more accurate output by stating "Probable IMMUNOGEN with a probability of 100%.".

3.2 MHC-I binding predictions

OMP was checked for MHC-I binding epitope predictions. The results related to the epitope analysis for MHC-I are presented in Table-1. According to MHC-I analysis guidelines, the peptides found were ranked based on their scores. The linear peptides with the best scores greater than 0.9 are shown in Table-1. All available alleles were selected under the default settings in IEDB MHC-I epitope prediction. According to the results, the maximum score was associated with "QEIGKLKKY". This sequence was also found for HLA-B*44:03. The allele frequency of HLA-B*44:03 was also checked via the allele frequencies database (Gonzalez-Galarza et al. 2020). The people who carry HLA-B*44:03 alleles are shown in Figure-1. Although Figure-1 shows the worldwide distribution of the HLA-B*44:03 alleles, the maximum percentage of individuals with the allele is 23.2, found in India East UCBB. Allele Frequency was also found to be 0.125.

Table 1 The MHC-I epitope prediction results for *C. canimorsus* OMP.

Allele	Sequence Number	Start	End	Length	Peptide	Score	Peptide Rank
HLA-B*44:03	3	15	23	9	QEIGKLKKY	0.994842	0.01
HLA-B*44:02	3	15	23	9	QEIGKLKKY	0.993719	0.01
HLA-A*68:01	4	15	23	9	EVVDEKAQR	0.981630	0.01
HLA-B*15:01	1	3	11	9	KQVIHSVVF	0.968909	0.01
HLA-A*11:01	1	15	23	9	ATTGLFAQK	0.961922	0.01
HLA-A*03:01	3	45	53	9	RLILRVINK	0.957827	0.01
HLA-B*15:01	1	21	29	9	AQKNMRIGY	0.948779	0.01
HLA-B*35:01	1	34	42	9	FILENVEEY	0.922386	0.03
HLA-B*44:03	1	40	49	10	EEYKIASAQF	0.906822	0.04
HLA-A*02:06	2	34	42	9	AILEHNLRV	0.900030	0.04

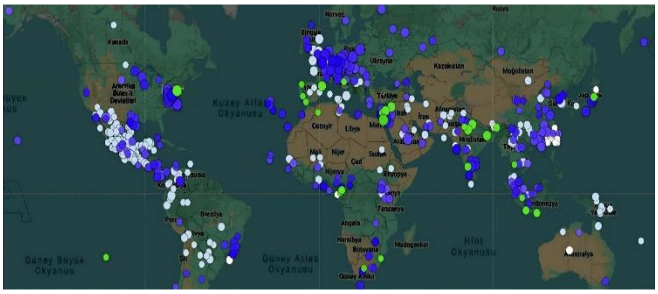

Fig. 1 Worldwide allele frequency of HLA-B*44:03 via Allele Frequencies.

3.3 MHC-II Epitope Binding Prediction Results

MHC-II Epitope binding predictions were carried out via IEDB.org. The best six results with scores higher than 0.7 are shown in Table-2. The results showed that the maximum score was found for "FNAVQEIGK" with respect to the allele "HLA-DRB5*01:01". This result is for HLA-DR in default settings. No data were found for HLA-DRB5*01:01 in the allele frequency database. However, the data was found for HLA-DRB1*07:01. This allele was very common in Central African Republic (Aka Pygmy) with 42.9% of individuals having the allele and its frequency being 0.2440. Figure-2 demonstrates the worldwide distribution of HLADRB1*07:01 alleles by using different colored markers, to distinguish various HLA alleles across different geographic regions.

Table 2 MHC-II epitope binding prediction results for OMP.

Allele	Start	End	Length	Core Sequence	Peptide Sequence	Score	%Rank
HLA-DRB5*01:01	128	142	15	FNAVQEIGK	DQVFNAVQEIGKLKK	0.8243	0.10
HLA-DRB1*07:01	38	52	15	YKIASAQFA	NVEEYKIASAQFAQQ	0.8171	0.43
HLA-DRB1*07:01	39	53	15	YKIASAQFA	VEEYKIASAQFAQQV	0.8066	0.45
HLA-DRB1*03:01	192	206	15	EVVDEKAQR	YDFEVVDEKAQRKAE	0.7268	1.20
HLA-DRB1*07:01	37	51	15	YKIASAQFA	ENVEEYKIASAQFAQ	0.7165	0.92
HLA-DRB1*15:01	97	111	15	LRVYQQEKF	EHNLRVYQQEKFGAE	0.7097	0.88

Table 3 T-cell epitopes with their prediction score.

Supertypes	#	Peptide Sequence	Predicted MHC Binding Affinity	Rescale Binding Affinity	C Terminal Cleavage Affinity	Transport Efficiency	Predictions Score
A1	149	KSDVSMLYS	0.3685	2.5024	0.0123	2.4410	2.3822
B44	135	QEIGKLKKY	0.2469	1.7072	0.9356	2.9180	1.9934
A3	15	ATTGLFAQK	0.6121	1.8229	0.9243	0.5990	1.9914
B27	228	QRLQEREQK	0.3227	1.5939	0.5686	0.6530	1.7118
B62	3	KQVIHSVVF	0.5345	1.3668	0.8092	2.8960	1.6330
A26	34	FILENVEEY	0.4460	1.2943	0.9988	2.8370	1.5859
B8	1	MKKQVIHSV	0.2751	1.3318	0.9660	0.4070	1.4971
B39	6	IHSVVFLLL	8.9900	1.2662	0.9987	1.0280	1.4674
A24	41	EYKIASAQF	0.8296	1.1351	0.9940	2.4260	1.4055
A2	34	AILEHNLRV	0.4226	1.0114	0.9941	0.6140	1.1912
B7	87	KDREQEIAI	0.2624	0.7277	0.1500	0.3920	0.7698
B58	139	KLKKYDFIF	0.1410	0.4877	0.9946	2.6290	0.7683

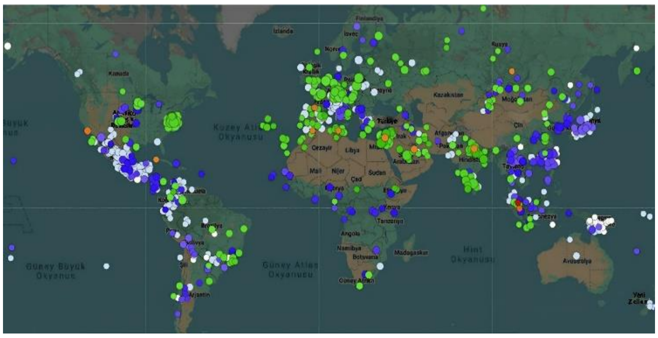

Fig.2. Worldwide allele frequency of HLA-DRB1*07:01 via Allele Frequencies

3.4 Prediction of T-cell epitope and cleavage sites

The data given in Table-3 demonstrate the predicted T-cell epitopes and their respective prediction scores for each supertype in detail. These scores contain multiple parameters such as MHC binding affinity, rescale binding affinity, C-terminal cleavage affinity, and TAP transport efficiency, which can be understood well from the overall prediction score. The data show the variability in peptide sequences and their corresponding immunogenic potential for each supertype. Supertypes with a high prediction score are likely to be recognized effectively by T-cells. All the peptide sequences for each supertype are ordered according to their prediction score, and the peptides with the highest scores for each supertype are placed in Table-3.

Cleavage predictions obtained from NetChop provide critical information about the immunogenic potential of the protein and its ability to be a candidate for vaccine development. Figure-3 demonstrates the predicted proteasomal cleavage sites of the OMP. While the green regions remain under observation, further analysis is conducted to determine their impact. The prediction score for the cleavage above the threshold (score ≥ 0.5) represents positive cleavage predictions, while pink regions, where the prediction score is below the threshold, suggest lower probabilities. The distribution of cleavage sites spread along the protein sequence with several high-scoring regions.

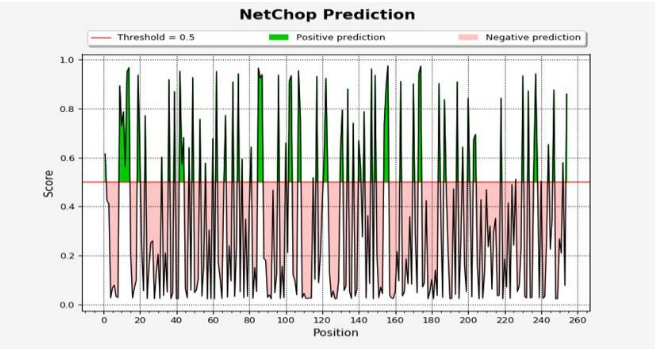

Fig. 3 Possible proteasomal cleavage sites of *C. canimorsus* OMP.

3.5 B-cell epitope predictions

For the prediction of potential B-cell epitopes, three immunoinformatics tools (BepiPred 2.0, ElliPro and

ABCpred) were used for the analysis of *C. canimorsus* OMP. Table-4 displays different probable epitope regions identified using various tools. Amino acid sequences with the prediction score over the threshold value were considered as potential B-cell epitopes. ABCPrep analysis identified multiple epitopes, with the highest-scoring peptide as KNMRIGYVDMDFILEN (0.91). Additionally, epitopes with high scores were: KESAEDRNKSMAELLK (0.86), EIAILEHNLRVYQQEK (0.84), and PELIKDREQEIAILEH (0.81). ElliPro analysis of the OMP of *C. canimorsus* revealed valuable information about predicted B cell epitopes. Two linear epitopes were identified, with lengths of 24 and 15 amino acids, respectively. The first epitope with the residues 1-24 (MKKQVIHSVVFLLLATTGLFAQKN) exhibits a high score of 0.791, indicating strong antigenicity. The second epitope consisting of residues 172-186 (NKKESAEDRNKSMAE) has a lower score of 0.583. BepiPred identified two potential longer linear B-cell epitopes, 82 and 72 residues long, and four potential shorter linear B-cell epitopes, 5, 1, 2, and 11 residues long, with specific sequences. The yellow area in Figure-4 demonstrates possible epitope regions of the amino acid sequences with the prediction scores over 0.5. Green regions, on the other hand, belong to the peptides with the lowest prediction scores.

Table 4 Linear B-cell epitope predictions and corresponding scores of *C. canimorsus* OMP using BepiPred, ABCPred, and ElliPro.

B-Cell Epitope Prediction Tools	Probable Linear B-Cell Epitope Sequences and Scores
BepiPred 2.0	QHNLS
	L
	RVINKKESAEDRNKSMAELLKENYDFEVVDEKAQRKAEIEQARQQRAQEREKQREAARQQRLQEREQKKKEAEERKKKLEEQ
	QD
	AQQVEQWEAEIEKRKTKIEAEKNKLEAEKPLLTPELIKDREQEIAILEHNLRVYQQEKFGAENGEYVKQKFMLAKP
	ENVEEYKIASA
ABCPred	KNMRIGYVDMDFILEN (0.91)
	KESAEDRNKSMAELLK (0.86)
	EIAILEHNLRVYQQEK (0.84)
	PELIKDREQEIAILEH (0.81)
	AEIEKRKTKIEAEKNK (0.81)
	EQKKKEAEERKKKLEE (0.81)
	DFIFEKSDVSMLYSNN (0.79)
	LKENYDFEVVDEKAQR (0.77)
	EAEKNKLEAEKPLLTP (0.74)
	KAEIEQARQQRAQERE (0.73)
	GAENGEYVKQKFMLAK (0.72)
	NLRVYQQEKFGAENGE (0.70)
	GKLKKYDFIFEKSDVS (0.70)
	LAKPIQDQVFNAVQEI (0.70)
ElliPro	MKKQVIHSVVFLLLATTGLFAQKN (0.79)
	NKKESAEDRNKSMAE (0.58)

Fig. 4 BepiPred positions of B-cell epitopes on OMP.

Seven discontinuous (conformational) epitopes were predicted with scores ranging from 0.975 (highest) to 0.574 (lowest) via Elliport (Table-5). The top-ranked discontinuous epitope consists of four residues (L247, E248, Q250, K251) with a score of 0.975. The most extensive epitope, consisting of 36 residues (A66–A101), has a score of 0.768. 3D structures for either continuous (linear) or discontinuous epitopes are shown in Figure-5 and Figure-6.

Table 5 Discontinuous B-cell epitopes of OMP predicted via ElliPro.

#	Residues	# Residues	Score
1	A:L247, A:E248, A:Q250, A:K251	4	0.975
2	A:Q235, A:K236, A:E239, A:A240, A:E241, A:R243, A:K244	7	0.897
3	A:Q4, A:V5, A:I6, A:H7, A:S8, A:V9, A:V10, A:F11,A:L12, A:L13, A:L14, A:A15, A:T16, A:T17,	19	0.795
4	A:G18, A:L19, A:F20, A:A21, A:Q22,A:K66, A:I67, A:E68, A:A69, A:E70, A:K71, A:N72, A:K73, A:L74, A:E75,A:A76, A:E77, A:K78, A:P79, A:L80, A:L81, A:T82, A:P83, A:E84,A:L85, A:I86, A:K87, A:D88, A:R89, A:E90, A:Q91, A:E92, A:I93,A:A94, A:I95, A:L96, A:E97, A:H98, A:N99, A:R101, A:V102	36	0.768
5	A:A215, A:R218, A:E219, A:K220, A:E223, A:A224, A:A225, A:R226,A:Q227, A:Q228, A:R229, A:L230, A:Q231, A:R233	14	0.683
6	A:E136, A:K173, A:K174, A:S176, A:A177, A:E178, A:D179,A:R180, A:N181, A:K182, A:S183, A:M184, A:A185, A:E186	14	0.598
7	A:A58, A:E59, A:I60, A:E61, A:K62, A:R63, A:K64, A:T65, A:L100	9	0.574

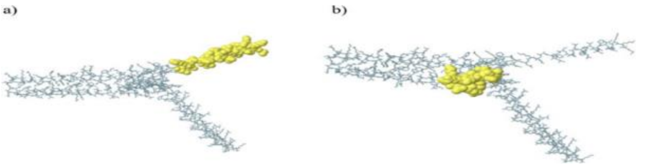

Fig. 5 3D structure of the predicted linear B-cell epitope regions for (a) the peptide sequence "MKKQVIHSVVFLLLATTGLFAQKN" (b) the peptide sequence "NKKESAEDRNKSMAE" in Table-4).

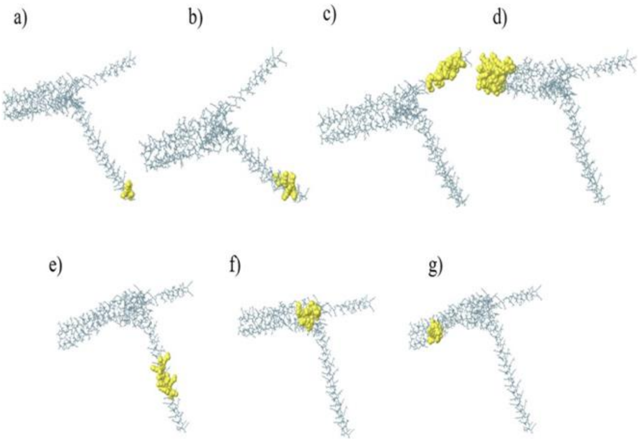

Fig. 6 3D structure of the location of predicted discontinuous B-cell epitopes of (a) sequence#1,(b) sequence#2, (c) sequence#3, (d) sequence#4, (e) sequence#5, (f) sequence#6, (g) sequence#7 via Ellipro.

3.6 Immunogenicity

The results for *C. canimorsus* OMP are given in Table-6. Those results demonstrate the probabilities of the different peptide sequences found in the OMP in generating an immune response when it enters the body. The peptide sequence "FILENVEEY" has the highest score (0.27271) meaning that it has a strong potential to generate an immune response. Similarly, peptides like RLILRVINK (0.22984) and AILEHNLRV (0.14344) demonstrate moderate immunogenic potential. Peptides with negative scores such as QEIGKLKKY (-0.45114) and EEYKIASAQF (-0.24089) have a lower probability of generating a significant immune response. The peptides with zero/near-zero scores, AQKNMRIGY (-0.06667), indicate a neutral activity, means that the peptide is unlikely to generate a strong immune response.

Table 6 Immunogenicity of MHC-I binding epitopes of *C. canimorsus* OMP.

Peptide	Length	Score
FILENVEEY	9	0.27271
RLILRVINK	9	0.22984
AILEHNLRV	9	0.14344
ATTGLFAQK	9	0.11144
KQVIHSVVF	9	0.08205
AQKNMRIGY	9	-0.06667
EVVDEKAQR	9	-0.10444
EEYKIASAQF	10	-0.24089
QEIGKLKKY	9	-0.45114
QEIGKLKKY	9	-0.45114

3.7 Prediction of signal peptides within protein sequence

Proteins containing signal peptides are commonly involved in virulence mechanisms and the SignalP 6.0 prediction diagram for the *C. canimorsus* OMP demonstrates the pres-ence of a Sec/SPI signal peptide (Antelmann et al. 2001). The initial segment of the signal peptide (positions 1–5) is high-lighted with a high probability for the N-region (Figure-7).

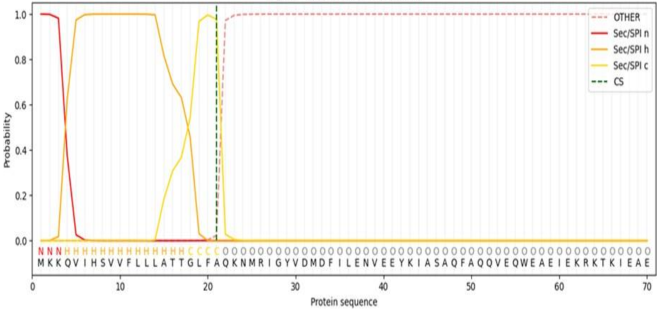

Fig. 7 Possible signal peptides on *C. canimorsus* OMP

This positively charged region plays a critical role in directing the protein to the secretion machinery. Following the N-region, the graph indicates a highly hydrophobic segment (positions 5-15), characteristic of the H-region. This hydrophobic side anchors the signal peptide in the membrane during translocation. The cleavage site was marked at positions 21-22, and the probability of this prediction is 0.9767. Beyond those positions, the probability passes to the "Other" category. While the probability of the sequence not having a signal peptide, categorized as 'Other,' is 0.0005, the likelihood for a classical signal peptide, categorized as 'Sec/SPI,' is 0.9986. The probability for lipoprotein signal peptide (Sec/SPII) is 0.0003. The probability of the other three types (Tat/SPI, Tat/SPII and Sec/SPIII) is 0.0002.

3.8 Population coverage

The results demonstrated that 94.57% of the population of Türkiye is covered by at least one epitope/HLA combination for combined MHC class I and II epitopes which means that the selected epitopes and HLA combinations affect large population coverage. On average, an individual recognizes approximately 25.2 epitope/HLA combinations. The minimum number of epitope/HLA combinations required per individual to achieve 90% population coverage (PC90) is 15.

Due to the absence of available allele frequency data for HLA-DRB5*01:01 for MHC-II, the population coverage analysis was conducted without including this allele. Despite this limitation, the global population coverage was calculated to be 96.45% which indicates that nearly the whole global population can recognize at least one epitope/HLA combination. On average, an individual can recognize 22.97 epitope/HLA combinations. Additionally, the PC90 value (the minimum number of epitope/HLA combinations required to cover 90% of the population) was found to be 13.34.

3.9 Kolaskar & Tongaonkar antigenity determination

Several peptide regions with high antigenicity scores (Table-7) have been identified in the Kolaskar and Tongaonkar antigenicity analysis for the OMP of *C. canimorsus*. The table highlights residues with scores exceeding 1.005. Among the top candidates, sequences such as "VFVLLLA" (1.239), "SVVFLLL" (1.231), and "VIHSVVF" (1.216) exhibit the highest scores.

The graphical representation (Figure-8) shows a distinction between high antigenicity regions (yellow) and less antigenic areas (green). Also, regions with residues from positions 9–15 and 165–171 demonstrate high antigenicity.

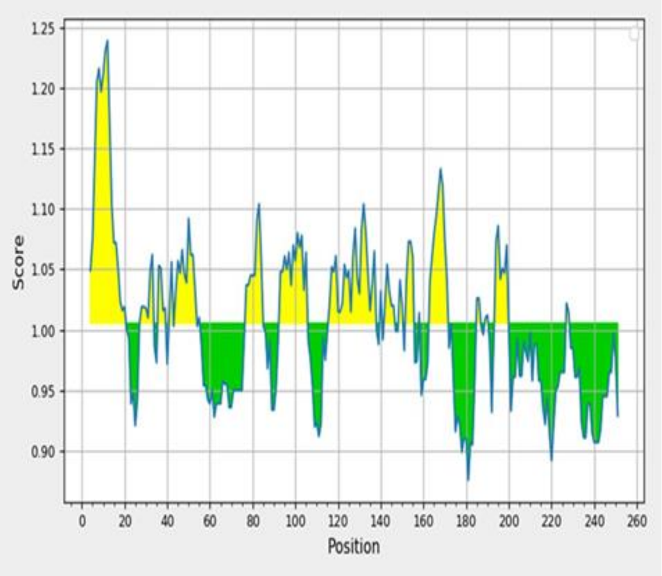

Fig. 8 Kolaskar & Tongaonkar antigenicity graphic of OMP.

Table 7 Predicted antigenic residues of OMP via Kolaskar & Tongaonkar Antigenicity.

Position	Residue	Start	End	Peptide	Score
12	L	9	15	VVFLLLA	1.239
11	F	8	14	SVVFLLL	1.231
8	S	5	11	VIHSVVF	1.216
10	V	7	13	HSVVFLL	1.211
7	H	4	10	QVIHSVV	1.205
9	V	6	12	IHSVVFL	1.197
13	L	10	16	VFLLLAT	1.171
6	I	3	9	KQVIHSV	1.140
168	L	165	171	RLILRVI	1.133
169	R	166	172	LILRVIN	1.119
167	I	164	170	SRLILRV	1.113
83	P	80	86	LLTPELI	1.104
132	N	129	135	QVFNAVQ	1.104
14	L	11	17	FLLLATT	1.103
166	L	163	169	LSRLILR	1.094
50	A	47	53	AQFAQQV	1.092
82	T	79	85	PLLTPEL	1.091
195	E	192	198	YDFEVVD	1.086
128	D	125	131	PIQDQVF	1.084
131	F	128	134	DQVFNAV	1.083
101	R	98	104	HNLRVYQ	1.080
133	A	130	136	VFNAVQE	1.080
165	R	162	168	NLSRLIL	1.080

3.10 Allergenity

Allergenicity of the protein sequences was analysed by using two different tools. AlgPred identified 85.64% (positive predictive value) and 67.96% (negative predictive value) of the sequences as potential allergens with a score of 1.1542393, based on the presence of IgE binding epitopes and motif analysis.

In AllerMatch, the sequence of OMP shows significant matches to known allergens, as indicated by the E-values (0.058) and the close identity percentages (20–26%). These results suggest that the sequence is likely allergenic, particularly due to its similarity to known allergens such as paramyosin from *Anisakis simplex* (*Ani s 2*) and *Anisakis pegreffii*.

4 Discussion

This investigation developed a multiepitope-based vaccine design against *C. canimorsus* through immunoinformatic approaches. The diseases caused by contact with pets such as a bite or lick, negatively affect patients' general health conditions who do not take any treatment (Beauruelle et al. 2022). It is well demonstrated that nearly the whole global population can develop immunogenicity against the epitope/HLA combination for *C. canimorsus* OMP. In a review written by Zajkowska et al. (2016), the danger of underestimating *C. canimorsus* infection is very well explained. Moreover, the authors mentioned that this bacterium could pose a significant risk for patients with asplenia, cirrhosis, or alcohol abuse. Since these conditions are not only valid for dog bites, but also for cat bites, vaccination might be necessary for some patients. Due to the conditions of the COVID-19 pandemic, the prevalence of pet ownership has increased all around the world (Ho et al. 2021). Therefore, even if the negative effects have not so far been published, possible peptide-based vaccines may be required for pet owners in the near future due to the increased number of dogs and cats as pets. According to a very recent case study reported by Yang et al. (2021), *Capnocytophaga*-based blebitis was reported in a case involving close contact with a dog including face licking (Yang et al. 2021). *C. canimorsus*-based endocarditis (Sandoe, 2004), meningitis and bacteraemia (Galles et al. 2020; Hannon et al. 2020, and purpura fulminans (Parisi and Pihán, 2023) were also discussed in the scientific literature. Due to the lack of any available specific vaccine for the bacterium, the latter disorders can be observed in people who have pets (Butler, 2015). Nowadays, immunoinformatics provides important contributions to the development of new and efficient vaccines (Kushwaha et al. 2024). This approach is suitable for the principles of reverse vaccinology and immunoinformatics, and it enables the identification of immunogenic targets by using computational tools (Masum et al. 2024). Such methodologies have a great potential to accelerate vaccine design. The ability to predict which proteins are most likely to generate immune responses allows researchers to increase productivity in discovering vaccines for various pathogenic species through the use of these tools. The results showed that *C. canimorsus* OMPs have demonstrated significant potential as vaccine and diagnostic candidates due to their immunogenic property. The epitope-rich regions of OMP are critical for their interaction with host immune cells, because those regions are the ones by which the bacterium is detected and recognized by T and B cells (Li and Wu, 2021). Krishnan et al. (2021) have also used similar tools for the development of T cell multi epitope dengue peptide vaccine. They studied non structural proteome. The authors also reported that the epitopes HTLWSNGVL and FTTNIWLKL are the most stable among the epitopes studied in their paper. This approach showed that the probability of the interaction between immune cells, like T and B cells, with epitopes has increased, leads to a stronger immune response. In this study, we have highlighted the structural and antigenic properties of *C. canimorsus* OMP. In this investigation, different *Capnocytophaga* genus members were also compared. The sequence of the OMPs of *C. canimorsus* (A0AAD0EAI0) was compared with those of *C. gingivalis* (A0A250FNB1) and *C. cynodegmi* (A0A250E913). Multiple sequence alignment analysis (Figure-9) revealed that different species within the genus *Capnocytophaga* may show a different amino acid sequence trend.

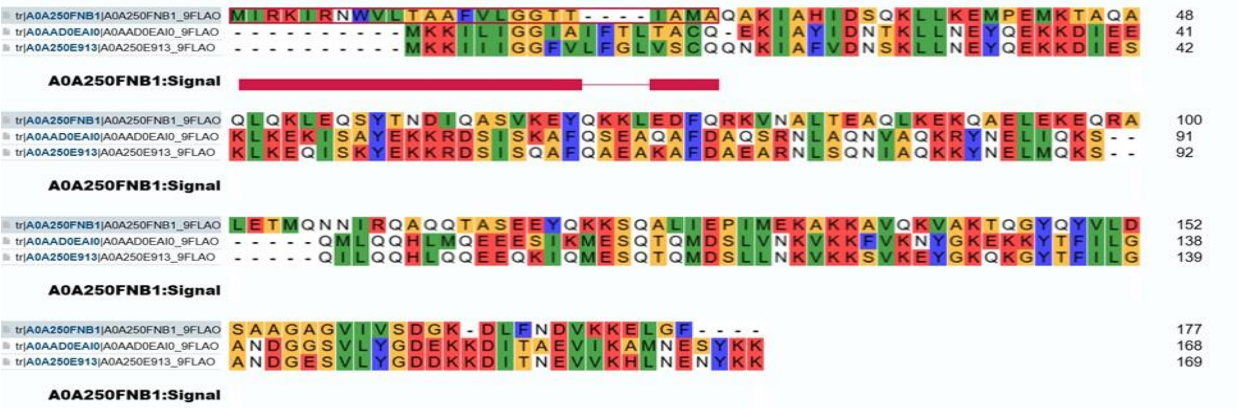

```
tr|A0A250FNB1|A0A250FNB1_9FLAO MIRKIRNWVLTAAFVLGGTT----IAMAQAKIAHIDSQKLLKEMPEMKTAQA  48
tr|A0AAD0EAI0|A0AAD0EAI0_9FLAO ----------MKKILIGGIAIFTLTACQ-EKIAYIDNTKLLNEYQEKKDIEE  41
tr|A0A250E913|A0A250E913_9FLAO ----------MKKIIIGGFVLFGLVSCQQNKIAFVDNSKLLNEYQEKKDIES  42

A0A250FNB1:Signal

tr|A0A250FNB1|A0A250FNB1_9FLAO QLQKLEQSYTNDIQASVKEYQKKLEDFQRKVNALTEAQLKEKQAELEKEQRA 100
tr|A0AAD0EAI0|A0AAD0EAI0_9FLAO KLKEKISAYEKKRDSISKAFQSEAQAFDAQSRNLAQNVAQKRYNELIQKS--  91
tr|A0A250E913|A0A250E913_9FLAO KLKEQISKYEKKRDSISQAFQAEAKAFDAEARNLSQNIAQKKYNELMQKS--  92

A0A250FNB1:Signal

tr|A0A250FNB1|A0A250FNB1_9FLAO LETMQNNIRQAQQTASEEYQKKSQALIEPIMEKAKKAVQKVAKTQGYQYVLD 152
tr|A0AAD0EAI0|A0AAD0EAI0_9FLAO -----QMLQQHLMQEEESIKMESQTQMDSLVNKVKKFVKNYGKEKKYTFILG 138
tr|A0A250E913|A0A250E913_9FLAO -----QILQQHLQQEEQKIQMESQTQMDSLLNKVKKSVKEYGKQKGYTFILG 139

A0A250FNB1:Signal

tr|A0A250FNB1|A0A250FNB1_9FLAO SAAGAGVIVSDGK-DLFNDVKKELGF----                       177
tr|A0AAD0EAI0|A0AAD0EAI0_9FLAO ANDGGSVLYGDEKKDITAEVIKAMNESYKK                       168
tr|A0A250E913|A0A250E913_9FLAO ANDGESVLYGDDKKDITNEVVKHLNENYKK                       169

A0A250FNB1:Signal
```

Fig. 9 Multiple sequence alignment analysis of *C. canimorsus* (A0AAD0EAI0), *C.gingivalis* (A0A250FNB1) and *C. cynodegmi* (A0A250E913).

Therefore, the vaccine developed based on *C. canimorsus* OMP may not show enough protection due to sequence differences. The antigenic potential of the *C. canimorsus* OMP was evaluated by using the VaxiJen v2.0, and 3.0 bioinformatics platform (Dimitrov et al. 2020). For this study, the protein sequences of *C. canimorsus* OMPs were input into the VaxiJen system. The antigenicity of the proteins has been calculated using the algorithm to analyze factors such as hydrophobicity, molecular weight, and amino acid composition. Based on this analysis, a ranked list of potential antigens has been created and the antigens that contain proteins with the highest scores were accepted as the most likely candidates for vaccine development. Notably, VaxiJen 2.0 showed significantly different results for three species. Although overall prediction of the protective antigen value was found to be 0.3977 for *C. gingivalis*, it was estimated to be 0.2776 and 0.3030 for *C. canimorsus* and *C. cynodegmi*, respectively. These results clearly showed that the selection of the correct sequence for immunoinformatics analysis is of great importance. The findings of our study demonstrated that the immunoinformatics approaches for designing multiepitope-based vaccines could be applied for *C. canimorsus* infections after *in vitro* and *in vivo* experiments. Joluvet-Gougeon et al. (2007) recommended that Imipenem /cilastatin, clindamycin, or beta-lactamase inhibitor combin-ations be used for antimicrobial therapy strategy against *Capnocytophaga* infections. Sandoe (2024) reviewed 12 cases of endocarditis caused by *C. canimorsus*, and the review underlined the importance of penicillins for the treatment of *C. canimorsus* infections. However, three cases were reported as deaths. Although most of the patients gave positive results after penicillin treatment, nonspecific symptoms of *C. canimorsus* can cause serious conditions such as septic shock and multiorgan failure (Meyer et al. 2021). According to a recent study on *Capnocytophaga* spp., minimum inhibitory concentrations (MIC) of various antibiotics and resistance genes were studied for 6 species under genus *Capnocytophaga* (Umeda et al. 2024). The researcher reported very low MIC values for imipenem and amoxicillin/clavulanic acid. It is very important to note that Umeda et al. (2024) reported a mutation in the quinolone resistance-determining region of gyrA .

As mentioned in the present study, there is a significant sequence variability in the OMPs among *Capnocytophaga* species which makes it difficult to identify vaccine targets. The variability observed in the multiple sequence alignment demonstrates the importance of selecting appropriate antigenic sequences for immunoinformatic analysis and vaccine development. Several factors are related to the absence of a traditionally developed vaccine against *C. canimorsus* infections. Primarily, the relatively low incidence of serious infections, reported at 0.67 infections per million, poses a significant challenge (Van Dam and Jansz, 2011). Furthermore, the genetic diversity of these pathogens, insufficient knowledge of host-pathogen interactions, lack of suitable cell lines, and absence of reliable animal models further block the traditional vaccine development efforts (Sunita et al. 2020). The absence of a specific vaccine against *C. canimorsus* can be attributed to several factors such as immunoinformatics-based studies have shown positive results for other related bacterial pathogens. For example, a multi-epitope vaccine that targets *C. gingivalis*, one of the bacterial species that is closely related within the same genus, was recently developed using similar methods (Repac et al. 2021). This shows the benefit of using computational tools to accelerate vaccine design. Nevertheless, the antigenic variations between *C. gingivalis* and *C. canimorsus* show that cross-protection will be insufficient due to the difference in the peptide sequences; and this demonstrates the critical need for species-specific vaccine development. A previous study also demonstrates that *C. canimorsus* OMP have relatively lower antigenic scores compared to other *Capnocytophaga* species. This explains the need for more research to improve vaccine efficacy. While immunoinformatics provides a strong infrastructure for the identification of vaccine candidates, there are several steps that should be taken to translate these findings into practical applications. *In vitro* and *in vivo* studies of predicted epitopes have great importance because experimental data help to confirm their immunogenicity. Furthermore, it is also crucial to understand the effectiveness and safety of the identified epitopes and confirm that those epitopes can generate a strong immune response without causing negative effects. Furthermore, verification of the epitopes that can generate a strong immune response without negative effects like immunopathology, autoimmunity, or hypersensitivity reactions is crucial for understanding their efficacy and safety (Cusick et al. 2012). While improving the stability, immunogenicity, and targeted delivery of the vaccine can-didates, researchers should carefully consider the combination of adjuvants and delivery systems to apply these findings. Adjuvants such as aluminium salts or saponins can increase the host immune response and activate both humoral and cellular immunity (Wang, 2021). Furthermore, designing appropriate vaccine delivery systems, such as nanoparticles, liposomes, or viral vectors, can protect the epitopes from degradation and maintain their release (Pati et al. 2018). These systems enhance their overall effectiveness. To determine the safety and immunogenicity of the vaccines, clinical tests are useful as they provide direct results on their effects on humans (Gebre et al. 2021; Vinusha and Girish, 2024). In addition, these tests helpful in determining the cross protective potential of vaccines against different pathogens. This is because different pathogens have different antigenicity and this difference may affect the efficacy of the vaccine (Warimwe et al. 2021). These varieties can also be easily detected and would be very useful in aiding the design of multi-epitope vaccines. This can be accomplished by using bioinformatics tools such as structural modeling and molecular docking, along with experimental data (Yurina and Adianingsih, 2022). Furthermore, to overcome the common issues that may be encountered when transferring from small scale to large scale manufacturing, it is important to focus on strong quality control measures and production plans for vaccine candidates that move from research to market (Buckland et al. 2024). During the manufacturing process, some of the important procedures are optimizing the protocols, production costs and following the guidelines of Good Manufacturing Practices (GMP) for the vaccines to be used in clinics and by patients (Silva et al. 2022).

5 Conclusion

This investigation shows the possibility that *C. canimorsus* OMPs can be used as vaccine candidates, and it also underlines the role of immunoinformatics in vaccine design. Although there are several limitations such as antigenic variability and the rarity of *C. canimorsus* in vaccine literature, our findings offer a starting point for further investigation. Applying computational predictions with experimental data and new vaccine delivery systems, considering the increasing demand for preventive strategies, especially due to the rise in pet ownership and the resulting zoonotic diseases, would be useful.

Acknowledgements

The authors would like to thank Dokuz Eylül University for providing computer support.

CRediT authorship contribution statement

Levent Cavas: Conceptualization, Investigation, Methodology, Resources, Supervision, Validation, Writing – review and editing.

Atakan Vatansever: Data curation, Formal analysis, Investigation, Methodology, Software, Validation, Visualization, Writing – original draft.

Funding

This research did not receive any specific grant from funding agencies in the public, commercial, or not-for-profit sectors.

Declaration of competing interest

The authors declare that they have no known competing financial interests or personal relationships that could have appeared to influence the work reported in this paper.

Data availability

All data generated and analyzed during this study are included in this published article.

References

Ammerman SM (2017). The Evolution of Animals through Domestication and other Human Relationships: An Animal-Centered Approach (Doctoral dissertation, UCLA).

Andreatta M, Nielsen M (2016) Gapped sequence alignment using artificial neural networks: application to the MHC class I system. Bioinformatics 32: 511-517 doi.org/10.1093/bioinformatics/btv639

Antelmann H, Tjalsma H, Voigt B, Ohlmeier S, Bron S, van Dijl JM, Hecker M (2001) A proteomic view on genome-based signal peptide predictions. Genome Res 11: 1484-1502 doi.org/10.1101/gr.182801

Authority EFS (2024) The European Union One Health 2023 Zoonoses report. EFSA J 22: 9106 doi.org/10.2903/j.efsa.2024.9106

Bateman A, Martin MJ, Orchard S, Magrane M, Ahmad S, Alpi E, Bowler-Barnett EH, Britto R, Cukura A, Denny P, Dogan T (2023) UniProt: the universal protein knowledgebase in 2023. Nucleic Acids Res 51: 523-531 doi.org/10.1093/nar/gkac1052

Beauruelle C, Plouzeau C, Grillon A, Isnard C, Corvec S, Degand N, Jacquier H, Amara M, Mizrahi A, Diedrich T, Piau C, Farfour E, Bonzon L, Le Brun C, Walewski V, Bille E, Dortet L, Guillard T, Soismier N, Le Guen R, Morand P, de Ponfilly GP, Le Monnier A, Le Monnier A, Héry-Arnaud G (2022) *Capnocytophaga* zoonotic infections: a 10-year retrospective study (the French CANCAN study). Eur J Clin Microbiol Infect Dis 41: 581-588 doi.org/10.1007/s10096-022-04402-x

Bobo RA, Newton EJ (1976) A previously undescribed gram-negative bacillus causing septicemia and meningitis. Am J Clin Pathol 65: 564-569 doi.org/10.1093/ajcp/65.4.564

Buckland B, Sanyal G, Ranheim T, Pollard D, Searles JA, Behrens S, Pluschkell S, Josefsberg J, Roberts CJ (2024) Vaccine process technology—A decade of progress. Biotechnol Bioeng doi.org/10.1002/bit.28703

Bui HH, Sidney J, Dinh K, Southwood S, Newman MJ, Sette A (2006) Predicting population coverage of T-cell epitope-based diagnostics and vaccines. BMC Bioinformatics 7: 1-5 doi.org/10.1186/1471-2105-7-153

Butler T (2015) *Capnocytophaga canimorsus* : an emerging cause of sepsis, meningitis, and post-splenectomy infection after dog bites. Eur J Clin Microbiol Infect Dis 34: 1271-1280 doi.org/10.1007/s10096-015-2360-7

Calado CR (2022) Antigenic and conserved peptides from diverse Helicobacter pylori antigens. Biotechnol Lett 44: 535-545 doi.org/10.1007/s10529-022-03238-x

Calis JJ, Maybeno M, Greenbaum JA, Weiskopf D, De Silva AD, Sette A, Keşmir C, Peters B (2013) Properties of MHC class I presented peptides that enhance immunogenicity. PLoS Comput Biol 9:1003266 doi.org/10.1371/journal.pcbi.1003266

Coudert E, Gehant S, De Castro E, Pozzato M, Baratin D, Neto T, Sigrist CJ, Redaschi N, Bridge A (2023) Annotation of biologically relevant ligands in UniProtKB using ChEBI Bioinformatics 39: 793 doi.org/10.1093/bioinformatics/btac793

Cusick MF, Libbey JE, Fujinami RS (2012) Molecular mimicry as a mechanism of autoimmune disease. Clin Rev Allergy Immunol 42: 102-111 doi.org/10.1007/s12016-011-8294-7

Damas MSF, Mazur FG, Freire CCDM, Cunha AFD, Pranchevicius MCDS (2022) A systematic immuno-informatic approach to design a multiepitope-based vaccine against emerging multiple drug resistant serratia marcescens. Front Immunol 13: 768569 doi.org/10.3389/fimmu.2022.768569

De Tiège A, Verpooten J, Braeckman J (2021) From animal signals to art: manipulative animal signaling and the evolutionary foundations of aesthetic behavior and art production. Q Rev Biol 96: 1-27 doi.org/10.1086/713210

Desvars-Larrive A, Vogl AE, Puspitarani GA, Yang L, Joachim A, Käsbohrer A (2024) A One Health framework for exploring zoonotic interactions demonstrated through a case study. Nat Commun15: 5650 doi.org/ 10.1038/s41467-024-49967-7

Dimitrov I, Zaharieva N, Doytchinova, I (2020) Bacterial immunogenicity prediction by machine learning methods. Vaccines 8: 709 doi.org/10.3390/vaccines8040709

Dogbey G, Dugah A, Abbiw RK, Agbolosu A, Asare-Dompreh K, Odoom T, Okine A, Amakye-Anim J, Otsyina HR, Enyetornye B (2024) Impact of COVID-19 on pets and pet owners: A survey conducted in selected veterinary clinics in Accra, Ghana. Heliyon 10 doi.org/ 10.1016/j.heliyon.2024.e37328

Esposito MM, Turku S, Lehrfield L, Shoman A (2023) The impact of human activities on zoonotic infection transmissions. Anim 13: 1646 doi.org/10.3390/ani13101646

Fiers MW, Kleter GA, Nijland H, Peijnenburg AA, Nap JP, Van Ham RC (2004) Allermatch™, a webtool for the prediction of potential allergenicity according to current FAO/WHO Codex alimentarius guidelines. BMC Bioinformatics 5: 1-6 doi.org/10.1186/1471-2105-5-133

Galibert F, Quignon P, Hitte C, André C (2011) Toward understanding dog evolutionary and domestication history. C R Biol 334: 190-196 doi.org/10.1016/j.crvi.2010.12.011

Galles A, Monlun E, Villeneuve L, Poirot-Mazères S (2020) Méningite à *Capnocytophaga canimorsus*. Med Mal Infect 50: 754-756 doi.org/10.1016/j.medmal.2020.09.001

Gebre MS, Brito LA, Tostanoski LH, Edwards DK, Carfi A, Barouch DH (2021) Novel approaches for vaccine development. Cell 184: 1589-1603 doi.org/10.1016/j.cell.2021.02.030

Gonzalez-Galarza FF, McCabe A, Santos, EJMD, Jones J, Takeshita L, Ortega-Rivera N D, Cid-Pavon G M D, Ramsbottom K, Ghattaoraya G, Alfirevic A, Middleton D, Jones A R (2020) Allele frequency net database (AFND) 2020 update: gold-standard data classification, open access genotype data and new query tools. Nucleic Acids Res 48: 783-788 doi.org/10.1093/nar/gkz1029

Hannon DM, Harkin E, Donnachie K, Sibartie S, Doyle M, Chan G (2020) A case of *Capnocytophaga canimorsus* meningitis and bacteraemia. Ir J Med Sci 189: 251-252 doi.org/10.1007/s11845-019-02045-0

Hedman HD, Krawczyk E, Helmy YA, Zhang L, Varga C (2021) Host diversity and potential transmission pathways of SARS-CoV-2 at the human-animal interface. Pathog 10: 180 doi.org/10.3390/pathogens10020180

Ho J, Hussain S, Sparagano O (2021) Did the COVID-19 pandemic spark a public interest in pet adoption?. Front Vet Sci 8: 647308 doi.org/10.3389/fvets.2021.647308

Jespersen MC, Peters B, Nielsen M, Marcatili P (2017) BepiPred-2.0: improving sequence-based B-cell epitope prediction using conformational epitopes. Nucleic Acids Res 45: 24-29 doi.org/10.1093/nar/gkx346

Jolivet-Gougeon A, Sixou JL, Tamanai-Shacoori Z, Bonnaure-Mallet M (2007) Antimicrobial treatment of *Capnocytophaga* infections. Int J Antimicrob Agent 29: 367-373 doi.org/10.1016/j.ijantimicag.2006.10.005

Jumper, J, Evans R, Pritzel A, Green, T, Figurnov M, Ronneberger, O, Tunyasuvunakool K, Bates R, Žídek A, Potapenko A, Bridgland A, Meyer C, Kohl SAA, Ballard AJ, Cowie A, Romera-Paredes B, Nikolov S, Jain R, Adler J, Black T, Pretersen S, Reiman D, Clancy E, Zielinski M, Steinegger M, Pacholska M, Berghammer T, Bodenstein S, Silver D, Vinyals O, Senior AW, Kavukcuoglu K, Kohli P, Hassabis D 2021 Highly accurate protein structure prediction with AlphaFold. Nature 596: 583-589

Ko AI, Goarant C, Picardeau M (2009) Leptospira: the dawn of the molecular genetics era for an emerging zoonotic pathogen. Nat Rev Microbiol 7: 736-747 doi.org/10.1038/nrmicro2208

Kolaskar AS, Tongaonkar PC (1990) A semi-empirical method for prediction of antigenic determinants on protein antigens. FEBS Lett. 276: 172-174 doi.org/10.1016/0014-5793(90)80535-Q

Krishnan S, Joshi A, Akhtar N, Kaushik V (2021) Immunoinformatics designed T cell multi epitope dengue peptide vaccine derived from non structural proteome. Microb Pathog 150: 104728 doi.org/10.1016/j.micpath.2020.104728

Kushwaha V, Prabha A, Sharma V, Devi A, Ramniwas S, Sharma A, Sharma AK, Sheikh I, Panwar A, Kaur D (2024) Immunoinformatics: computational keys to immune system secrets. Bioinform Drug Discov 123 doi.org/10.1515/9783111568584-007

Lee K, McGregor S, Strowd L (2020) Noninflammatory Retiform Purpura: Answer. Am J Dermatopathol 42: 893-894 doi.org/10.1097/DAD.0000000000001552

Larsen MV, Lundegaard C, Lamberth K, Buus S, Lund O, Nielsen M (2007) Large-scale validation of methods for cytotoxic T-lymphocyte epitope prediction. BMC Bioinformatics 8: 1-12 doi.org/10.1186/1471-2105-8-424

Larsen JEP, Lund O, Nielsen M (2006) Improved method for predicting linear B-cell epitopes. Immunome Res 2: 1-7 doi.org/10.1186/1745-7580-2-2

Li D, Wu M (2021) Pattern recognition receptors in health and diseases. Signal Transduct Target Ther 6: 291 doi.org/10.1038/s41392-021-00687-0

Lion C, Escande F, Burdin JC (1996) *Capnocytophaga canimorsus* infections in human: review of the literature and cases report. Eur J Epidemiol 12: 521-533 doi.org/10.1007/BF00144007

Lundegaard C, Lamberth K, Harndahl M, Buus S, Lund O, Nielsen M (2008) NetMHC-3.0: accurate web accessible predictions of human, mouse and monkey MHC class I affinities for peptides of length 8–11. Nucleic Acids Res 36: 509-512 doi.org/10.1093/nar/gkn202

Mader N, Luehrs F, Langenbeck M, Herget-Rosenthal S (2020) *Capnocytophaga canimorsus*–a potent pathogen in immunocompetent humans–systematic review and retrospective observational study of case reports. Infect Dis 52: 65-74 doi.org/10.1080/23744235.2019.1687933

Masum MHU, Wajed S, Hossain MI, Moumi NR, Talukder A, Rahman MM (2024) An mRNA vaccine for pancreatic cancer designed by applying *in silico* immunoinformatics and reverse vaccinology approaches. PLoS One 19: 0305413 doi.org/10.1371/journal.pone.0305413

Meyer EC, Alt-Epping S, Moerer O, Büttner B (2021) Fatal septic shock due to *Capnocytophaga canimorsus* bacteremia masquerading as COVID-19 pneumonia-a case report. BMC Infect Dis 21: 1-6 doi.org/10.1186/s12879-021-06422-y

Nielsen M, Lundegaard C, Lund O, Keşmir C (2005) The role of the proteasome in generating cytotoxic T-cell epitopes: insights obtained from improved predictions of proteasomal cleavage. Immunogenet 57: 33-41 doi.org/10.1007/s00251-005-0781-7

Oltenacu EAB (2004) Domestication of animals. Encycl Anim Sci 294-296

O'Riordan, F Ronayne A, Jackson A (2021) *Capnocytophaga canimorsus* meningitis and bacteraemia without a dog bite in an immunocompetent individual. BMJ Case Rep 14: 242432 doi.org/10.1136/bcr-2021-242432

Ortega-Tirado D, Arvizu-Flores AA, Velazquez C, Garibay-Escobar A (2020) The role of immunoinformatics in the development of T-cell peptide-based vaccines against Mycobacterium tuberculosis. Expert Rev Vaccines 19: 831-841 doi.org/10.1080/14760584.2020.1825950

Owji H, Nezafat N, Negahdaripour M, Hajiebrahimi A, Ghasemi Y (2018) A comprehensive review of signal peptides: Structure, roles, and applications. Eur J Cell Biol 97: 422-441 doi.org/10.1016/j.ejcb.2018.06.003

Parisi X, Pihán G (2023) Purpura fulminans due to *Capnocytophaga canimorsus*. Br J Haematol 202 doi.org/10.1111/bjh.18837.

Pati R, Shevtsov M, Sonawane A (2018) Nanoparticle vaccines against infectious diseases. Front Immunol 9: 2224 doi.org/10.3389/fimmu.2018.02224

Pieracci EG, Williams CE, Wallace RM, Kalapura CR, Brown CM (2021) US dog importations during the COVID-19 pandemic: Do we have an erupting problem?. PLoS One, 16: 0254287 doi.org/10.1371/journal.pone.0254287

Ponomarenko J, Bui HH, Li W, Fusseder N, Bourne PE, Sette A, Peters B (2008) ElliPro: a new structure-based tool for the prediction of antibody epitopes. BMC Bioinformatics 9: 1-8. doi.org/10.1186/1471-2105-9-514

Popiel KY, Vinh DC (2013) 'Bobo-Newton syndrome': An unwanted gift from man's best friend. Can J Infect Dis Med Microbiol 24: 209 doi.org/10.1155/2013/930158

Powell L, Lavender TM, Reinhard CL, Watson B (2022) Pet Owners' Perceptions of COVID-19, zoonotic disease, and veterinary medicine: The impact of demographic characteristics. Vet Sci 9: 195 doi.org/10.3390/vetsci9050195

Rees EM, Minter A, Edmunds WJ, Lau CL, Kucharski AJ, Lowe R (2021) Transmission modelling of environmentally persistent zoonotic diseases: a systematic review. Lancet Planet Health 5: 466-478 doi.org/10.1016/S2542-5196(21)00137-6

Repac J, Mandić M, Lunić T, Božić B, Božić Nedeljković B (2021) Mining the capacity of human-associated microorganisms to trigger rheumatoid arthritis—A systematic immunoinformatics analysis of T cell epitopes. PLoS One 16: 0253918 doi.org/10.1371/journal.pone.0253918

Saha S, Raghava GPS (2006) AlgPred: prediction of allergenic proteins and mapping of IgE epitopes. Nucleic Acids Res 34: 202-209 doi.org/10.1093/nar/gkl343

Saha S, Raghava GPS (2006) Prediction of continuous B-cell epitopes in an antigen using recurrent neural network. Proteins:Struct Funct Bioinf 65: 40-48 doi.org/10.1002/prot.21078

Saklani S, Barsola, B, Pathania D, Sonu S, Kumari P, Singh P, Taha BA, Rustagi S, Thakur P, Narayan M, Chaudhary V (2024) Nanomaterials-integrated electrochemical biosensors as pioneering solutions for zoonotic disease diagnosis. J Electrochem Soc171: 087502 doi.org/10.1149/1945-7111/ad65bb

Sandoe JA (2004) *Capnocytophaga canimorsus* endocarditis. J Med Microbiol 53: 245-248 doi.org/10.1099/jmm.0.05274-0

Schleidt WM, Shalter MD (2003) Co-evolution of humans and canids. Evol Cogn 9: 57-72

Shamakhi A, Kordbacheh E (2021) Immunoinformatic design of an epitope-based immunogen candidate against *Bacillus anthracis*. Inform Med Unlocked 24: 100574 doi.org/10.1016/j.imu.2021.100574

Shin H, Mally M, Kuhn M, Paroz C, Cornelis GR (2007) Escape from immune surveillance by *Capnocytophaga canimorsus*. J Infect Dis 195: 375-386 doi.org/10.1086/510243

Silva DN, Chrobok M, Ahlén G, Blomberg P, Sällberg M, Pasetto A (2022) ATMP development and pre-GMP environment in academia: a safety net for early cell and gene therapy development and manufacturing. Immuno-Oncol Technol 16: 100099 doi.org/10.1016/j.iotech.2022.100099

Sunita, Sajid, A., Singh, Y. and Shukla, P., 2020. Computational tools for modern vaccine development. Hum. Vaccines Immunother. 16: 723-735 doi.org/10.1080/21645515.2019.1670035

Teufel F, Almagro Armenteros JJ, Johansen AR, Gíslason MH, Pihl SI, Tsirigos KD, Winther O, Brunak S, von Heijne G, Nielsen H (2022) SignalP 6.0 predicts all five types of signal peptides using protein language models. Nat Biotechnol 40: 1023-1025 doi.org/10.1038/s41587-021-01156-3

Umeda K, Suzuki M, Imaoka K (2024) Investigation of antimicrobial susceptibility and resistance gene prevalence in *Capnocytophaga* spp. isolated from dogs and cats and characterization of novel class A β-lactamase CST-1. Eur J Clin Microbiol Infect Dis 1-11 doi.org/10.1007/s10096-024-05025-0

Van Dam AP, Jansz A (2011) *Capnocytophaga canimorsus* infections in The Netherlands: a nationwide survey. Clin Microbiol Infect 17: 312-315 doi.org/10.1111/j.1469-0691.2010.03195.x

Van Samkar A, Brouwer MC, Schultsz C, van der Ende A, van de Beek D (2016) *Capnocytophaga canimorsus* meningitis: three cases and a review of the literature. Zoonoses Public Health 63: 442-448 doi.org/10.1111/zph.12248

Vigne JD, Guilaine J, Debue K, Haye L, Gérard P (2004) Early taming of the cat in Cyprus. Science 304: 259-259 doi.org/10.1126/science.1095335.

Vinusha V, Girish C (2024) Discovering vaccines: the trial tale. Naunyn-Schmiedeb. Arch Pharmacol 1-15 doi.org/10.1007/s00210-024-03368-1

Wang P, Sidney J, Dow C, Mothé B, Sette A, Peters B (2008) A systematic assessment of MHC class II peptide binding predictions and evaluation of a consensus approach. PLoS Computut Biol 4: 1000048 doi.org/10.1371/journal.pcbi.1000048

Wang P, Sidney J, Kim Y, Sette A, Lund O, Nielsen M, Peters B (2010) Peptide binding predictions for HLA DR, DP and DQ molecules. BMC Bioinformatics 11:1-12. doi.org/10.1186/1471-2105-11-568

Wang P (2021) Natural and synthetic saponins as vaccine adjuvants vaccines 2021: 9, 222 doi.org/10.3390/vaccines9030222

Warimwe GM, Francis MJ, Bowden TA, Thumbi SM, Charleston B (2021) Using cross-species vaccination approaches to counter emerging infectious diseases. Nat Rev Immunol 21: 815-822 doi.org/10.1038/s41577-021-00567-2

Yang MC, Ling J, Mosaed S (2021) *Capnocytophaga canimorsus* blebitis: case report and review of literature. BMC Ophthalmol 21:1-5 doi.org/10.1186/s12886-021-01823-8

Yurina V, Adianingsih OR (2022) Predicting epitopes for vaccine development using bioinformatics tools. Ther Adv Vaccines Immunother 10: 25151355221100218 doi.org/10.1177/25151355221100218

Zaharieva N, Dimitrov I, Flower DR, Doytchinova I (2019) VaxiJen dataset of bacterial immunogens: an update. Curr Comput-Aided Drug Des 15: 398-400. doi.org/10.2174/1573409915666190318121838

Zaharieva N, Dimitrov I, Flower D, Doytchinova I (2017) Immunogenicity prediction by VaxiJen: a ten year overview. J Proteom Bioinform 10: 10-4172 doi.org/10.4172/jpb.1000454

Zajkowska J, Król M, Falkowski D, Syed N, Kamieńska A (2016) *Capnocytophaga canimorsus*–an underestimated danger after dog or cat bite–review of literature. Prz Epidemiol 70: 289-295